

**Non-linear Model Reduction and Control of Molten Carbonate
Fuel Cell Systems with Internal Reforming**

Dissertation

zur Erlangung des akademischen Grades

Doktoringenieur

(Dr.-Ing.)

von M.Sc. Min Sheng

geb. am 4. Januar 1973 in Hunan, P.R.China

genehmigt durch die Fakultät für Elektrotechnik und Informationstechnik
der Otto-von-Guericke-Universität Magdeburg

Gutachter:

Herr Prof. Dr. A. Kienle

Herr Prof. Dr. K. Sundmacher

Herr Dr. M. Mangold

Promotionskolloquium am 12. Oktober 2007

Acknowledgements

I express my gratitude to the German people for giving me the opportunity of working in the Max-Planck-Institut für Dynamik Komplexer Technischer Systeme in Magdeburg under ideal scientific conditions. In the institute I met the most brilliant colleagues I have ever known and I was favored by stimulating discussions and warm friendship with some of them.

I would like to express my gratitude to Dr.-Ing. Dr. h.c. mult. E. D. Gilles, the founding director of the institute, for making possible for me to work under such ideal conditions.

I gratefully acknowledge Prof. Dr.-Ing. Achim Kienle for the enthusiastic discussions and supervising tasks during the development of this research project.

I wish to express my gratitude to Dr.-Ing. Michael Mangold for his comments and careful attention to detail. His valuable contribution has enabled me to free the text from various errors and some inconsistencies, but the errors remained are my sole responsibility.

To:

My parents, my wife and my daughter

Abstract

Currently, the process design of fuel cells and the development of control strategies is mainly based on heuristic methods. Fuel cell models are often too complex for control purposes, or they are developed for a specific type of fuel cell and valid only in a small range of operation conditions. The application of fuel cell models to controller design is still limited. Furthermore, suitable and simple-to-implement design strategies for fuel cell control remain an open area. There is thus a motivation for simplifying dynamic models for process control applications and for designing suitable control strategies for fuel cells. This is the main objective of this work. As an application example, the 250 kW industrial molten carbonate fuel cell (MCFC) system HotModule by MTU CFC Solutions, Germany is considered.

A detailed dynamic two-dimensional spatially distributed cross-flow model of a MCFC from literature is taken as a starting point for the investigation. In Chapter 2, two simplified model versions are derived by incorporating additional physical assumptions. One of the simplified models is extended to a three-dimensional stack model to deal with physical and chemical phenomena in the stack. Simulations of the stack model are performed in Chapter 3 in order to calculate the mass and temperature distributions in the direction perpendicular to the electrode area. The other simplified model forms the basis for a low order reduced model that is derived in Chapter 4.

The reduced-order model is constructed by application of the Karhunen-Loève Galerkin method. The spatial temperature, concentration and potential profiles are approximated by a set of orthogonal time independent spatial basis functions. Problem specific basis functions are generated numerically from simulation data of the detailed reference model. The advantage of this approach is that a small number of basis functions suffices in order to approximate the solution of the detailed model very well. The resulting reduced order model is of considerably lower order than the

detailed model and requires much less computation time. It is used for the development of a model based control strategy in Chapter 5.

The purpose of control is to guarantee a fast and safe dynamic response of the fuel cell system during load changes; an optimal steady state electric efficiency is also desired. Taking both considerations a control strategy with three main loops is designed. The first loop is composed of a master controller that imposed a load change and sets fuel gas, the steam to carbon ratio, air number and cathode gas recycle ratio to their corresponding conditions for optimal steady state electric efficiency. The other two loops are feedback PID controllers that for given temperature limits (maximum temperature and maximum temperature difference) respond by changing the air ratio and steam to carbon ratio around the default sets by the master controller. It turns out that for load changes, the PID controllers can successfully take the maximum temperatures as well as the spatial temperature differences to their desired set-points.

In cases, where the maximum temperature and the maximum temperature difference cannot be measured directly, the proposed control scheme has to be combined with a state estimator. A suitable state estimator is developed based on the reduced-order model and the control strategy with the observer shows reasonable results.

Kurzzusammenfassung

Derzeit beruht die Entwicklung von Brennstoffzellensystemen und zugehörigen Prozessführungskonzepten hauptsächlich auf heuristischen Methoden. Verfügbare Brennstoffzellenmodelle sind oft zu kompliziert für die Anwendung auf Regelungsprobleme, oder sie sind nur für ein ganz spezielles Brennstoffzellensystem und nur in engen Betriebsbereichen gültig. Daher existieren sehr wenige modellbasierte Regelungskonzepte für Brennstoffzellen. Darüber hinaus existiert ein Bedarf an geeigneten und einfach zu implementierenden Regelungsstrategien für Brennstoffzellen. Daraus ergibt sich die Motivation, dynamische Brennstoffzellenmodelle im Hinblick auf Prozessführungsaufgaben zu vereinfachen und mit Hilfe dieser Modelle Regelungsstrategien für Brennstoffzellen zu entwickeln. Dies ist das Hauptziel dieser Arbeit. Als Anwendungsbeispiel wird das industrielle Schmelzkarbonatbrennstoffzellensystem (MCFC-System) HotModule der Firma MTU CFC Solutions betrachtet, das eine elektrische Leistung von bis zu 250 kW liefert.

Als Ausgangspunkt für die Untersuchungen dient ein detailliertes dynamisches, örtlich zweidimensionales Brennstoffzellenmodell aus der Literatur. In Kapitel 2 werden von diesem Modell durch zusätzliche physikalische Annahmen zwei vereinfachte Varianten abgeleitet. Die eine Modellvariante wird zu einem dreidimensionalen Modell des Brennstoffzellenstapels erweitert, um zusätzliche chemische und physikalische Phänomene im Zellstapel zu erfassen. In Kapitel 3 werden Simulationen mit dem Modell des Brennstoffzellenstapels durchgeführt, um Konzentrations- und Temperaturverteilungen senkrecht zur Elektrodenfläche zu erfassen. Die zweite vereinfachte Modellvariante dient als Grundlage für ein reduziertes Modell sehr niedriger Ordnung, das in Kapitel 4 hergeleitet wird.

Das reduzierte Modell wird mit Hilfe der Karhunen-Loève-Galerkin-Methode bestimmt. Dazu werden die örtlichen Temperatur-, Konzentrations- und Potenzialprofile mit Hilfe zeitlich konstanter orthonormaler Basisfunktionen approximiert. Aus Simulationsdaten, die mit Hilfe des detaillierten Modells gewonnen wurden, werden auf numerischem Wege problemangepasste Basisfunktionen generiert. Diese Methode bietet den Vorteil, dass eine kleine Anzahl von Basisfunktionen ausreicht, um die Lösung des detaillierten Modells mit guter Genauigkeit zu approximieren. Das resultierende reduzierte Modell ist von viel niedrigerer Ordnung als das detaillierte Modell und benötigt erheblich weniger Rechenzeit. Es dient als Grundlage für die Entwicklung eines modellgestützten Regelungskonzepts für das HotModule, das in Kapitel 5 entwickelt wird.

Die Regelung hat die Aufgabe, ein schnelles und sicheres dynamisches Verhalten des Brennstoffzellensystems bei Lastwechseln zu garantieren. Darüber hinaus ist eine optimale Effizienz des Systems im stationären Fall wünschenswert. Unter Berücksichtigung dieser beiden Anforderungen wird ein Regelungskonzept aus einer Vorsteuerung und zwei PID-Reglern entwickelt. Die Vorsteuerung setzt die Brennstoffdurchflussmenge, das Verhältnis zwischen Dampf und Methan im Anodenzufluss, die Luftzahl des Brenners sowie den Anteil des zum Brenner zurückgeführten Kathodenabgases auf die optimalen stationären Werte bei einer gegebenen Lastanforderung. Die beiden PID-Regler dienen dazu, die örtlich höchste Temperatur sowie den örtlichen Temperaturgradienten auf vorgegebene Maximalwerte zu begrenzen. Sie korrigieren dazu die Luftzahl und die Zusammensetzung des Brenngases um die von der Vorsteuerung vorgegebenen Werte. Simulationsstudien zeigen, dass diese Strategie Erfolg versprechend ist.

In Fällen, wo die Maximaltemperatur und der maximale Temperaturgradient nicht gemessen werden können, muss das vorgeschlagene Regelungskonzept um eine Zustandsschätzung erweitert werden. Dazu wird basierend auf dem reduzierten Modell ein Beobachter entworfen und mit dem Regler kombiniert. Dies führt in Testsimulationen zu guten Ergebnissen.

Contents

1	Notations	xi
1	Introduction	1
1.1	Background	1
1.2	Objectives.....	2
1.3	Outline of the Thesis	3
1.4	Originality	4
2	Background to MCFC Principle and MCFC Modeling	5
2.1	Overview of MCFC	5
2.2	MCFC Working Principle	6
2.3	MCFC Modeling with respect to Process Control Purposes.....	11
2.3.1	A 2-D MCFC model developed by Heidebrecht (2005)	12
2.3.2	A simplified 2-D MCFC model based on Heidebrecht (2005)	23
2.3.3	A nonlinear 3-D MCFC model with IIR internal reforming section	26
3	Model comparison and validation	31
3.1	Introduction.....	31
3.2	Validation of the simplified model	31
3.3	Simulation results of 3-D stack model without DIR.....	33
4	Nonlinear Model Reduction of a Two-Dimensional MCFC Model with Internal Reforming	38
4.1	Introduction.....	38
4.2	Derivation of the Reduced MCFC Model.....	38
4.2.1	Galerkin procedure.....	38
4.2.2	The Karhunen-Loève decomposition.....	41
4.2.3	Choice of snapshots	45
4.2.4	Treatment of boundary conditions	46
4.3	Simulation Results of the Reduced MCFC Model.....	47
4.4	Summary	51
5	Model-Based Dynamic Performance and Control of a Molten Carbonate Fuel Cell System	53
5.1	Introduction.....	53

5.2 The Control Strategy	54
5.2.1 Steady state optimization	57
5.2.2 Solid temperature response analysis	60
5.2.3 Control results and analysis	65
5.2.4 State estimator	68
5.3 Development of a Luenberger Observer for Model Based Measurement ..	68
5.3.1 Structure of the Observer	69
5.3.2 Observer model	70
5.3.3 Observability and placement of sensors.....	71
5.3.4 Observer correction term.....	71
5.3.5 Test of the observer	73
5.3.6 Control results with the observer model	75
5.4 Summary	79
6 Conclusions	82
Bibliography	84

Notations

Latin symbols

Arr_j	Arrhenius number of reaction j
C	Correlation matrix
c	Surface related charge capacity
c_p	Molar heat capacity
Da_j	Damköhler number of reaction j
$E_{A,j}$	Activation energy of reaction j
F	Dimensionless Faradaic constant
G	Molar flow $mol \cdot s^{-1}$
g	Mass flow density $mol \cdot m^{-2} \cdot s^{-1}$
H_{feed}	Combustion enthalpy of the fuel gas
$h_{a/c}$	Height m
I_{cell}	Total cell current
I_n	$n \times n$ identity matrix
i	Current density
K_j	Equilibrium constant of reaction j
k_e	Ion conductivity of electrolyte $m^{-1} \cdot \Omega^{-1}$
k^h	Heat exchange coefficient $W \cdot m^{-2} \cdot K^{-1}$
L_K	Cell size in direction k
l_2	Geometric aspect ratio
l_3	Geometric aspect ratio
N	Number of snapshots
n_i	Mass exchange flux density of component i
n_j	Number of electrons transferred in electrochemical reaction j
P	Electric power
Pe_s	Peclet number
p	Pressure
q	Heat exchange flux density
q_s	Heat source density
R	Gas constant

r_j	Reaction rate of reaction j
R_{back}	The cathode gas recycle ratio
S/C	Steam to carbon ratio
St	Stanton number
T	Temperature K
t	Time s
U_{cell}	Cell voltage
V	Volume
z_k	Spatial coordinate k m

Greek symbols

$\alpha_{j,\pm}$	Transition factors for reaction j
Γ	Total molar flow
γ	Molar flow density
$\Delta_c h_i^0$	Standard combustion enthalpy of component i
$\Delta_R g_{Cj}$	Free enthalpy of reaction j
$\Delta_R h_j^0$	Standard enthalpy of reaction j
ε	Residual error
ζ_d	Spatial coordinate
η	Electric efficiency
ϑ	Temperature
κ_e	Ion conductivity
λ	Eigenvalue
λ_{air}	Air number
λ_s	Thermal conductivity $W \cdot m^{-1} \cdot K^{-1}$
μ_j	Lagrangian multiplier
$\nu_{i,j}$	Stoichiometric coefficient of component i in reaction j
$\bar{\nu}_j$	Total mole change in reaction j
ξ	Average mean-square residual error
τ	Time
φ_i	Partial pressure of component i
Φ	Electric potential
ϕ	Orthonormal basis function
$\sigma_{i,j}$	Component i mass source due to the reaction j

$\sigma_{\vartheta,j}$	Reaction heat due to the reaction j
v_i	Snapshot
χ_i	Mole fraction of component i
ψ	Integration variable, temperature

Lower indexes

<i>a</i>	Anode gas phase
<i>air</i>	Burner air
<i>as</i>	Anode / solid phase exchange
<i>b</i>	Boundary
<i>back</i>	Cathode recycle
<i>c</i>	Cathode gas phase
<i>cs</i>	Cathode / solid phase exchange
<i>diff</i>	Difference
<i>e</i>	Electrolyte
<i>FC</i>	Fuel cell stack
<i>feed</i>	Fuel cell feed
<i>i</i>	(usually) chemical species, component
<i>in</i>	Inlet
<i>j</i>	(usually) chemical reaction
<i>l</i>	Chemical species, component
<i>max</i>	Maximum
<i>min</i>	Minimum
<i>out</i>	Outlet
<i>r</i>	Indirect internal reforming section
<i>s</i>	Solid phase
<i>t</i>	Total

Upper indexes

<i>0</i>	Thermodynamic standard
θ	System specific standard
\sim	(usually) dimensional variable
\wedge	Approximation
<i>T</i>	Transported matrix

Chapter 1

Introduction

1.1 Background

Fuel cell-based power plants convert the chemical energy in a fuel directly to electricity without the requirement of conversion of energy into heat. This results in high efficiency (50 - 60% before heat recovery). The molten carbonate fuel cell (MCFC) is a high-temperature fuel cell operated at 600°C - 700°C. Due to its high operation temperature, the MCFC offers advantages for the co-generation of heat and electricity. Furthermore, the high operation temperature enables internal reforming and makes the MCFC flexible with respect to the sorts of fuel that can be used. On the other hand, the operation temperatures and consequently the demands of the MCFC on thermal stability of the used materials are below those of solid oxide fuel cells (Carrette, Friedrich & Stimming, 2001). Those properties make the MCFC an attractive candidate for decentralized power generation. The first commercial MCFC systems are now close to market (Bischoff & Huppmann, 2002).

Currently, the development and operation of MCFCs as of other high temperature fuel cells is mainly based on experimental and empirical knowledge. However, an intuitive process understanding is difficult in this case, as an MCFC system is a highly integrated process whose behavior depends on numerous interactions between the electrochemical reaction steps, the internal reforming, mass transport processes, and the heat transfer inside a cell or stack. A deeper understanding of the physico-chemical processes in an MCFC can be obtained from mathematical models based on physical conservation principles. Model based process control and process design strategies can lead to a much better use of the fuel cells' capacities

and increase the efficiency of the system, but require suitable dynamic process models. Such models should offer good extrapolation qualities on the one hand, but must also be solvable in the framework of a real-time process control environment or an optimization algorithm. Today, the majority of MCFC models available in open literature are steady state models and therefore not suitable for process control (a survey is given in (Koh, Kang & Lim, 2001)). Only very few detailed dynamic MCFC models have been published (He & Chen, 1998; Heidebrecht & Sundmacher, 2002; Heidebrecht & Sundmacher, 2003). Those models consist of systems of algebraic and nonlinear partial differential equations in several space coordinates, which are too complex for many process control purposes. As a consequence, most control studies of the MCFC have to rely on rather simple dynamical models, black-box type input output models, or qualitative knowledge-based approaches (Lucas, Lee & Ghezal-Ayagh, 2002; Kang, Koh & Lim, 2001; Shen *et al.* 2002; Sun, Cao & Zhu, 2001).

The main contribution of the thesis is to develop suitable dynamic models for control purposes and to design a practicable control strategy for MCFC systems. The thesis focuses on three-dimensional MCFC stack model development; MCFC model reduction; temperature control of MCFC with internal reforming and state estimator design.

1.2 Objectives

In particular this thesis develops a simplified form of a detailed two-dimensional spatially distributed MCFC model. This model serves as a basis for the model reduction. A three-dimensional model for a MCFC stack is developed in order to have a better understanding of how the actual fuel cell stack performs and how the temperature in the stack distributes. The thesis then focuses on the development of the reduced-order model, which is also a basis of the temperature controller and the observer design.

The objectives include:

(1) A detailed two-dimensional spatially distributed model of a planar MCFC with cross flow is derived from energy, mass, and charge balances. This model is used as a starting-point and reference for the reduced model. A reduced set of model equations is developed by applying the Karhunen-Loève Galerkin method to the reference model. The resulting model approximates a detailed spatially distributed model with good accuracy.

(2) A three-dimensional model based on a ‘HotModule’ stack is established to deal with physical and chemical phenomena in the stack and to calculate the mass distribution in the direction perpendicular to the electrode area.

(3) A control system framework based on a ‘HotModule’ fuel cell is constructed to satisfy high electric efficiency over a long range of electric load change and to keep the fuel cell safe.

(4) A Luenburger state observer is designed based on a reduced model of the ‘HotModule’ fuel cell. The state estimator and the control scheme are combined together in order to obtain a practical application of the control scheme.

1.3 Outline of the Thesis

Chapter 2 first briefly reviews some general methods for fuel cell modeling and control, and then focuses on a detailed nonlinear dynamic model of a planar MCFC with direct internal reforming (DIR) that serves as a reference and a basis for the approaches proposed in this work. A simplified model and three-dimensional stack model are then built based on this detailed model.

Chapter 3: The simplified model built in Chapter 2 is validated by comparison to the detailed model and also presents the three-dimensional simulation.

A reduced form of the nonlinear dynamic model of the planar MCFC is described in Chapter 4.

A control scheme based on the detailed dynamic model is designed in Chapter 5. Its practical application is implemented by incorporating a state estimator which is constructed based on the reduced order model.

The main benefit of the work is summarized in Chapter 6.

1.4 Originality

The three-dimensional model simulation, the nonlinear model reduction using Galerkin Karhunen-Loève approach and the temperature control strategy are all original. The work has been presented at various symposia and conferences (Mangold & Sheng, 2003; Mangold et al. 2004a; Mangold et al. 2005), published in Chemical Engineering Science (Mangold et al. 2004b), in Fuel Cells (Mangold & Sheng, 2004), in a book chapter (Mangold & Sheng, 2006), and also in the Journal of Power Sources (Sheng, Mangold & Kienle 2006).

Chapter 2

Background to the MCFC Principle and MCFC Modeling

First this chapter briefly reviews the basic principle of MCFC, and then introduces a two-dimensional MCFC model developed by Heidebrecht (2005), which serves as a basic model for the three-dimensional stack model, model reduction and controller design proposed in the later chapters.

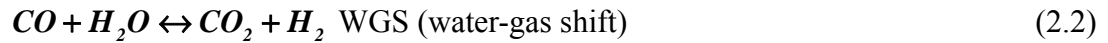
2.1 Overview of MCFC

Among the various fuel cell types, the molten carbonate fuel cell (MCFC) is a very promising technique which is now about to become commercially used. It will mainly be applied for stationary generation of electric energy together with the production of highly valuable heat and is thus suitable for many industrial applications as well as for decentralized power supply. Although, natural gas is the preferred fuel, the cell can be fed by a wide variety of fuels containing non-oxidized carbon or hydrogen, as can be found in many industrial processes. Due to high operating temperatures, internal reforming can be applied in this fuel cell type. The MCFC with an internal reforming is very attractive for the co-generation of electricity and heat. However, it requires further research efforts to make high temperature fuel cells economically competitive. A better process understanding and an improved process operation can help to exploit the potential of the cells to a higher degree than it is done today. Process operation is challenging, because industrial high temperature fuel cell stacks are highly integrated processes, which combine the internal generation of hydrogen by steam reforming, the mass coupling between anode and cathode gas channels, and the heat integration of endothermic reforming reactions and exothermic electrochemical reactions in one apparatus. The process operation is further complicated by the limited measurement information

available online. Currently, most high temperature fuel cell stacks are operated manually, based on experience and heuristic knowledge. This approach requires large safety factors and therefore is unsatisfactory.

2.2 MCFC Working Principle

The basic structure and the working principle of an MCFC with direct internal reforming (DIR) is shown in Figure 2-1. The MCFC consists of two porous electrodes, an electrolyte layer between them and gas channels above each electrode. Necessary fuel and oxidant reactants are conveyed and distributed onto anode and cathode electrode through gas channels. In order to make full use of the fuel gas and to improve the performance of fuel cell, special baffles are introduced in the anode gas channel (Figure 2-2), which results in an even distribution of the fuel gas. The anode channel is fed with a mixture of natural gas (methane), carbon monoxide, carbon dioxide, hydrogen and steam which come from a pre-reformer. The following reactions occur in the pre-reformer:



In the anode gas channel, the natural gas that is not completely reacted in the pre-reformer continues to be oxidized to hydrogen and carbon monoxide in an internal reforming step. Then both H_2 and CO are oxidized electrochemically, consuming carbonate ions from the molten salt electrolyte and producing free electrons on the anode electrode:



The anode exhaust gases consist of unreformed feed gas, reforming products and oxidation products. The anode exhaust gases are mixed with fresh air, and in some cases with a part of cathode exhaust gas and then fed into a catalytic combustion section (also named as burner or Anode Gas Oxidizer). In the burner, all combustible species are completely oxidized. The outlet of the burner (a mixture of

O_2 and CO_2) is then fed back into the fuel cell cathode gas channel. The oxygen and carbon dioxide in the oxidant stream undergo a reduction reaction under consumption of electrons from the electrode to form new carbonate ions CO_3^{2-} :



The electrons from the anode are transferred to the cathode via an external electric circuit, where they perform electric work.

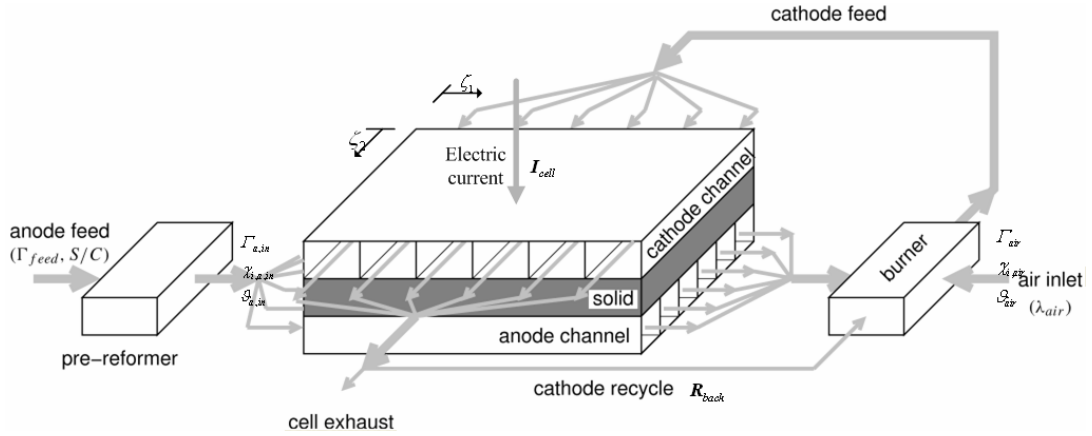


Figure 2 - 1: Considered scheme of the MCFC system, which consists of a pre-reformer, the cell stack, and a burner between anode side and cathode side.

The input parameters of the model describe the amount of anode feed gases (in terms of dimensionless molar flows, Γ), their composition (in terms of mole fractions, χ_i) and their temperature (ϑ) as well as at the air inlet to the burner and the cathode gas recycle ratio (R_{back}). Depending on the operation mode of the cell, either the cell voltage $\Delta\phi$ (potentiostatic operation) and the cell current I_{cell} (galvaniostatic operation) or the resistance of an external electric load can be considered as further input variables. The output variables are identical to the state variables. The remaining variables are fluxes of mass, energy and charge, among them is the current density i . All constants describing the properties of the system are system parameters.

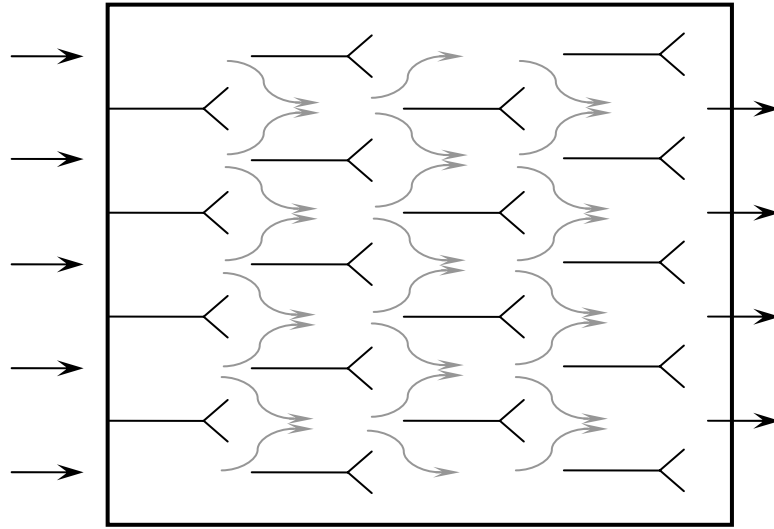
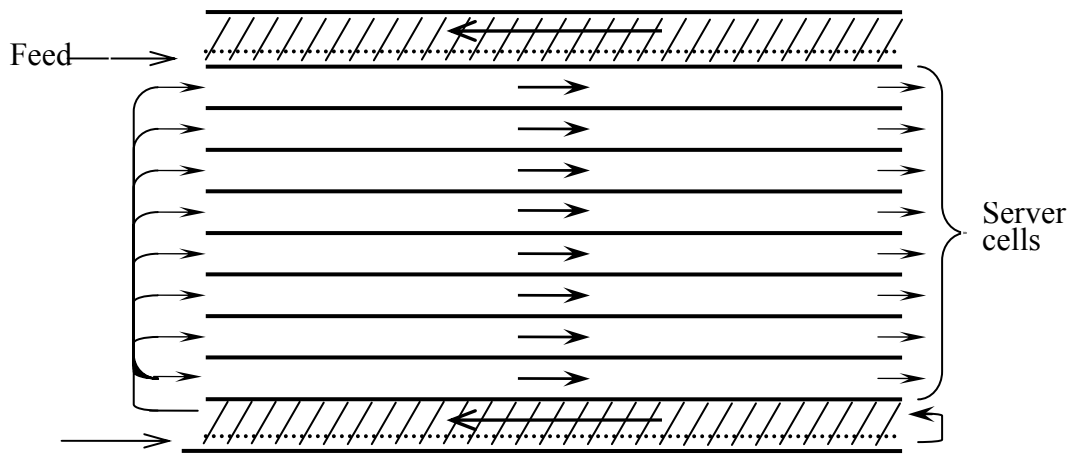


Figure 2 - 2: Top view of anode gas channels

In order to provide enough electrical power density, individual fuel cells are aggregated to a cell stack. A MCFC stack generally consists of several fuel cells and indirect internal reforming sections between several, e.g. eight to ten fuel cells. The power generated by a fuel cell stack depends on the number and size of single fuel cells. A basic MCFC stack structure is shown in figure 2 - 3, in which natural gas is internally reformed to hydrogen, partially in an internal reforming unit and partially at the cells' anode gas channels, which is a combination of indirect internal reforming (IIR) and direct internal reforming (DIR). Top and bottom of the stack are two indirect internal reforming sections. The gas phase through the reformer is in counter-flow to the anode gas channels in order to provide better temperature distribution. The structure of an indirect internal reforming section is shown in Figure 2 - 4. Not all MCFC stacks consider both steps, some may have no reforming catalysts in the cell anode gas channels and hence have no direct internal reforming step.



Flow direction of anodes (cathode in cross flow)

Figure 2 - 3: basic cell stack structure with internal reforming

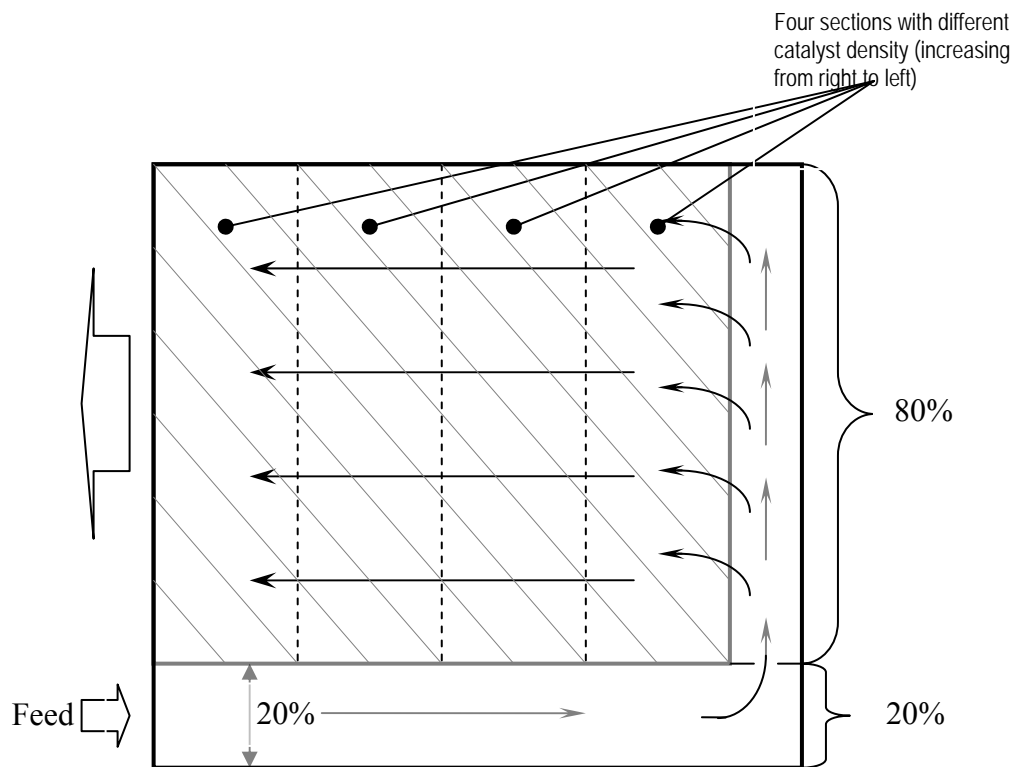


Figure 2 - 4: Top view of indirect internal reforming

A complete MCFC system is a highly integrated process that may couple the dynamics of several hundreds fuel cells in one single vessel with a thermal management system, anode gas burner/oxidizer (AGO), and power conditioning unit. In other words, a complete MCFC system is the sum of all equipment for safe operation as well as the technical coordination of all concerned parts of a power plant. An example of the MCFC system is the HotModule by MTU CFC Solutions, Germany (Bischoff & Huppmann, 2002), which includes 342 fuel cells that can deliver up to 200 kW of electrical power. A pilot plant installation of the HotModule exists at the Magdeburg university hospital, Germany (Figure 2 - 5). The name of the HotModule was chosen to highlight the fact that all hot cell parts are assembled in just one single vessel. Further devices are assembled in the so-called media supply. Here, a desulphurizer with activated carbon, a heat exchanger and a humidifier, an external pre-reformer and several heat exchangers serve for the pre-treatment of the fuel gas. Within this work, the focus is on the cell stack vessel, the media supply is not treated.

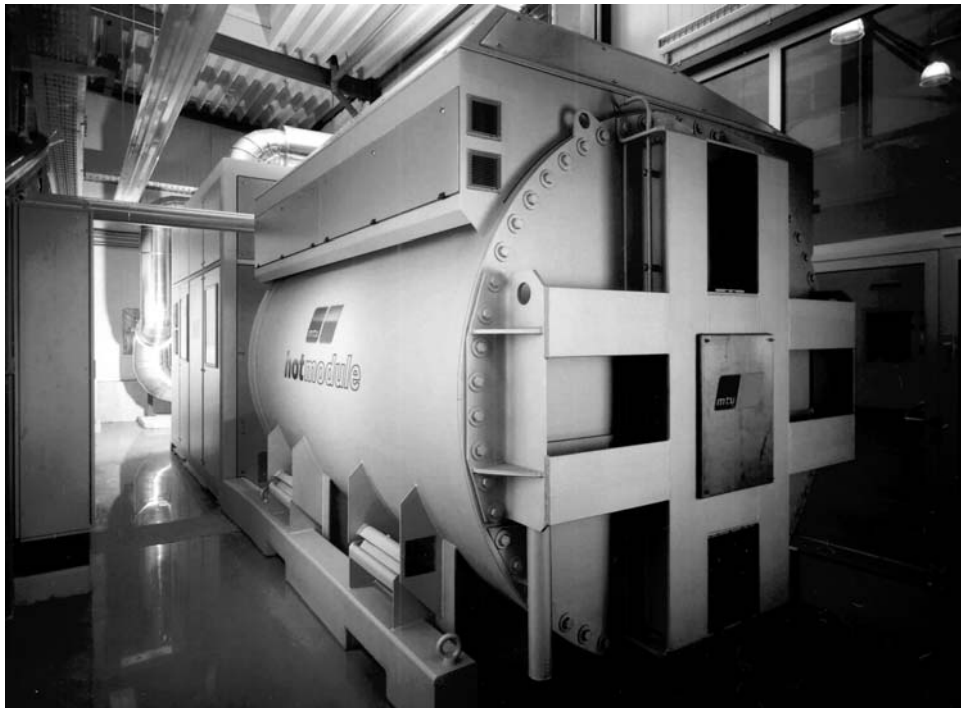


Figure 2 - 5: The HotModule exists at the Magdeburg university hospital, Germany

2.3 MCFC Modeling with respect to Process Control Purposes

Mathematical modeling of fuel cells has concentrated on such issues as physical and transport properties, kinetics, and static performance. Simple dynamic representations of fuel cells and peripheral components (thermal management system, anode gas burner, and power conditioning unit) are instead preferred for use in control applications. To this end, several developments have been reported in the literature based on particular assumptions. In literature one can find a number of steady state models for MCFCs, most of them considering the system under various aspects such as temperature distribution or pressure profile, electric efficiency or fuel usage (Yoshida et al., 1998; Bosio, Costamagna, & Parodi, 1999). Many of these models contain strongly empirical approaches, valid only for the system discussed in the respective article. Also assumptions are made that only apply to a few cases. The number of transient models is far smaller. Cell geometry effects and complex mass distributions have been included in a dynamic model for a MCFC with external reforming (He, 1994; He & Chen, 1995). Alternatively, a dynamic model for a MCFC with internal reforming has been developed assuming chemical reactions at equilibrium and negligible mass storage (Ernest, Ghezal-Ayagh & Kush, 1996). He and Chen (1998) developed a transient stack model using a computational-fluid-dynamics (CFD) program in order to simulate the temperature profile in a MCFC stack. But the model describes only the states of the temperature in the stack. Lukas, Lee & Ghezal-Ayagh (2002) have developed a model for a single cell with indirect and direct internal reforming based on the assumption of lumped parameters. The model cannot describe spatial distributions in the cell. Heidebrecht & Sundmacher (2003) developed a transient mathematical model for a single counter-flow cell of a molten carbonate fuel cell. Heidebrecht (2005) also developed a two dimensional cross-flow MCFC model. The model is based on the description of physical phenomena related to the concentration, temperature and potential field within the gas and solid phases. The model results include the steady states of the system as well as the transient functions of concentrations, temperature,

current densities and cell voltage. But the model consists of systems of algebraic and nonlinear partial differential equations in several space coordinates, which are too complex for many process control purposes. As a consequence, most control studies of the MCFC have to rely on rather simple dynamic models, black-box type input/output models, or qualitative knowledge-based approaches (Shen et al. 2002; Kang, Koh & Lim, 2001; Sun, Cao & Zhu, 2001; Aguiar et al. 2005).

2.3.1 A 2-D MCFC model developed by Heidebrecht (2005)

This thesis is mostly concerned with the experimental and theoretical analysis of the so-called HotModule by MTU CFC Solutions, Germany (Bischoff & Huppmann, 2002), a detailed model for this particular system was developed by Heidebrecht (2005).

The model by Heidebrecht (2005) is based on a simplified scheme of the MCFC system as depicted in Figure 2 - 1. The fresh anode feed consisting of steam and methane first enters a pre-reformer where a part of the methane is converted to hydrogen, and then is distributed to the anode gas channels of the cell stack. The outlet flow on anode side goes into a burner. The burner is supplied with air from the ambient and oxidizes unconsumed methane and hydrogen. The burner outlet is fed to the cathode gas channels. Finally, a part of the cathodic exhaust gases may be recycled to the burner.

The Heidebrecht model serves as a reference and as a basis for the model reduction, state estimator and controller design in this thesis. The main assumptions of the model are:

- The gas phases are isobaric and behave like ideal gases
- In all channels, plug flow is assumed
- In the fuel cell, spatial gradients in the direction of ζ_1 and ζ_2 axis, i.e. in the direction of the anodic and cathodic gas fluxes are taken into account

- A pseudo-homogeneous energy balance is formulated for the solid parts of the cell, assuming an identical temperature in the anode, the electrolyte and the cathode
- Reversible potential kinetics is used to describe the internal reforming in the cell; for the electrochemical reactions, Butler-Volmer kinetics are used
- The electrodes possess infinite electrical conductivity
- Charge transport in the electrolyte occurs only perpendicular to the ζ_1 and ζ_2 axis; the electrolyte is modeled as a ohmic resistance, the concentration of carbonate ions is assumed to be constant; a spatially distributed potential field and a spatially distributed current density field are computed
- The pre-reformer has a negligible hold-up; all reactions in the pre-reformer occur instantaneously; CO is converted completely to CO_2 ; a constant rate of conversion for CH_4 is assumed
- The burner has a negligible hold-up and works with total conversion

Dimensionless numbers

The Heidebrecht model equations were written completely in dimensionless terms. The meanings and physical interpretations of all state variables, the cell current and the most important model parameters are given in the following. The list of dimensionless quantities can be found in Heidebrecht (2005).

Because the mole fraction x_i in a dimensional equation system already is dimensionless it can be used directly. Only a Greek symbol is used to distinguish dimensionless equations from dimensional ones.

$$\chi_i = x_i \quad (2.6)$$

The partial pressures, p_i , are related to a standard pressure, p^θ .

$$\varphi_i = \frac{p_i}{p^\theta} \quad (2.7)$$

The temperature, T , is made dimensionless by relating it to a standard temperature, T^θ .

$$\vartheta = \frac{T}{T^\theta} \quad (2.8)$$

Extensive molar flows, G , are related to a standard value of a molar flow which is characteristic for the MCFC operation, G^θ .

$$\Gamma = \frac{G}{G^\theta} \quad (2.9)$$

In gas channels the intensive molar flow density, g , is related to a standard molar flow density, g , resulting from the division of the standard molar flow by the respective cross sectional area.

$$\gamma_a = \frac{g_a L_2 h_a}{G^\theta} \quad (2.10)$$

$$\gamma_c = \frac{g_c L_1 h_c}{G^\theta} \quad (2.11)$$

The electric potential, ϕ , becomes dimensionless by multiplying it by the Faraday constant, \tilde{F} , and dividing it by the gas constant, R , and the standard temperature, T^θ .

$$\phi = \tilde{\phi} \cdot \frac{\tilde{F}}{RT^\theta} \quad (2.12)$$

The dimensionless total cell current, I_{cell} , is defined as the dimensional total cell current divided by the stoichiometrically possible current under standard conditions, I^θ .

$$I_{cell} = \frac{\tilde{I}_{cell}}{I^\theta} \quad (2.13)$$

The Damköhler number for the quasi-homogeneous gas phase reactions in the anode channel reads:

$$Da_{ref} = \frac{r_{ref}^\theta L_1 L_2 h^\theta}{G^\theta} \quad (2.14)$$

The Damköhler number for the electrochemical (surface) reactions is defined as:

$$Da_{ox,red} = \frac{r_{ox,red}^\theta L_1 L_2}{G^\theta} \quad (2.15)$$

In both cases a characteristic volume or surface related reaction rate under certain conditions (standard concentrations and temperature) is divided by a characteristic volume or surface related molar flow density.

The Arrhenius number describes the temperature dependence of a reaction rate. It is defined as:

$$Arr_j = \frac{E_{A,j}}{RT^\theta} \quad (2.16)$$

$E_{A,j}$ is activation energy of reaction j.

The Stanton number is a measure for the heat exchange capability at certain interfaces. Here a heat exchange coefficient for the complete exchange interface is related to the heat capacity of the standard convective flow:

$$St = \frac{k^h L_1 L_2}{G^\theta c_p^\theta} \quad (2.17)$$

The heat conductivity of the solid phase is described by the Peclet number. In analogy to the Stanton number it relates a characteristic measure for the conductive heat flux to the characteristic convective heat flux:

$$\frac{1}{Pe} = \frac{h_s \lambda_s}{G^\theta c_p^\theta} \quad (2.18)$$

Directly connected to the Peclet number is the ratio of the geometrical cell dimensions.

$$l_2 = \frac{L_2}{L_1} \quad l_3 = \frac{L_3}{L_1} \quad (2.19)$$

The equations and boundary conditions of the model are introduced in the following.

Material balances

Component and total material balances on the anode side:

$$\frac{V_a}{\vartheta_a} \frac{\partial \chi_{i,a}}{\partial \tau} = -\gamma_a \frac{\partial \chi_{i,a}}{\partial \zeta_1} + n_{i,as} - \chi_{i,a} \sum_l n_{l,as} + \sum_{j=ref} (v_{i,j} - \chi_{i,j} \bar{v}_j) Da_j r_j \quad (2.20)$$

$$0 = -\frac{\partial \gamma_a \vartheta_a}{\partial \zeta_1} + \frac{1}{c_{p,a}} \left(\sum_i n_{i,as}^+ \cdot \int_{\vartheta_a}^{\vartheta_s} c_{p,i}(\Psi) d\Psi + \sum_{j=ref} (-\Delta_R h_j^0(\vartheta_a)) Da_j r_j + q_{as} \right) + \vartheta_a \sum_i n_{i,as} + \vartheta_a \sum_{j=ref} \bar{v}_j Da_j r_j \quad (2.21)$$

$$n_{i,as} = \sum_{j=ox} \nu_{i,j} Da_j r_j \quad (2.22)$$

In the above equations, the subscript a stands for the anode, s means the solid and c is the cathode; the subscript i is a component index for the seven gas components CH₄, H₂O, H₂, CO, CO₂, O₂, N₂; V is volume; ζ_1 is spatial coordinate; $n_{i,as}$ is mass exchange flux density from solid to anode; $\nu_{i,j}$ is the stoichiometric coefficient of component i in reaction j ; $\bar{v}_j = \sum_i \nu_{i,j}$ is total mole change in reaction j ; r_j is the dimensionless reaction rate; $c_{p,i}$ and $c_{p,a}$ is molar heat capacity; $\Delta_R h_j^0$ is standard enthalpy of reaction j ; q is heat exchange flux density; the other variables are constant model parameters.

The first term of the Equation 2.20 on the right hand side describes the effect of convection of the gas through the anode channel along the ζ_1 coordinate. The second and third terms describe the effect of mass exchange between gas phase and electrode. The second term simply considers the direct effect of mass entering or leaving the gas phase. The third term can be interpreted to compensate mole fraction changes due to the dilution effects of overall mass transfer between the gas phase and the solid phase. The last term expresses an increase or a decrease in molar gas flow density along the channel for the gas phase reforming reactions. While the first part describes the source density for component i due to the reforming reactions the second one calculates the dilution/concentration effect of reactions with changes in total mole numbers.

As for the total mass balance Equation 2.21. The first term is the spatial derivative of a product of the molar flow density and the temperature. The next three terms

consider thermal expansion effects due to the temperature change connected to mass exchange with the electrode, heat of reforming reaction and convective heat transfer. The last two terms consider the increase of total molar flow due to mass exchange between gas and electrode as well as due to the reforming reactions.

In the following, a justification of Equations 2.20 and 2.21 will be given. In fact, the Equation 2.20 comes from a dimensional form of the partial mass balance Equation 2.23 and total mass balance 2.24:

$$\frac{\partial c_{i,a}}{\partial t} = -\frac{\partial}{\partial z_1} (g_a \cdot \chi_{i,a}) + \frac{n_{i,as}}{d_a} + \sum_{j=ref} v_{i,j} r_j \quad (2.23)$$

$$\frac{\partial c_{t,a}}{\partial t} = -\frac{\partial g_a}{\partial z_1} + \frac{n_{t,as}}{d_a} + \sum_{j=ref} \bar{v}_j r_j \quad (2.24)$$

As

$$\frac{\partial \chi_{i,a}}{\partial t} = \frac{\partial}{\partial t} \left(\frac{c_{i,a}}{c_{t,a}} \right) = \dots = \frac{1}{c_{t,a}} \cdot \frac{\partial c_{i,a}}{\partial t} - \frac{\chi_{i,a}}{c_{t,a}} \cdot \frac{\partial c_{t,a}}{\partial t} \quad (2.25)$$

Insert into the above Equations 2.23 and 2.24, which will lead to the Equation 2.20 in dimensional form. As for the Equation 2.21, only after the total mass balance 2.24 and enthalpy balance in temperature form 2.33 are inserted into:

$$\frac{\partial c_{t,a}}{\partial t} = \frac{p}{R} \frac{\partial T_a^{-1}}{\partial t} = -\frac{p}{RT_a^2} \cdot \frac{\partial T_a}{\partial t} = -\frac{c_{t,a}}{T_a} \cdot \frac{\partial T_a}{\partial t} \quad (2.26)$$

by some manipulation, the dimensional form of Equation 2.21 can be achieved. The detailed derivation can be found in (Heidebrecht 2005). In above equations, z_k is the spatial coordinate, and t is the time.

The boundary conditions for Equation 2.20 and 2.21 read:

$$\chi_{i,a}(\zeta_1 = 0, \zeta_2, \tau) = \chi_{i,a,in}(\tau) \quad (2.27)$$

$$\gamma_a(\zeta_1 = 0, \zeta_2, \tau) = \gamma_{a,in}(\tau) = \Gamma_{a,in}(\tau) \quad (2.28)$$

In a similar way, component and total material balances on the cathode side can be derived:

$$\frac{V_c}{\vartheta_c} \frac{\partial \chi_{i,c}}{\partial \tau} = -\gamma_c \frac{\partial \chi_{i,c}}{\partial \zeta_2} + n_{i,cs} - \chi_{i,c} \sum_l n_{l,cs} \quad (2.29)$$

$$0 = -\frac{\partial \gamma_c \vartheta_c}{\partial \zeta_2} + \frac{I}{c_{p,c}} \left(\sum_i n_{i,cs}^+ \cdot \int_{\vartheta_a}^{\vartheta_c} c_{p,i}(\Psi) d\Psi + q_{cs} \right) + \vartheta_c \sum_i n_{i,cs} \quad (2.30)$$

The boundary conditions for Equation 2.29 and 2.30 read:

$$\chi_{i,c}(\zeta_1, \zeta_2 = 0, \tau) = \chi_{i,c,in}(\tau) = \chi_{i,m}(\tau) \quad (2.31)$$

$$\gamma_c(\zeta_1, \zeta_2 = 0, \tau) = \gamma_{c,in}(\tau) = \Gamma_m(\tau) \quad (2.32)$$

The first term of the Equation 2.29 on the right hand side describes the effect of convection of the gas through the cathode channel along the ζ_2 coordinate. The second and third terms describe the effect of mass exchange between gas phase and electrode.

As for the total mass balance Equation 2.30. The first term is the spatial derivative of a product of the molar flow density and the temperature. The next two terms consider thermal expansion effects due to the temperature change connected to mass exchange with the electrode and convective heat transfer. The last terms consider the increase of total molar flow due to mass exchange between gas and electrode.

Energy balances

Anode side:

$$V_a \frac{c_{p,a}}{\vartheta_a} \frac{\partial \vartheta_a}{\partial \tau} = -\gamma_a c_{p,a} \frac{\partial \vartheta_a}{\partial \zeta_1} + \sum_i n_{i,as}^+ \cdot \int_{\vartheta_a}^{\vartheta_s} c_{p,i}(\Psi) d\Psi + \sum_{j=ref} (-\Delta_R h_j^0(\vartheta_a)) Da_j r_j + q_{as} \quad (2.33)$$

Equation 2.33 is the dynamic enthalpy balance in temperature form for the anode gas. Convective enthalpy transport is considered in the first term on the equation's right hand side. The second term is heat transfer due to the mass flow densities between gas phase and electrode pores. The heat of the reforming reactions is considered in the third term, while the last term describes the convective heat exchange between gas and solid phase.

The boundary conditions for Equation 2.33 read:

$$\vartheta_a(\zeta_1 = 0, \zeta_2, \tau) = \vartheta_a, in(\tau) \quad (2.34)$$

Cathode side:

$$V_c \frac{c_{p,c}}{\vartheta_c} \frac{\partial \vartheta_c}{\partial \tau} = -\gamma_c c_{p,c} \frac{\partial \vartheta_c}{\partial \zeta_2} + \sum_i n_{i,cs}^+ \cdot \int_{\vartheta_c}^{\vartheta_s} c_{p,i}(\Psi) d\Psi + q_{cs} \quad (2.35)$$

Equation 2.35 is similar to the Equation 2.33. Convective enthalpy transport is considered in the first term on the equation's right hand side. The second term is heat transfer due to the mass flow densities between gas phase and electrode pores, while the last term describes the convective heat exchange between gas and solid phase.

The boundary conditions for Equation 2.35 read:

$$\vartheta_c(\zeta_1, \zeta_2 = 0, \tau) = \vartheta_{c,in}(\tau) = \vartheta_m(\tau) \quad (2.36)$$

Solid side:

$$c_{p,s} \frac{\partial \vartheta_s}{\partial \tau} = \frac{l_2}{Pe_s} \frac{\partial^2 \vartheta_s}{\partial \zeta_1^2} + \frac{l}{Pe_s l_2} \frac{\partial^2 \vartheta_s}{\partial \zeta_2^2} + \sum_i (-n_{i,as}^-) \cdot \int_{\vartheta_s}^{\vartheta_a} c_{p,i}(\Psi) d\Psi + \sum_i (-n_{i,cs}^-) \cdot \int_{\vartheta_s}^{\vartheta_c} c_{p,i}(\Psi) d\Psi - q_{as} - q_{cs} + q_s \quad (2.37)$$

The first two terms on the right hand side of the enthalpy balance describe the heat conduction along both coordinates. The next two terms consider the temperature effect caused by components flowing into the porous electrodes and being heated up or cooled down to solid temperature. The fifth and sixth term stand for the convective heat exchange between both gas phases and the solid phase. The last term contains all heat induced into the solid by the electrochemical reactions.

The boundary conditions for Equation 2.37 read:

$$\left. \frac{\partial \vartheta_s}{\partial \zeta} \right|_{\partial \zeta} = 0 \quad (2.38)$$

$$\vartheta_s(\zeta_1, \zeta_2, \tau = 0) = \vartheta_{s,0}(\zeta_1, \zeta_2) \quad (2.39)$$

In the above equations, l_2 is Geometric aspect ratio, that equal to Cathode channel length divided by Anode channel length; Pe_s is Peclet number.

Reaction kinetics

In this model two different kinds of reactions occur: the chemical reactions of the methane reforming process in the anode channel and the electrochemical reactions inside the electrode pores. These are the methane steam reforming reaction (indexed "ref1"), the water-gas shift reaction (indexed "ref2"), the anode oxidation reactions of hydrogen (indexed "ox1") and carbon monoxide (indexed "ox2") and the reduction of oxygen (indexed "red") at the cathode.

The kinetic expressions are listed in the following:

$$r_{ref1} = \exp\left(Arr_{ref1} \cdot \left(\frac{1}{\vartheta_{ref1}^0} - \frac{1}{\vartheta_a} \right) \right) \cdot \left(\chi_{CH_4,a} \chi_{H_2O,a} - \frac{1}{K_{ref1}(\vartheta_a)} \chi_{CO,a} \chi_{H_2,a}^3 \right) \quad (2.40)$$

$$r_{ref2} = \exp\left(Arr_{ref2} \cdot \left(\frac{1}{\vartheta_{ref2}^0} - \frac{1}{\vartheta_a} \right) \right) \cdot \left(\chi_{CO,a} \chi_{H_2O,a} - \frac{1}{K_{ref2}(\vartheta_a)} \chi_{CO_2,a} \chi_{H_2,a} \right) \quad (2.41)$$

$$r_{ox1} = \exp\left(Arr_{ox1} \cdot \left(\frac{1}{\vartheta_{ox1}^0} - \frac{1}{\vartheta_s} \right) \right) \cdot \left\{ \begin{aligned} & \varphi_{H_2,ac} \cdot \exp\left(\alpha_{ox1,+} \cdot n_{ox1} \frac{(\Phi_a^S - \Phi_a^L) - \Delta\Phi_{ox1,0}(\vartheta_s)}{\vartheta_s} \right) \\ & - \varphi_{H_2O,ac} \varphi_{CO_2,ac} \cdot \exp\left(-(1 - \alpha_{ox1,+}) \cdot n_{ox1} \frac{(\Phi_a^S - \Phi_a^L) - \Delta\Phi_{ox1,0}(\vartheta_s)}{\vartheta_s} \right) \end{aligned} \right\} \quad (2.42)$$

$$r_{ox2} = \exp\left(Arr_{ox2} \cdot \left(\frac{1}{\vartheta_{ox2}^0} - \frac{1}{\vartheta_s} \right) \right) \cdot \left\{ \begin{aligned} & \varphi_{CO,ac} \cdot \exp\left(\alpha_{ox2,+} n_{ox2} \frac{(\Phi_a^S - \Phi_a^L) - \Delta\Phi_{ox2,0}(\vartheta_s)}{\vartheta_s} \right) \\ & - (\varphi_{CO_2,ac})^2 \cdot \exp\left(-(1 - \alpha_{ox2,+}) n_{ox2} \frac{(\Phi_a^S - \Phi_a^L) - \Delta\Phi_{ox2,0}(\vartheta_s)}{\vartheta_s} \right) \end{aligned} \right\} \quad (2.43)$$

$$r_{red} = \exp\left(Arr_{red} \cdot \left(\frac{1}{\vartheta_{red}^0} - \frac{1}{\vartheta_s} \right) \right) \cdot \left\{ \begin{aligned} & (\varphi_{CO_2,cc})^{a1} \cdot \exp\left(\alpha_{red,+} \frac{(\Phi_c^S - \Phi_c^L) - \Delta\Phi_{red,0}(\vartheta_s)}{\vartheta_s} \right) \\ & - (\varphi_{O_2,cc})^{a2} (\varphi_{CO_2,cc})^{a3} \cdot \exp\left(-\alpha_{red,-} \frac{(\Phi_c^S - \Phi_c^L) - \Delta\Phi_{red,0}(\vartheta_s)}{\vartheta_s} \right) \end{aligned} \right\} \quad (2.44)$$

In the above equations, Φ is Electric potential, φ_i is Partial pressure of component i.

Charge balances

The density of current production by the reactions is calculated from a dimensionless Faraday law:

$$i_a(\Phi_a^L) = \sum_{j=ox} n_j F D a_j r_j(\Phi_a^L) \quad (2.45)$$

$$i_c(\Phi_c^L, \Phi_c^S) = - \sum_{j=red} n_j F D a_j r_j(\Phi_c^L, \Phi_c^S) \quad (2.46)$$

The ionic current through the electrolyte is assumed to be linearly depending on the corresponding potential difference:

$$i_e(\Phi_a^L, \Phi_c^L) = k_e \cdot (\Phi_a^L - \Phi_c^L) \quad (2.47)$$

The total currents are calculated from:

$$I_a = \int_A i_a d\zeta \quad ; \quad I_e = \int_A i_e d\zeta \quad ; \quad I_c = \int_A i_c d\zeta \quad (2.48)$$

The spatially distributed potentials in the electrode near the anode and cathode double layer change depending on the current density from the electrode, i , and the current density produced by the electrochemical reaction, i_a and i_c , respectively:

$$\frac{\partial \Phi_a^L}{\partial t} = - \frac{I}{c_a} \cdot (i - i_a) \quad (2.49)$$

$$\frac{\partial \Phi_c^L}{\partial t} = - \frac{I}{c_a} \cdot (i - i_a) - \frac{I}{c_e} \cdot (i - i_e) \quad (2.50)$$

The cathode electrode potential depends on the differences of the overall currents produced by the electrochemical reactions respectively the overall current through the electrolyte from the given total cell current:

$$\frac{d\Phi_c^S}{dt} = \frac{I_a - I_{cell}}{c_a} + \frac{I_c - I_{cell}}{c_c} + \frac{I_e - I_{cell}}{c_e} \quad (2.51)$$

In the above equations, i_a is the electrical current densities of anode, and cathode; Φ_a^S , Φ_c^S are the electrical potentials of the anode and the cathode; Φ_a^L , Φ_c^L are the electrical potentials of the electrolyte membrane on anode side and on cathode side;

n_j is number of electrons transferred in oxidation reactions; F is the dimensionless Faraday constant; the factor, k_e , is the dimensionless ion conductivity of the electrolyte layer.

The resulting model is a system of hyperbolic and parabolic partial differential equations for the temperatures in the gas and solid phases, for the composition of the gases, and for the electrical potentials. It describes the concentration in the anode and cathode channels, temperatures in gas and solid phase as well as the potential field in the electrode/electrolyte compound. The whole model is derived in dimensionless form describing characteristic properties of the system. It consists of 17 hyperbolic and parabolic partial differential equations, 2 ordinary differential equations in space, 8 ordinary differential equations in time, and additional algebraic equations.

2.3.2 A simplified 2-D MCFC model based on Heidebrecht (2005)

Heidebrecht's model (2005) serves as a reference and as a basis for the model reduction, state estimator and controller design in this thesis. The model reduction will be done in two steps. In a first step, which is described in this section, some additional physical assumptions are made in order to simplify the model equations slightly. In the second step, mathematical projection techniques will be used to achieve a stronger reduction in the system order. This will be the topic of Chapter 4. The time constants of electric potential equations and the time constants in the gas phases are much smaller than the time constant of the energy balance of the solid. As the slow dynamics of the solid temperature dominates many process control problems, the electric potential fields as well as the anode and cathode gas channels can be considered as quasi-stationary. And for conveniences of numerical solution, some other parts (constant heat capacities, constant heat of reaction) also have been simplified. However, the use of a dynamic equation for the cathode gas temperature turns out to be advantageous for the numerical solution. The reason is that a change

of the cell current causes a jump of the cathode gas temperature if quasi-stationarity is assumed.

Material balances

Assuming quasi-stationarity in the anode gas channels, Equations 2.20, 2.21 and 2.22 can be combined to yield the following simplified component material balances:

$$-\frac{\partial(\gamma_a \chi_{i,a})}{\partial \zeta_1} + n_{i,as} + \sigma_{i,ref} = 0 \quad i = CH_4, H_2O, CO_2 \quad (2.52)$$

$$\chi_{H_2,a} = 1.0 - \chi_{CH_4,a} - \chi_{H_2O,a} - \chi_{CO,a} - \chi_{CO_2,a} \quad (2.53)$$

$$\chi_{CO,a} = -1.5\chi_{CH_4,a} + 0.5\chi_{H_2O,a} - 0.5\chi_{CO_2,a} + \gamma_{in,a} / \gamma_a \times (\chi_{CO,in,a} + 1.5\chi_{CH_4,a,in} - 0.5\chi_{H_2O,a,in} + 0.5\chi_{CO_2,a,in}) \quad (2.54)$$

$$\sigma_{i,ref} = \sum_{j=ref} v_{i,j} Da_j r_j \quad (2.55)$$

The Equation 2.54 comes from the following derivation:

$$0 = -\frac{\partial(\gamma_a \chi_{CH_4,a})}{\partial \zeta_1} - Da_{ref1} r_{ref1} \quad (2.56)$$

$$0 = -\frac{\partial(\gamma_a \chi_{H_2O,a})}{\partial \zeta_1} + Da_{ox1} r_{ox1} - Da_{ref1} r_{ref1} - Da_{ref2} r_{ref2} \quad (2.57)$$

$$0 = -\frac{\partial(\gamma_a \chi_{CO,a})}{\partial \zeta_1} - Da_{ox2} r_{ox2} + Da_{ref1} r_{ref1} - Da_{ref2} r_{ref2} \quad (2.58)$$

$$0 = -\frac{\partial(\gamma_a \chi_{CO_2,a})}{\partial \zeta_1} + Da_{ox1} r_{ox1} + 2Da_{ox2} r_{ox2} + Da_{ref2} r_{ref2} \quad (2.59)$$

$2 \times (2.58) + 3 \times (2.56) - (2.57) + (2.59)$ will lead to:

$$0 = -\frac{\partial}{\partial \zeta_1} \left(\gamma_a (2\chi_{CO,a} + 3\chi_{CH_4,a} - \chi_{H_2O,a} + \chi_{CO_2,a}) \right) \quad (2.60)$$

From Equation 2.60, the following equation can be get:

$$\begin{aligned} \gamma_a \left(2\chi_{CO,a} + 3\chi_{CH_4,a} - \chi_{H_2O,a} + \chi_{CO_2,a} \right) &= \mathbf{const.} \\ &= \gamma_{a,in} \left(2\chi_{CO,a,in} + 3\chi_{CH_4,a,in} - \chi_{H_2O,a,in} + \chi_{CO_2,a,in} \right) \end{aligned} \quad (2.61)$$

Summation of the above equations 2.52, 2.53 and 2.54 yields to total material balance of anode side:

$$-\frac{\partial \gamma_a}{\partial \zeta_1} + \sum n_{i,as} + \sigma_{t,ref} = \mathbf{0} \quad (2.62)$$

$$\sigma_{t,ref} = \sum_i \sigma_{i,ref} \quad (2.63)$$

For cathode side; one obtains:

$$-\frac{\partial (\gamma_c \chi_{i,c})}{\partial \zeta_2} + n_{i,cs} = \mathbf{0} \quad i = CO_2 \quad (2.64)$$

$$\chi_{H_2O,c} = \chi_{H_2O,c,in} \gamma_{c,in} / \gamma_c \quad (2.65)$$

$$\chi_{N_2,c} = \chi_{N_2,c,in} \gamma_{c,in} / \gamma_c \quad (2.66)$$

$$\chi_{O_2,c} = \mathbf{1.0} - \chi_{CO_2,c} - \chi_{H_2O,c} - \chi_{N_2,c} \quad (2.67)$$

Also summation of the equations 2.64, 2.65, 2.66 and 2.67 yields the total material balance of cathode side:

$$-\frac{\partial \gamma_c}{\partial \zeta_2} + \sum n_{i,cs} = \mathbf{0} \quad (2.68)$$

The boundary conditions remain unchanged.

Energy balances

For the energy balances, quasi-stationarity was applied to the anode side and constant heat capacity was assumed, which lead to:

$$0 = -\gamma_a c_{p,a} \frac{\partial \vartheta_a}{\partial \zeta_1} + \sum n_{i,as} \cdot c_{p,a} + h_{as} + \sigma_{\vartheta,ref} + q_{as} \quad (2.69)$$

h_{as} is enthalpy flux density from solid to anode, defined as:

$$h_{as} = c_{p,a} \left(n_{H_2O,as} + n_{CO_2,as} \right) \times (\vartheta_s - \vartheta_a) \quad (2.70)$$

$\sigma_{\vartheta,ref}$ is reaction heat due to the reforming reaction, defined as:

$$\sigma_{\vartheta,ref} = \sum_{j=ref} -\Delta_R h_j^0(\vartheta_a) Da_j r_j \quad (2.71)$$

All other equations remain unchanged.

Reaction kinetics

This part remains unchanged.

Charge balances

$$i_a = i_c = i_e = -\sum_{j=ox} n_j F Da_j r_j \quad (2.72)$$

$$I_{cell} = \int_A i_e d\zeta \quad (2.73)$$

$$U_{cell} = \Phi_c^S - \Phi_a^S = (\Phi_c^S - \Phi_c^L) + (\Phi_c^L - \Phi_a^L) + (\Phi_a^L - \Phi_a^S) \quad (2.74)$$

In the above equations, I_{cell} is the total cell current; U_{cell} is the total electric potential.

2.3.3 A nonlinear 3-D MCFC model with IIR internal reforming section

The two-dimensional dynamic model is useful for providing possible solutions for control strategy of fuel cells, especially during start-up, shut-down and the load changes. The two-dimensional models assume that all cells behave more or less in the same fashion. Because of that, the 2-D models neglect the influence of both ends of the fuel cell stack, that is the system boundary. So the 2-D model only can provide the average two-dimensional spatial temperature distribution of the fuel stack. In order to have a better understanding of how the actual fuel cell stack performs and how the temperature in the stack distributes, a three-dimensional model is necessary.

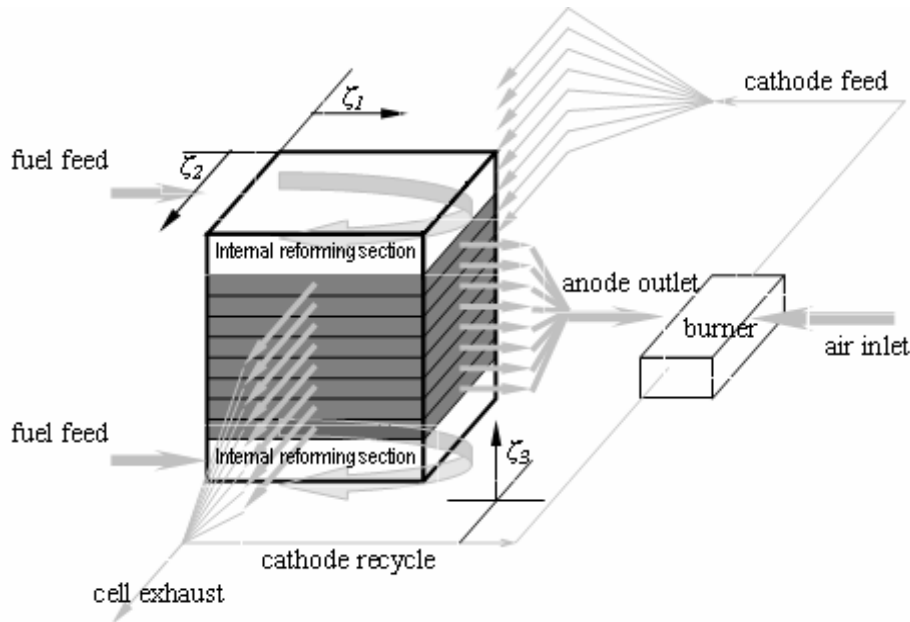


Figure 2 - 6: Scheme of the MCFC system, which consists of two indirect internal reformers, eight fuel cells, and a burner between anode side and cathode side.

The cell stack structure considered here is shown in Figure 2 - 6, which is an integrated MCFC system with a cell stack of eight cells; above and below those cells there are two reforming sections. The fresh fuel gas, consisting of steam and methane, first enters both indirect reforming sections, where most of the methane is converted to hydrogen, and then is distributed into the anode gas channels of eight cells. The flows on anode and on cathode side are orthogonal to each other, thereby inducing a cross flow. In this cell structure, both indirect internal reforming and direct internal reforming are considered.

Due to limited computational resources, it is necessary to simplify the 2-D model of 2.3.2 further. In order to enable the simulation of the total cell stack, the following additional model assumptions are made:

- Identical temperatures of anode gases, solid and cathode gases are assumed. The uniform temperature distribution is computed from a pseudo-homogeneous energy balance of all three phases.

- The oxidation reaction $CO + CO_3^{2-} \rightarrow 2CO_2 + 2e^-$ is neglected.

Indirect internal reforming section

In the indirect internal reforming section, the two reactions 2.1 and 2.2 were considered.

Reaction kinetics of indirect internal reforming section

The reaction kinetics 2.40 and 2.41 are used for these reactions.

Energy balance of the indirect internal reforming section

The energy balance is expressed as enthalpy balance in dimensionless temperature:

$$0 = -V_r \frac{c_{p,r}}{\vartheta_r} \frac{\partial \vartheta_r}{\partial \tau} - \gamma_r c_{p,r} \frac{\partial \vartheta_r}{\partial \zeta_1} + \sum_{j=ref} v_{i,j} Da_j r_j + St_{rFC} (\vartheta_{FC} - \vartheta_r) + St_{rb} (\vartheta_b - \vartheta_r) \quad (2.75)$$

The boundary conditions read:

$$\vartheta_r(\tau, \zeta_z, \zeta_2) = \vartheta_{r,in}(\tau, \zeta_2)$$

$$\left. \frac{\partial \vartheta_r}{\partial \zeta_1} \right|_{\tau, \zeta_z, \zeta_2} = 0 \quad (2.76)$$

In the above equations, the $c_{p,r}$ is the total thermal capacity of the system; St_{rFC} and St_{rb} are the Stanton numbers, that can be used as a dimensionless heat transfer coefficient between the indirect internal reforming section and the cells/boundary; the subscript FC means fuel cell and b suggests the boundary.

Material balances of the indirect internal reforming section

$$0 = -\frac{\partial(\gamma_r \chi_{i,r})}{\partial \zeta_1} + \sum_{j=ref} v_{i,j} Da_j r_j \quad i = CH_4, H_2O, CO_2, CO, H_2 \quad (2.77)$$

$$\mathbf{0} = -\frac{\partial \gamma_r}{\partial \zeta_1} + \sum_i \sum_{j=ref} v_{i,j} Da_j r_j \quad (2.78)$$

Reaction kinetics of the MCFC stack

For the anode reactions in the cell, we consider reaction 2.3. The reaction rates for the electrochemical reaction are the same as 2.42.

For the cathode reactions in the cell, we consider reaction 2.5. The reaction rate for this reaction in MCFC is usually running backwards with the same reaction rate expression.

The current density is connected to this reaction rate by a conversion factor F which is the same as 2.72.

Except the above reactions, for the anode side direct internal reforming reactions also have been considered here which can be switched off. The reaction kinetics are nearly the same as Equation 2.53 and 2.54, only the dimensionless temperature of indirect internal reforming section ϑ_r was replaced by the dimensionless pseudo homogeneous temperature of stack ϑ_{FC} .

Energy balance of the MCFC stack

The energy balance of the MCFC stack in the form of a parabolic partial differential equation of the temperature has the following structure, where a pseudo-homogeneous temperature is assumed:

$$\mathbf{0} = \left(-V_a \frac{c_{p,a}}{\vartheta_{FC}} - c_{p,s} - V_c \frac{c_{p,c}}{\vartheta_{FC}} \right) \frac{\partial \vartheta_{FC}}{\partial \tau} - \gamma_a c_{p,a} \frac{\partial \vartheta_{FC}}{\partial \zeta_1} - \gamma_c c_{p,c} \frac{\partial \vartheta_{FC}}{\partial \zeta_2} - \left(\frac{l_2}{Pe_s} \frac{\partial^2 \vartheta_{FC}}{\partial \zeta_1^2} + \frac{1}{l_2 Pe_s} \frac{\partial^2 \vartheta_{FC}}{\partial \zeta_2^2} \right) + \sigma_{\vartheta,ox} + \sigma_{\vartheta,red} + \sigma_{\vartheta,ref} + (\Phi_a^L - \Phi_c^L) i_e + \frac{l_2}{l_3^2 Pe_s} \frac{\partial^2 \vartheta_{FC}}{\partial \zeta_3^2} \quad (2.79)$$

The boundary conditions read:

$$\begin{aligned}
\vartheta_{FC}(\tau, \zeta_1, 0, \zeta_3) &= \vartheta_{a,in}(\tau, \zeta_1) & \vartheta_{FC}(\tau, 0, \zeta_2, \zeta_3) &= \vartheta_{c,in}(\tau, \zeta_2) \\
\left. \frac{\partial \vartheta_{FC}}{\partial \zeta_1} \right|_{\tau, \zeta_1, L_z} &= 0 & \left. \frac{\partial \vartheta_{FC}}{\partial \zeta_2} \right|_{\tau, L_y, \zeta_2} &= 0 \\
\left. \frac{\partial \vartheta_{FC}}{\partial \zeta_3} \right|_{\tau, \zeta_1, \zeta_2, L_N} &= St_{rFC} (\vartheta_r - \vartheta_{FC}(\tau, \zeta_1, \zeta_2, L_N)) \\
\left. \frac{\partial \vartheta_{FC}}{\partial \zeta_3} \right|_{\tau, \zeta_1, \zeta_2, L_I} &= St_{rFC} (\vartheta_{FC}(\tau, \zeta_1, \zeta_2, L_I) - \vartheta_r)
\end{aligned} \tag{2.80}$$

In the above equations, $\sigma_{\vartheta,ox}$ is reaction heat term due to oxidation reactions; $\sigma_{\vartheta,red}$ is reaction heat term due to reduction reactions; $\sigma_{\vartheta,ref}$ is the heat source due to DIR; $\sigma_{\vartheta,ref}$ will vanish, if no DIR takes place; l_3 is Geometric aspect ratio, that equals to fuel cell thickness divided by Anode channel length;

Material balances and charge balances of the MCFC stack are identical with the simplified model which was described in section 2.3.2.

Chapter 3

Model comparison and validation

3.1 Introduction

In Chapter 2, a 2-D MCFC model developed by Heidebrecht (2005) was first reviewed. A pseudo-homogeneous temperature 3-D stack model with/without DIR and a quasi-stationary simplified 2-D model were then built based on the detailed model. In this Chapter, the simplified 2-D model will be validated at the beginning, and then the simulation results of the 3-D stack model without DIR will be shown.

All these models are implemented in the process modeling tool ProMoT (Tränkle, et al. 2000). A finite volume method is used for the spatial discretization of the partial differential equations. The resulting differential algebraic system is solved by the simulation tool DIVA (Köhler et al. 2001).

3.2 Validation of the simplified model

As a validation experiment for the simplified model introduced in 2.3.2, the cell current is varied randomly between 0.7 with 0.8. Figure 3 - 1 shows the comparison between the simplified model and the detailed model. All diagrams in Figure 3 - 1 use a dimensionless time coordinate, one dimensionless time unit corresponding to about 12.15 s of real time.

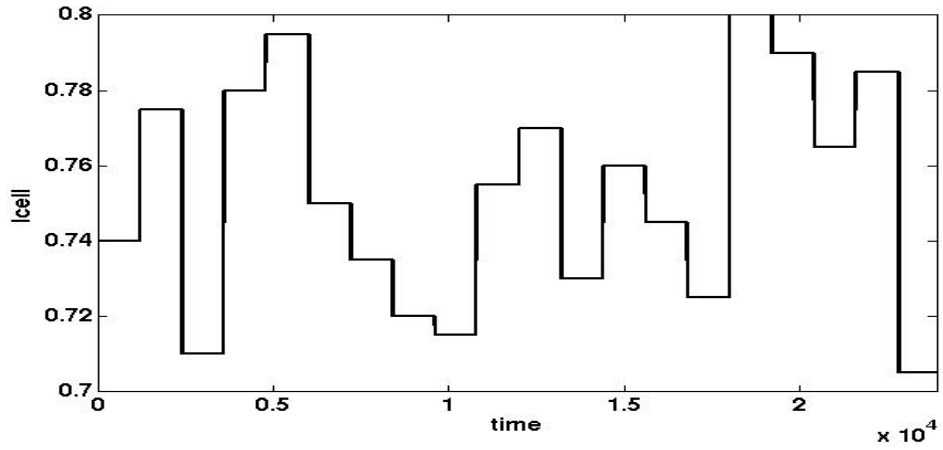


Figure 3 - 1(a): Random input signal (the dimensionless cell current)

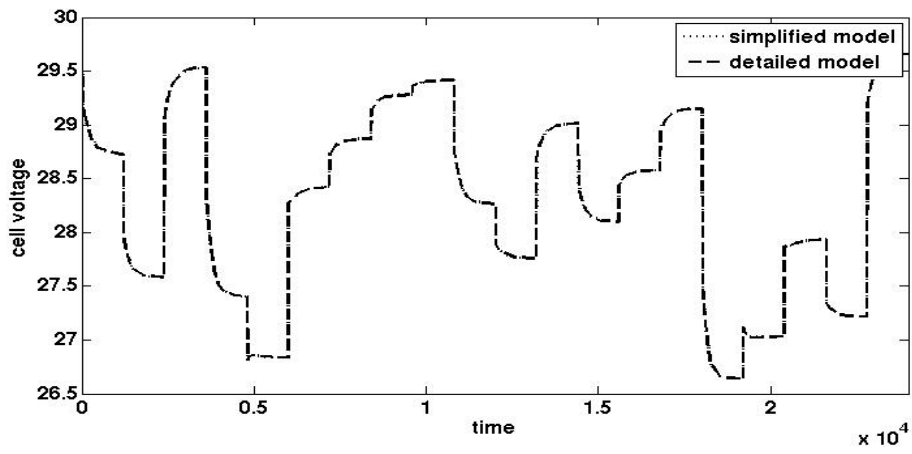


Figure 3 - 1(b): Cell voltage of the simplified model and the detailed model

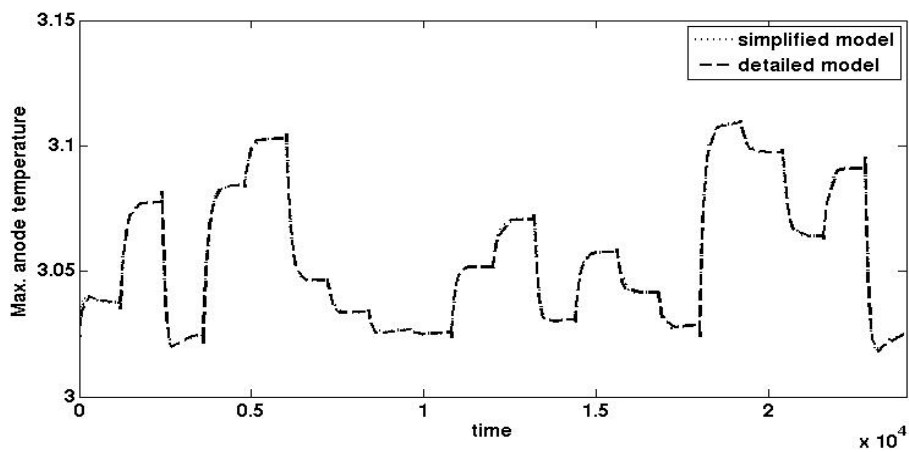


Figure 3 - 1(c): Maximum anode temperature of the simplified model and the detailed model

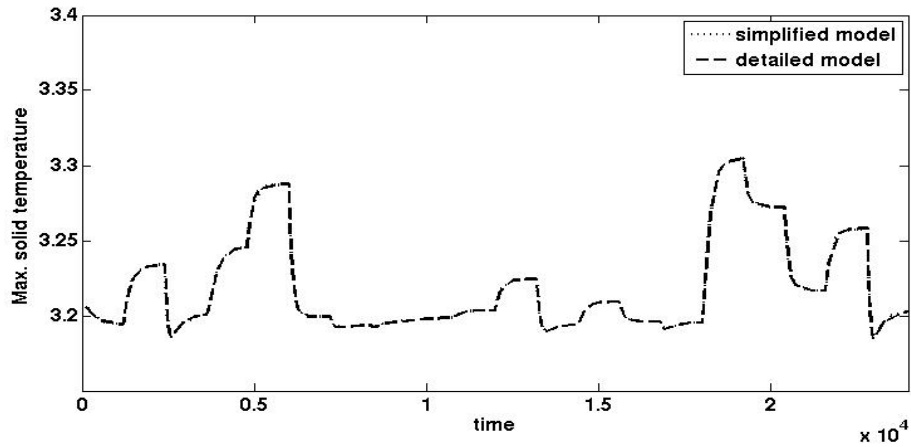


Figure 3 - 1(d): Maximum solid temperature of the simplified model and the detailed model

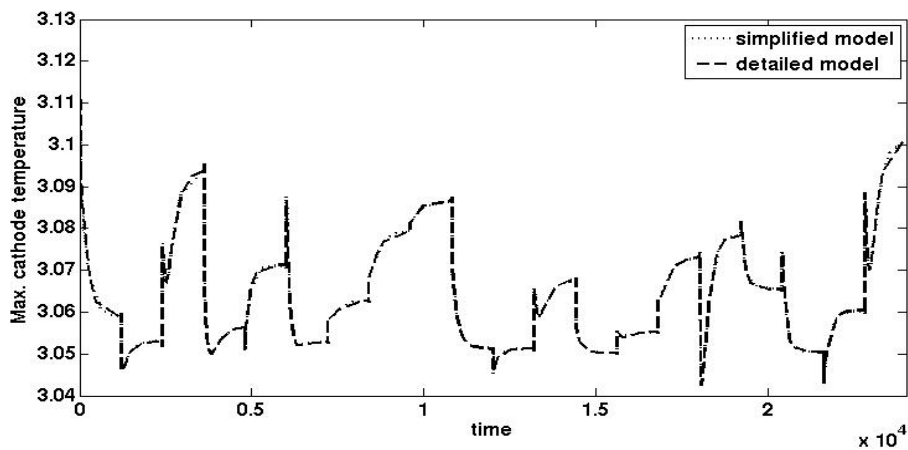


Figure 3 - 1(e): Maximum cathode temperature of the simplified model and the detailed model

From these tests it can be seen that the simplified model describes the behaviour of the MCFC system with good accuracy and can be used as a basis for model reduction.

3.3 Simulation results of the 3-D stack model without DIR

Using the model derived in 2.3.3, it is possible to simulate the steady state as well as the dynamic behaviour of the cell over a wide range of electrical load changes.

One of the 3-D simulated results of most interest is the spatial temperature distribution, which is shown in Figure 3 - 2. Because the cell stack structure is symmetrical, only the results of the first reforming section and the cells 1 - 4 are shown. In the reforming section, the temperature decreases very fast in ζ_1 -direction (Figure 3 - 2 (a)) due to the strong cooling effect of the reforming reaction, the heat exchange between the reforming section and fuel cells causes temperature gradients also in ζ_2 -direction. As no internal reforming takes place in cells, the exothermic electrochemical reaction causes a temperature increase in the cell, and the cell is only cooled by the incoming gas flows and heat transfer between cells and the reforming section. Therefore, the mean temperature increases from cell 1 - 4 (Figure 3 - 2 (b)-(e)).

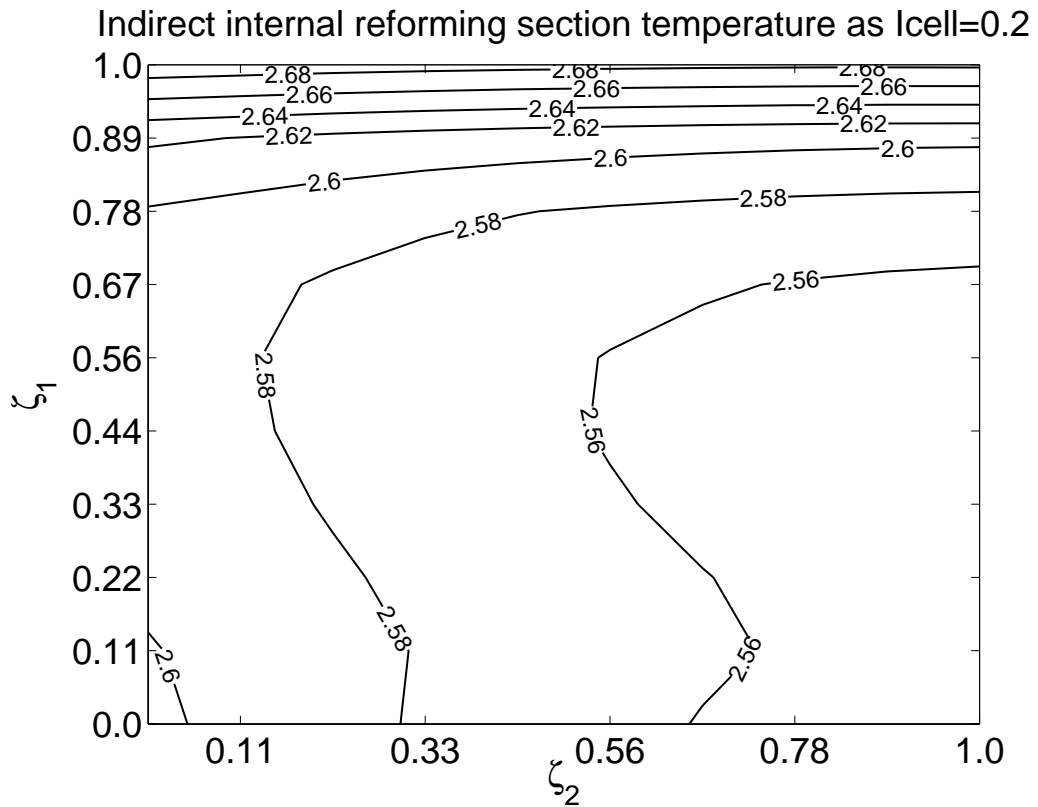


Figure 3 - 2 (a): Temperature distribution in the first reforming section

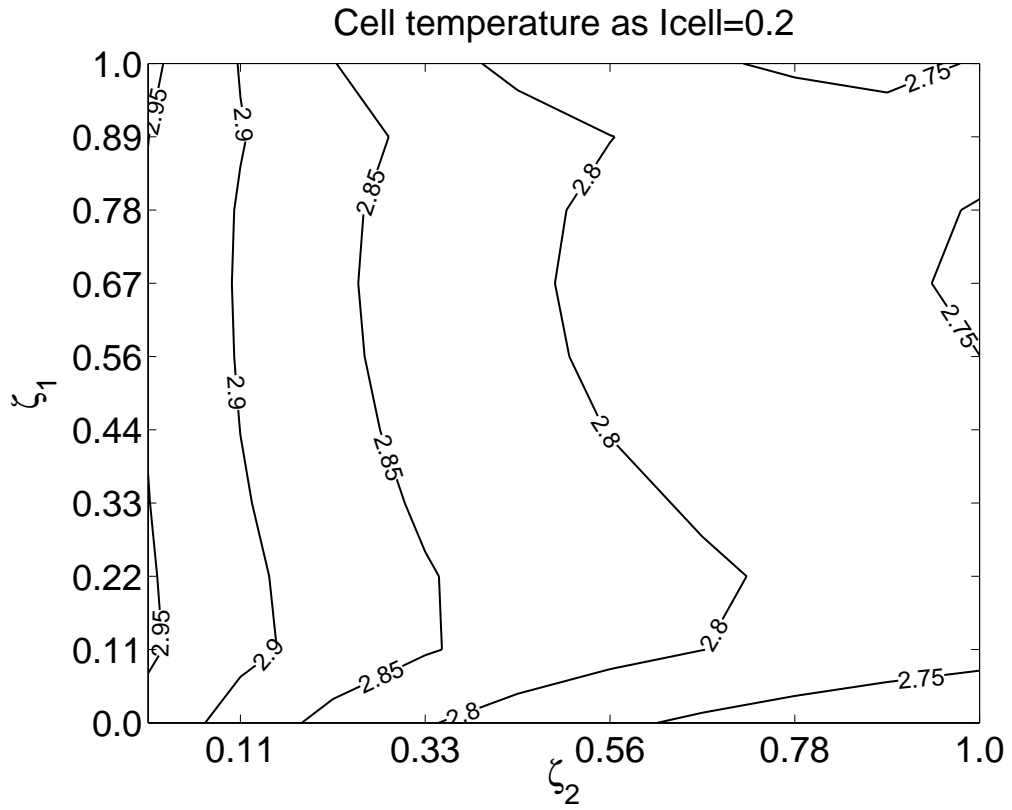


Figure 3 - 2 (b): Temperature distribution in cell 1

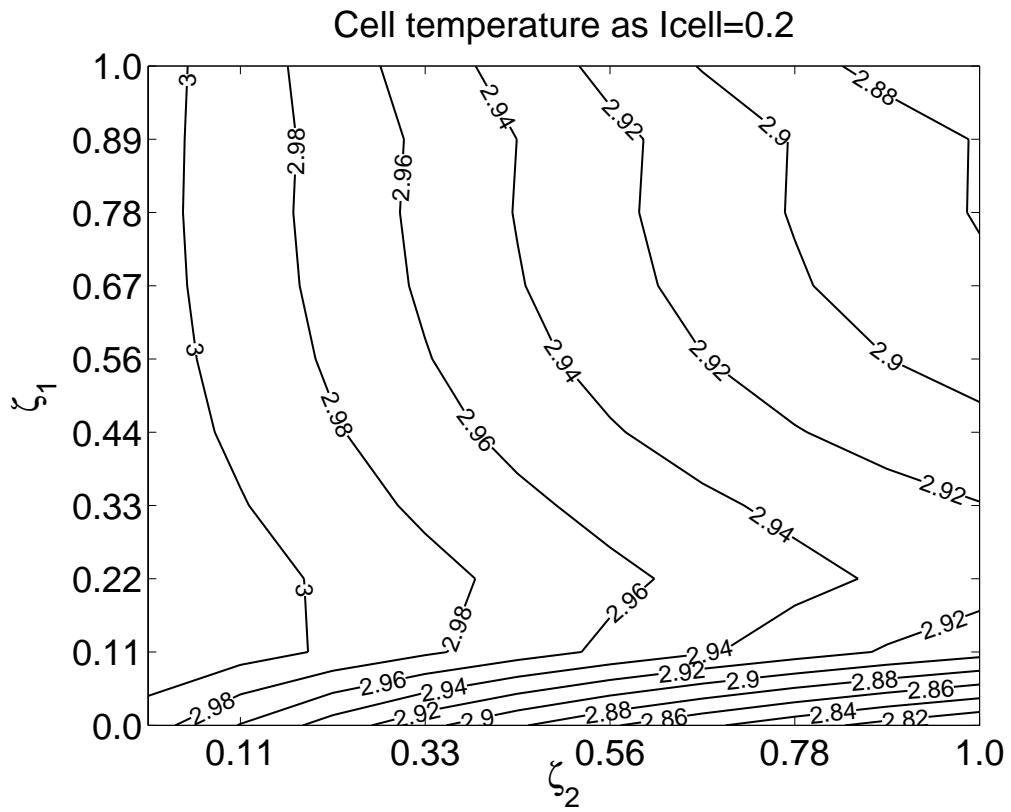


Figure 3 - 2 (c): Temperature distribution in cell 2

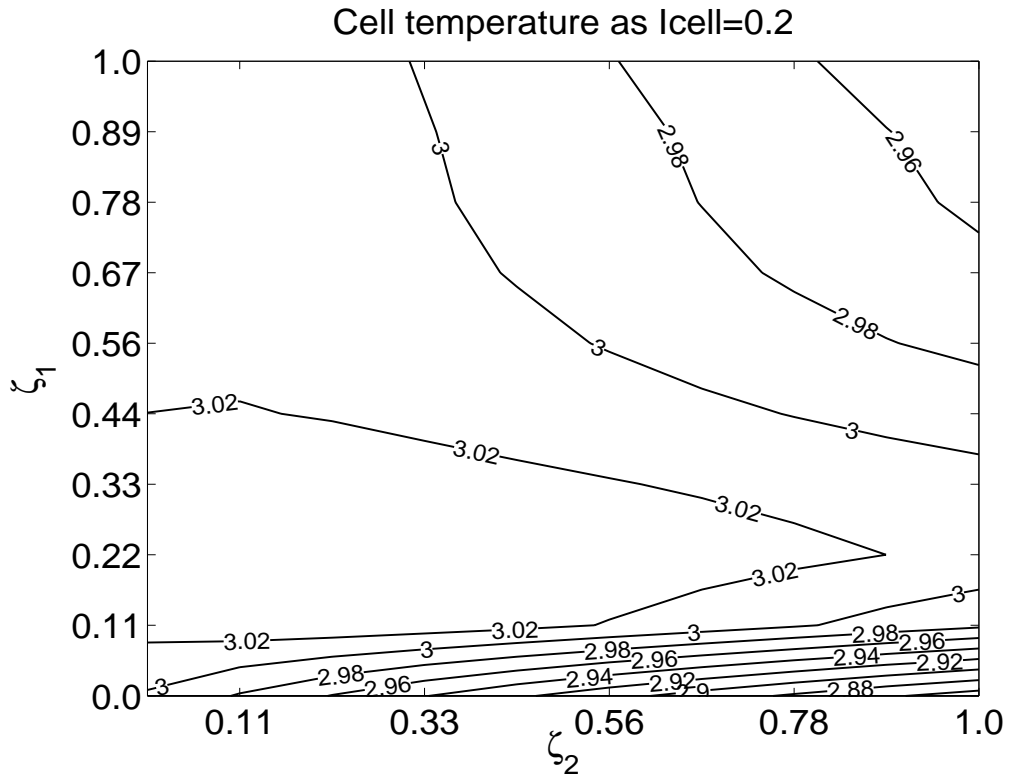


Figure 3 - 2 (d): Temperature distribution in cell 3

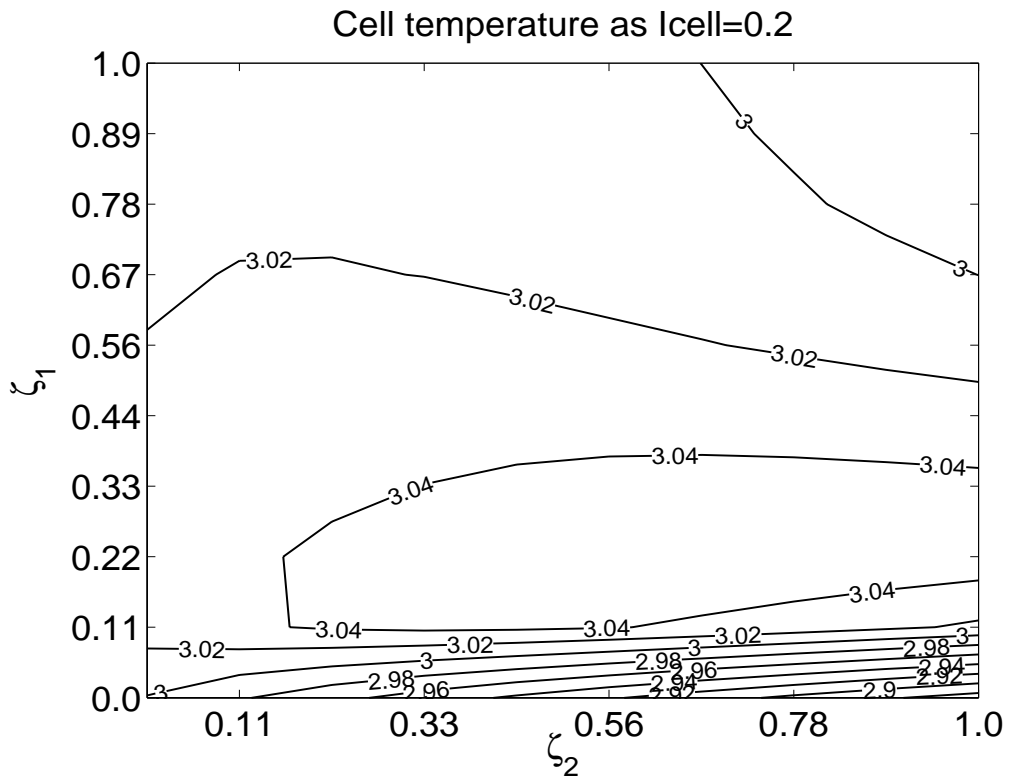


Figure 3 - 2 (e): Temperature distribution in cell 4

Most parts of this model are developed based on the 2-D model (Heidebrecht & Sundmacher 2003), so the benefits of that 2-D model are carried on, for instance, the dimensionless notation. This work can be applied for system analysis with respect to multiple steady states, sensitivity and stability. As can be seen in this model, the indirect internal reforming section greatly influences the behaviour of the cell stack. This model makes it possible to directly compare the effectiveness of different operating parameters for the MCFC with indirect internal reforming, and make better operating strategies. But the drawback of the 3-D model is also obvious: the 3-D model takes much more CPU time, and the 3-D model is much harder to solve. From the above results, one can find when the IIR was introduced, that the 2-D model cannot always replace the 3-D stack model. The cooling effect of the reforming section strong influences the temperature distribution of nearby fuel cells. Nevertheless, experimental validations of the 2-D model show that the 2-D model describes the process behaviour of the HotModule with sufficient accuracy for process control purposes (Gundermann, 2006). Therefore, in the remainder of this work, the 2-D model is used as a basis for process control design.

Chapter 4

Nonlinear Model Reduction of a Two-Dimensional MCFC Model with Internal Reforming

4.1 Introduction

Fuel cells utilizing internal reforming of natural gas can eliminate the need for a large external reformer to produce hydrogen fuel and can simplify the plant configuration. A rigorous spatially distributed model of the HotModule system was developed by Heidebrecht (2005) and has been reviewed in Chapter 2. But for process control purposes, simple dynamic models are required. A simplified form of this detailed model was developed in chapter 2 and validated in chapter 3. A reduced set of model equations is derived by applying the Karhunen-Loève Galerkin procedure to the simplified model. The reduced model is of considerably lower order than the original one and requires much less computation time. Finally, the reduced model is validated in test simulations by comparison with the detailed model.

4.2 Derivation of the Reduced MCFC Model

4.2.1 Galerkin procedure

For the model reduction of parabolic partial differential equations (PDEs) like (2.37), orthogonal projection methods have become a frequently used technique (Hoo & Zheng, 2001; Baker & Christofides, 2000; Atwell & King, 2001).

The basic idea is to represent the unknown variable, e.g. the solid temperature ϑ_s , by an infinite sum of products.

$$\vartheta_s(\zeta_1, \zeta_2, \tau) = \sum_{i=1}^{\infty} \vartheta_{i,s}(\tau) \phi_i^\vartheta(\zeta_1, \zeta_2) \quad (4.1)$$

In Equation (4.1), $\phi_i^\vartheta(\zeta_1, \zeta_2)$ are orthonormal basis functions with the following property:

$$\int_{\zeta_1=0}^{L_{\zeta_1}} \int_{\zeta_2=0}^{L_{\zeta_2}} \phi_i^\vartheta(\zeta_1, \zeta_2) \phi_j^\vartheta(\zeta_1, \zeta_2) d\zeta_1 d\zeta_2 = \begin{cases} 0 & \text{for } i \neq j \\ 1 & \text{for } i = j \end{cases} \quad (4.2)$$

The model reduction is achieved by approximating the infinite sum by a series with a finite number of elements and neglecting the higher order terms:

$$\hat{\vartheta}_s(\zeta_1, \zeta_2, \tau) = \sum_{i=1}^{N^\vartheta} \vartheta_{i,s}(\tau) \phi_i^\vartheta(\zeta_1, \zeta_2) \quad (4.3)$$

In general, the approach (4.3) will not solve the equation (2.37) exactly, but a nonzero residual Re_s will remain. The Galerkin method of weighted residuals requires that the residual Re_s must vanish, if weighted by a basis function, i.e

$$\int_{\zeta_1=0}^{L_{\zeta_1}} \int_{\zeta_2=0}^{L_{\zeta_2}} \text{Re}_s \phi_i^\vartheta d\zeta_1 d\zeta_2 = 0 \quad i = 1, \dots, N^\vartheta \quad (4.4)$$

This approach leads to N^ϑ conditions for the time dependent functions $\tilde{\vartheta}_i(\tau)$.

Consequently, the partial differential equation (2.37) is replaced by N^ϑ ordinary differential equations in the reduced model.

For the model reduction of the MCFC model, not only the profile of the temperature, but also those of the molar fractions in the anode and in the cathode gas channels, as well as the profiles of the total molar flow rates have to be approximated by basis functions. Using the notation

$$\hat{\chi}_{j,a}(\zeta_1, \zeta_2, \tau) := \sum_{i=1}^{N^{zj}} \chi_{j,a,i}(\tau) \phi_i^{\chi_{j,a}}(\zeta_1, \zeta_2) \quad j = \text{CH}_4, \text{H}_2\text{O}, \text{CO}_2 \quad (4.5)$$

$$\hat{\chi}_{j,c}(\zeta_1, \zeta_2, \tau) := \sum_{i=1}^{N^{zj,c}} \chi_{j,c,i}(\tau) \phi_i^{\chi_{j,c}}(\zeta_1, \zeta_2) \quad j = \text{CO}_2 \quad (4.6)$$

$$\hat{\gamma}_a := \sum_{i=1}^{N^{\gamma_a}} \gamma_{a,i}(\tau) \phi_i^{\gamma_a}(\zeta_1, \zeta_2) \quad (4.7)$$

$$\hat{\gamma}_c := \sum_{i=1}^{N^{\gamma_c}} \gamma_{c,i}(\tau) \phi_i^{\gamma_c}(\zeta_1, \zeta_2) \quad (4.8)$$

$$\Delta \hat{\Phi}_a := \sum_{i=1}^{N^{\Delta \Phi_a}} \Delta \Phi_a(\tau) \phi_i^{\Delta \Phi_a}(\zeta_1, \zeta_2) \quad (4.9)$$

one obtains the following set of reduced model equations by applying the weighted residual condition to the energy, material balances and charge balances:

$$0 = \iint \left\{ \gamma_a c_{p,a} \frac{\partial \vartheta_a}{\partial \zeta_1} + \sum n_{i,as} \cdot c_{p,a} - \sigma_{i,ref} + q_{as} \right\} \phi_j^{\vartheta_a} d\zeta_1 d\zeta_2 \quad (4.10)$$

$$V_c c_{p,c} \frac{\partial \vartheta_{i,c}}{\partial \tau} = \iint \left\{ \gamma_c c_{p,c} \frac{\partial \vartheta_c}{\partial \zeta_2} + \sum n_{i,cs} \cdot c_{p,c} + q_{cs} \right\} \vartheta_c \phi_j^{\vartheta_c} d\zeta_1 d\zeta_2 \quad (4.11)$$

$$c_{p,s} \frac{\partial \vartheta_{i,s}}{\partial \tau} = \iint \left\{ \frac{l_2}{Pe_s} \frac{\partial^2 \vartheta_s}{\partial \zeta_2^2} + \frac{1}{Pe_s l_2} \frac{\partial^2 \vartheta_s}{\partial \zeta_1^2} \right. \\ \left. + \sum -n_{i,as} \cdot c_{p,a} + \sum -n_{i,cs} \cdot c_{p,c} - q_{as} - q_{cs} + q_s \right\} \phi_j^{\vartheta_s} d\zeta_1 d\zeta_2 \quad (4.12)$$

$$0 = \iint \left\{ -\frac{\partial(\gamma_a \chi_{i,a})}{\partial \zeta_1} + n_{i,as} + v_{i,ref1} r_{ref1} + v_{i,ref2} r_{ref2} \right\} \phi_j^{\chi_{i,a}} d\zeta_1 d\zeta_2 \\ i = CH_4, H_2O, CO_2 \quad (4.13)$$

$$0 = \iint \left\{ -\frac{\partial(\gamma_c \chi_{i,c})}{\partial \zeta_2} + n_{i,cs} \right\} \phi_j^{\chi_{i,c}} \quad i = CO_2 \quad (4.14)$$

$$0 = \iint \left\{ -\frac{\partial \gamma_a}{\partial \zeta_1} + \sum n_{i,as} + r_{ref} \right\} \phi_j^{\gamma_a} d\zeta_1 d\zeta_2 \quad (4.15)$$

$$0 = \iint \left\{ -\frac{\partial \gamma_c}{\partial \zeta_2} + \sum n_{i,cs} \right\} \phi_j^{\gamma_c} d\zeta_1 d\zeta_2 \quad (4.16)$$

$$0 = \iint U_{cell} \phi_j^{\Phi_a} d\zeta_1 d\zeta_2 - \iint (\Phi_c^S - \Phi_c^L) \phi_j^{\Phi_a} d\zeta_1 d\zeta_2 \\ - \iint (\Phi_c^L - \Phi_a^L) \phi_j^{\Phi_a} d\zeta_1 d\zeta_2 - \iint (\Phi_a^L - \Phi_a^S) \phi_j^{\Phi_a} d\zeta_1 d\zeta_2 \quad (4.17)$$

$$0 = \iint i_e \phi_j^{\phi_c} d\zeta_1 d\zeta_2 + \sum_{j=0x} n_j F D a_j r_j \phi_j^{\phi_c} d\zeta_1 d\zeta_2 \quad (4.18)$$

The charge balances and (2.59) complete the reduced model. In summary, the reduced model is a differential algebraic system of differential index one for the unknowns $\hat{\vartheta}_i, \hat{\chi}_{i,a}, \hat{\chi}_{i,c}, \hat{\gamma}_a, \hat{\gamma}_c, \Delta \hat{\Phi}_a, \Delta \hat{\Phi}_s, \Delta \hat{\Phi}_c$. The quality of the reduced model, i.e. its deviation from the original model, mainly depends on two factors. The first one is the number of terms considered in the approximations (4.3), (4.5) - (4.9). The second is the choice of the basis functions. A good approximation of the complete model by a low order reduced model is achievable, if suitable problem-specific basis functions are chosen. One possibility would be to linearize the original spatially distributed system and to use the eigenfunctions of the linearized problem as basis functions (Hoo & Zheng, 2001). In this contribution, another approach, the Karhunen-Loève decomposition method is applied, because by that method it is also possible to incorporate the nonlinear behavior of the system in the basis functions.

4.2.2 The Karhunen-Loève decomposition

The Karhunen-Loève decomposition (K-L decomposition) was originally developed for the description of stochastic data (Loève, 1955), also known as principal component analysis (PCA). By applying the K-L decomposition to a given stochastic field, eigenfunctions are obtained that can reproduce the data with a certain accuracy and with a minimum number of degrees of freedom.

For the solution of partial differential equations, the K-L decomposition method can be used to generate basis functions for the Galerkin procedure (Park & Cho, 1996).

The key issue in this approach is to determine suitable basis functions from simulation results with the original model, taken at discrete time points $t_i, i=1, \dots, N$. The simulation results are called snapshots and are denoted as $\mathbf{v}_i(\zeta_1, \zeta_2)$. By the K-L decomposition, it is possible to extract the most typical or characteristic

structure from these snapshots in the form of empirical eigenfunctions $\phi_i(\zeta_1, \zeta_2)$.

As it is shown in (Park & Cho, 1996), the basis functions $\phi_i(\zeta_1, \zeta_2)$ can be written as:

$$\phi_i(\zeta_1, \zeta_2) = \sum_{i=1}^N \alpha_i^T \cdot \mathbf{v}_i(\zeta_1, \zeta_2) \quad (4.19)$$

In (4.19), α_i is the eigenvector of an $N \times N$ matrix C whose elements are given by:

$$C_{i,j}^M = \frac{1}{N} \int_{\zeta_1=0}^{L_{\zeta_1}} \int_{\zeta_2=0}^{L_{\zeta_2}} \mathbf{v}_i(\zeta_1, \zeta_2) \cdot \mathbf{v}_j(\zeta_1, \zeta_2) d\zeta_1 d\zeta_2 \quad (4.20)$$

$$C^M \alpha_i = \lambda_i \alpha_i \quad (4.21)$$

For the eigenvalue λ_i , the following correlation holds (Christofides & Daoutidis, 1996):

$$\langle \mathbf{v}_n \rangle := \frac{1}{N} \sum_{n=1}^N \mathbf{v}_n(\zeta_1, \zeta_2) \quad (4.22)$$

$$(\phi_i, \mathbf{v}_n) := \int_{\zeta_1=0}^{L_{\zeta_1}} \int_{\zeta_2=0}^{L_{\zeta_2}} \phi_i(\zeta_1, \zeta_2) \cdot \mathbf{v}_n(\zeta_1, \zeta_2) d\zeta_1 d\zeta_2 \quad (4.23)$$

$$\lambda_i = \langle (\phi_i, \mathbf{v}_n)^2 \rangle \quad (4.24)$$

Therefore, λ_i may be interpreted as a measure of how well an eigenfunction ϕ_i is able to approximate the time average of the snapshots. In this sense, the eigenfunction ϕ_l corresponding to the largest eigenvalue λ_l is the most typical structure of the snapshots.

The derivation of how the basis functions can be obtained from the K-L decomposition method is as follows:

Consider N snapshots $\mathbf{v}_j \in \mathfrak{R}^k$ (k is the order of the vector space), $j = 1, \dots, N$, for which a basis ϕ is to be determined in such way that an approximation $\hat{\mathbf{v}}_j$ of \mathbf{v}_j can be obtained by a linear combination of m orthogonal basis vectors:

$$\hat{v}_j = \sum_{i=1}^m \lambda_{i,j} \phi_i \quad j = 1, \dots, N \quad (4.25)$$

By the orthogonality of ϕ_i ($i=1, \dots, N$) and by the imposition of an additional constraint that ϕ_i has the unit norm, it follows:

$$\begin{aligned} \phi_i^T \phi_i &= 1 \\ \phi_i^T \phi_j &= 0 \quad i \neq j \end{aligned} \quad (4.26)$$

Where $\lambda_{i,j}$ is the weighting coefficient of basis vector ϕ_i formed by taking the inner product of v_j with ϕ_i :

$$\lambda_{i,j} = v_j^T \phi_i \quad (4.27)$$

Now, the problem is to obtain the basis functions ϕ_i such that the residual error in approximating v_j with \hat{v}_j is minimized:

$$\varepsilon_j = v_j - \hat{v}_j = \sum_{i=m+1}^k \lambda_{i,j} \phi_i \quad j = 1, \dots, N \quad (4.28)$$

A suitable criterion is the minimization of the average mean-square residual error:

$$\xi = \frac{1}{N} \sum_{j=1}^N |v_j - \hat{v}_j|^2 = \frac{1}{N} \sum_{j=1}^N \varepsilon_j^T \varepsilon_j \quad (4.29)$$

Since the basis functions ϕ_i are orthonormal it follows that:

$$\xi = \frac{1}{N} \sum_{j=1}^N \left(\sum_{i=m+1}^k \lambda_{i,j} \phi_i^T \right) \left(\sum_{i=m+1}^k \lambda_{i,j} \phi_i \right) = \frac{1}{N} \sum_{j=1}^N \sum_{i=m+1}^k \lambda_{i,j}^2 \quad (4.30)$$

From Equation 4.27, one can see that:

$$\lambda_{i,j}^2 = (v_j^T \phi_i)^2 = (\phi_i^T v_j)(v_j^T \phi_i) = \phi_i^T v_j v_j^T \phi_i \quad (4.31)$$

Defining $C_j = v_j v_j^T$, we arrive at the final form for the quantity ξ to be minimized:

$$\xi = \frac{1}{N} \sum_{j=1}^N \sum_{i=m+1}^k \phi_i^T C_j \phi_i = \sum_{i=m+1}^k \phi_i^T \left(\frac{1}{N} \sum_{j=1}^N C_j \right) \phi_i = \sum_{i=m+1}^k \phi_i^T C \phi_i \quad (4.32)$$

We can express the minimization as a multi-variate differential equation by using a

set of Lagrangian multipliers μ_j , the equation will be written in:

$$F(\phi_i) = \sum_{i=m+1}^k \phi_i^T C \phi_i + \mu_i (1 - \phi_i^T \phi_i) \quad (4.33)$$

After that, the derivative of the expectation of the mean-square error with respect to the basis components ϕ_j is set to zero.

$$\frac{\partial}{\partial \phi_i} F(\phi_i) = 2(C\phi_i - \mu_i \phi_i) = 0 \quad \text{Where } i = m+1, \dots, k \quad (4.34)$$

It is well known that the solutions to this equation constitute the eigenvectors of the correlation matrix C . Thus, the problem is equivalent to finding the eigenvectors of the correlation matrix C . Since the columns of Φ are now determined to be the eigenvectors, we can re-express the residual error as the sum of the eigenvalues of the unused portion of the basis:

$$\xi = \sum_{i=m+1}^k \mu_i \quad (4.35)$$

And the solution to the minimization reduces to ordering the basis vector ϕ_i such that the columns with the smallest eigenvalues occur in the unused portion of the basis.

In order to determine suitable basis functions for the MCFC model, the response of the complete model to an increase of the cell current from 0.7 to 0.8 and subsequent decrease to 0.7 is computed numerically by using the method of lines. The basis functions for the reduced model are computed from the transient solution of the complete model. For the temperature profile, 8 basis functions are chosen. For the other variables of the reduced model, anode side: χ_{CH_4} , 7; χ_{CO_2} , 10; χ_{H_2O} , 6; γ_a , 10; $n_{CO_2,as}$, 8; $n_{CO,as}$, 6; $n_{H_2,as}$, 6; cathode side: CO_2 , 2; γ_c , 9; $n_{CO_2,cs}$, 8; $n_{O_2,cs}$, 6; for other components: $\Delta\Phi_a$, 10 and $\Delta\Phi_c$, 9 basis functions are found to be sufficient.

4.2.3 Choice of snapshots

An important factor that affects the accuracy of the reduced model, i.e. its deviation from the simplified model is the choice of the basis functions. The K-L decomposition method uses numerical simulation results at discrete time points, so-called snapshots, obtained from dynamic simulations with the simplified model. In the case of MCFC system, the snapshots $v_j \in R^n$, $j = 1, 2, 3, \dots, J$ give the value of the state vector at discrete time points. Since the system is rather complex, the simulation process may generate tens of thousands of snapshots. The number of snapshots may cause numerical trouble in order to solve the constructed covariance matrix C from these snapshots. Therefore, some representatives should be chosen from these snapshots in order to get a complete picture of the possible solution profiles of the simplified model. Prud'Homme *et al.* (2002) developed guidelines for certain linear problems, but to our knowledge, there are no strict rules on how to choose snapshots for a nonlinear problem as considered here. A practical approach is to perform a high number of test simulations under different operation conditions and obtain a huge number of snapshots. From all these snapshots only several hundreds are chosen from the following procedure as representatives.

In the MCFC system considered, each spatially discretized state variable describes a curve in the $n \times n$ dimensional space. During one simulation process, the system generate tens of thousands points (snapshots) to describe the curve. The aim is to choose a few hundred from all these tens of thousands snapshots to depict the curve as well as possible. To achieve this, the following heuristic procedure is used in this work. A reference distance is first chosen. From a selected starting point (snapshot), record the distance between this point and the next. If the distance is less than the reference distance, the next point is neglected; otherwise select this point and continue searching from this point. Repeat this searching procedure until all the points are visited. If the number of selected points is too large, re-choose the reference distance until the number of selected points is in the order of hundreds.

4.2.4 Treatment of boundary conditions

There are several approaches to take care of the boundary conditions in the Galerkin approach. The first one used e.g. in (Park & Cho, 1996) is to include the boundary condition in the weak problem formulation through integration by parts. However, this approach cannot guarantee that the approximate solution resulting from the Galerkin method fulfills the boundary conditions accurately. In the case of the HotModule, this approach leads to poor results.

Another method suggested by Finlayson (1972) for one-dimensional problems is to replace some of the residual conditions (4.4) by the boundary conditions (2.39). By this way, the approximate solution resulting from the Galerkin method will fulfill the boundary conditions exactly. However, there is no guideline, which residual condition should be dropped, and the extension of the method to a two-dimensional problem is difficult.

A different approach is tried in this work. Instead of dropping residual conditions, additional variables are introduced in order to fulfill the boundary conditions. The additional variables are the values of the states at the boundary points, e.g. $\vartheta^{s,*}(\zeta_2, \tau)$ for $\vartheta(0, \zeta_2, \tau)$. These variables are still undefined because of the way how the basis functions ϕ_i are determined: The ϕ_i follow from a numerical solution of the detailed reference model using a spatial discretization on finite volumes, are only known at discrete grid points. In a next step, the spatial gradient $\partial\vartheta/\partial\zeta_1$ or $\partial\vartheta/\partial\zeta_2$ is approximated by finite differences and inserted into the boundary conditions in order to obtain equations for the newly introduced variables, e.g.

$$\left. \frac{\partial\vartheta}{\partial\zeta_1} \right|_{0, \zeta_2} \approx \frac{\vartheta(\Delta\zeta_1, \zeta_2, \tau) - \vartheta^{s,*}(\zeta_2, \tau)}{\Delta\zeta_1} = 0 \quad (4.36)$$

Finally, the boundary values are used in the numerical quadrature of the integrals terms in Equation (4.4). As the above equation can be solved explicitly for $\vartheta^{s,*}(\zeta_2, \tau)$, the introduction of additional unknowns does not increase the order of the reduced model.

4.3 Simulation Results of the Reduced MCFC Model

Test simulations are made in order to validate the reduced model by comparison with the original Heidebrecht model. Special emphasis is laid on the extrapolation qualities of the reduced model. The first test consists in the simulation of a randomly varying cell current identical to the test signal for the validation of the simplified model in chapter 3 Figure 3 - 4(a). The results for a cell are shown in Figure 4 - 1. It can be seen that the maximum temperature error of the anode, cathode and solid phase between the detailed model and reduced model is quite small. The cell voltage of the reduced model matches the result of the detailed model nearly perfectly. The K-L decomposition technique leads to a considerable reduction in terms of the order of the system as well as in terms of the computation time. This is also illustrated from Figure 4 - 1: After a spatial discretization, the complete model consists of about 4,759 equations. Its numerical solution requires about 3200 s of a CPU time on a PC (AMD Athlon(tm) 64 3200+). In comparison, the reduced model consists of 131 equations. Its numerical solution takes about 82s of CPU time on the same PC. The decrease of the computational time achieved by the model reduction is not quite as strong as the decrease of the order of the system. The reason is that the evaluation of the reduced model equations is more complicated as it requires a numerical quadrature.

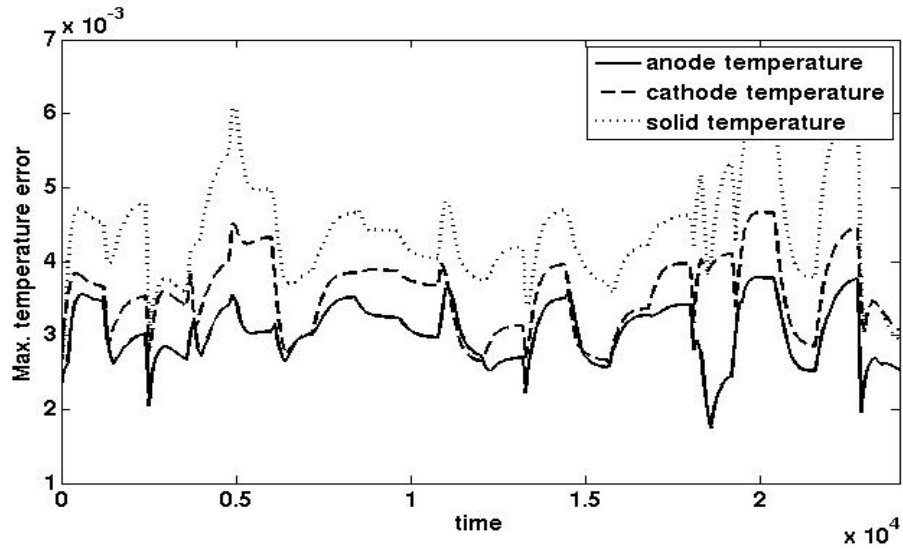


Figure 4 - 1 (a): Maximum temperature error of the reduced model

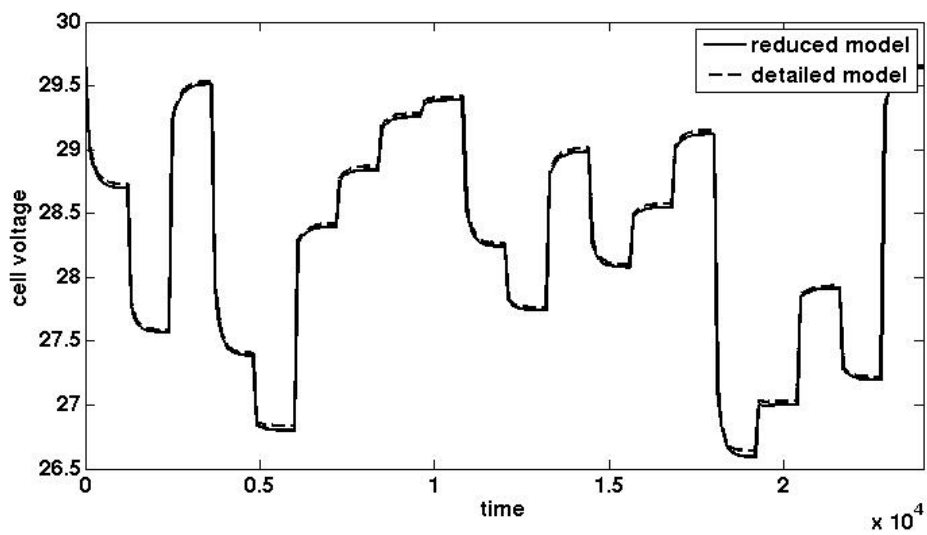


Figure 4 - 1(b): Cell voltage of the reduced and the detailed model

A second test is the response of the reduced model to a change of the steam-to-carbon ratio in the feed. This test is more challenging than the first one, because the basis functions for the reduced model were obtained from simulations with a fixed steam-to-carbon ratio. Nevertheless, the agreement between the reduced and the detailed model is still very good, as can be seen in Figure 4 - 2.

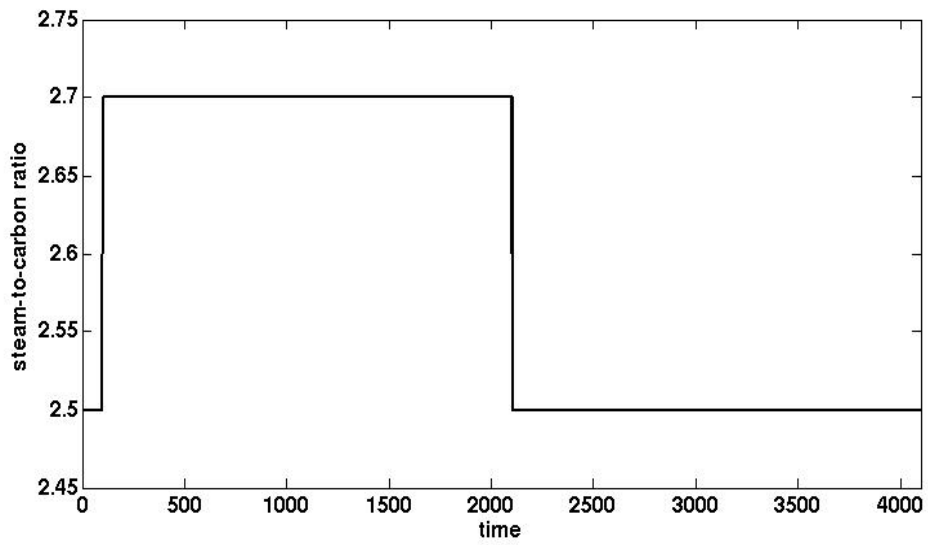


Figure 4 - 2 (a): Ratio of the water and methane concentration in the feed

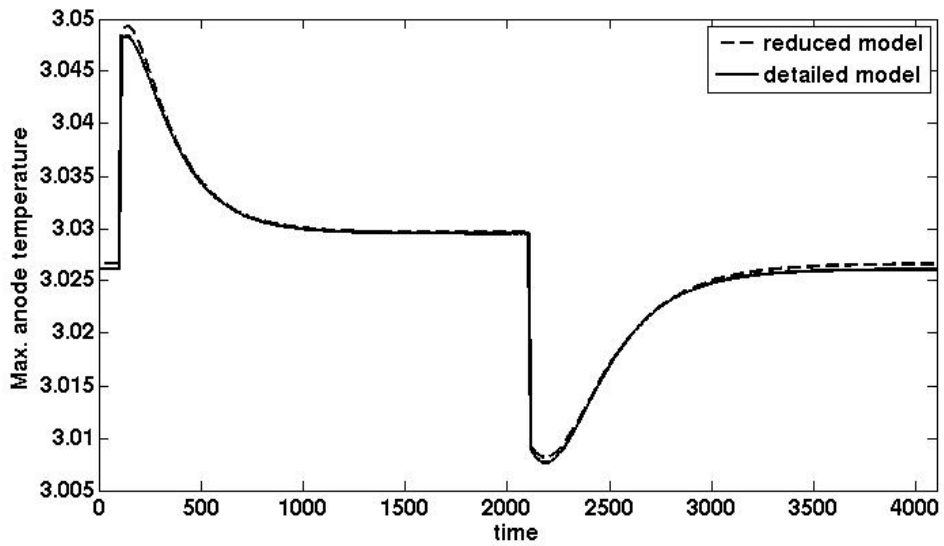


Figure 4 - 2 (b): Maximum anode temperature of the reduced and the detailed model

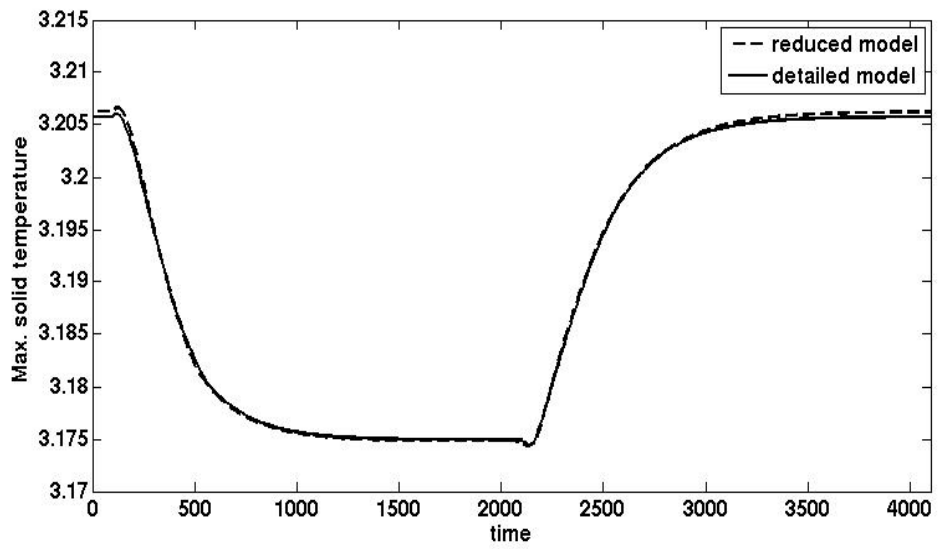


Figure 4 - 2 (c): Maximum solid temperature of the reduced and the detailed model

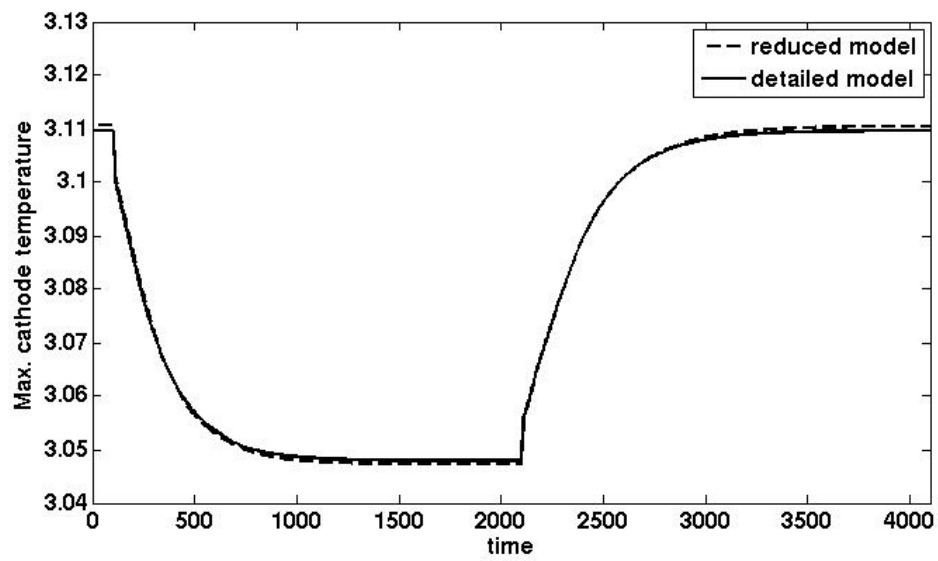


Figure 4 - 2 (d): Maximum cathode temperature of the reduced and the detailed model

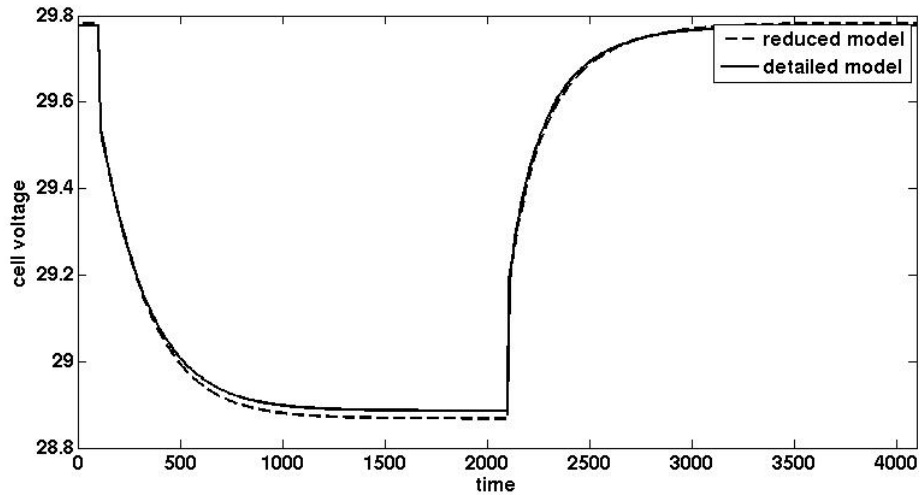


Figure 4 - 2(e): Cell voltage of the reduced and the detailed model

4.4 Summary

The detailed physical modeling of fuel cell systems deepens the process understanding and is an important first step in the design of process control strategies. Dynamic spatially distributed models, however, are too complex for many real-time applications. In this chapter, a reduced model of a MCFC was obtained by applying the Karhunen-Loève Galerkin method to a simplified model of a two-dimensional spatially distributed cross-flow model which was described in chapter 2. The basic idea of the method is to approximate the profiles of the spatially distributed variables by basis functions obtained from test simulations with a detailed reference model. For the MCFC model considered here, this technique proves to be successful. The reduced model produces results that are very close to those of the detailed model, and it reduces the computation time significantly.

It may be regarded as a certain drawback of the K-L decomposition method that the resulting eigenfunctions depend on the choice of the numerical test simulations or snapshots. However, the results of the previous section indicate satisfactory extrapolation qualities of the reduced model of the MCFC. That may be explained by the fact that only the basis functions of the reduced model are obtained

numerically. The reduced model itself is given in an analytical form and still contains the information on the physical correlations in the detailed model.

Due to its properties, the reduced model seems to be suitable for applications in the field of model based process control. An example are model based measuring techniques, where the reduced model can be used in the framework of a Luenberger observer or a Kalman filter in order to estimate quantities of a fuel cell that are not accessible to direct measurements. The reduced model developed here will be used in the next chapter for the design of a Luenberger observer to aid the realization of the proposed control strategy.

Chapter 5

Model-Based Dynamic Performance and Control of a Molten Carbonate Fuel Cell System

5.1 Introduction

Temperature is always a main issue in high temperature fuel cell operation. In an MCFC stack a high temperature may cause carbonization, carbon deposition in the anode channel, and the temperature difference may cause mechanical damage of the fuel cell.

An industrial MCFC stack is characterized by a high degree of system integration, as the process behavior depends on numerous interactions between the electro-chemical reaction steps, the internal reforming, mass transport processes, and the heat transfer inside a cell or stack. An understanding of the physical-chemical processes in an MCFC can be obtained from mathematical models based on physical conservation principles as was shown in the previous chapters. Model based process control and process design strategies can lead to a much better use of the fuel cells' capacities and increase the efficiency of the system.

As the overall fuel-to-electricity conversion efficiency is the most important for power industries, a maximum electric efficiency is desired not only when the cell is operated at constant load over a long period of time but also during dynamic load changes. In the former situation an optimal electric efficiency can be achieved through a steady state optimization procedure (Heidebrecht, 2005); whilst in the latter situation a fast and safe transition must also be taken into consideration. To keep the process safe, the solid temperature must not exceed a minimum and a

maximum temperature, and also the maximum temperature difference within the solid phase is limited. This chapter tries to construct a framework (Aguilar, 2005) for satisfying high electric efficiency over a larger range of operation points and at the same time controlling the solid temperature when power load changes. For simulation, optimization and control of MCFC processes mathematical models are required. The detailed spatially two-dimensional model of the MCFC presented in previous publications (Heidebrecht & Sundmacher, 2002; 2003) was introduced in Chapter 2. A control strategy is constructed based on this model, which achieves the optimal electric efficiency by a steady state optimization and at the same time satisfies the solid temperature constraints by involving two PID controllers. As will be shown in the later sections, the control approach proposed includes the control of spatial dependencies (the control of stack temperature difference). It combines a feed-forward branch based on a detailed physical model and feedback PID controllers. A suitable state estimator is finally designed to make the control method applicable. The reduced version of the model derived using the model reduction method proposed in Chapter 3 serves as the basis for the state estimator.

5.2 The Control Strategy

Performance and availability of molten carbonate fuel cells stack are greatly dependent on their operating temperature. Control of the operating temperature within a specified range and reduction of temperature fluctuation are highly desirable. The models of MCFC stacks existing are too complicated to be suitable for design of a controller because of the lack of clear input-output relations. In literature, only a few publications about model based control of MCFC are available. Lucas & Lee (2005) describe a first principle-based non-linear dynamic model and also obtain reduced-order models, but no spatial gradients are considered. Kang, Koh & Lim (2001) derive a linear 3×3 transfer function matrix model from an experimental study, which will simplify the design of controllers but will limit application of the controller to the vicinity of a chosen operating point. Shen *et al.* (2002) present an adaptive fuzzy control procedure for the temperature of a MCFC

stack based on a neural network identification model. As the dynamic model is also empirical, the applicability of the controller is restricted to operating conditions, where this model is valid. Because of the assumptions they made, these models have limitations for control with large-scale load changes.

Lukas, Lee & Ghezel-Ayagh (2002) presented a simulation of a group of control loops in an MCFC power plant with cycling load demand. The control loops involved such as stack temperature, stack differential pressure, natural gas flow, *etc.* are all single-loop and PI-type. Although these control loops are practically important, the coupling between various loops was not taken into consideration, and the spatial gradient was also not considered.

Golbert & Lewin (2004) describe a model-based controller for the regulation of a proton exchange membrane (PEM) fuel cell. The model accounts for spatial dependencies of voltage, current, material flows, and temperatures in the fuel channel. Analysis of the process model shows that the effective gain of the process undergoes a sign change in the normal operating range of the fuel cell, indicating that it cannot be stabilized using a linear controller with integral action. Consequently, a nonlinear model-predictive-controller based on a simplified model has been developed, enabling the use of optimal control to satisfy power demands robustly. The model predictive control framework tackles problems such as nonlinearity in the vicinity of the peak power density and assurance of efficient operation during transients and when extreme load changes are imposed.

Model predictive control (MPC) is part of a family of optimization-based control methods, which are based on on-line optimization of future control actions. Using a process model, the optimizer predicts the effect of past inputs on future outputs. Then, using the same model, it computes a sequence of future control actions, such that an objective function, including penalties on the trajectory of the predicted tracking error, is minimized. The first part of the future control actions is implemented, and the entire optimization is repeated from the next step on, and so

on, and infinitum. Feedback is used to compensate for the model's inaccuracies and to ensure convergence. But because of the on-line optimization requirement, MPC will consume more CPU resources than regular PID controllers. When the plant model is too complex, the optimization may require more powerful calculation tools which may be very hard to be implemented on line.

Aguiar, Adjiman & Brandon (2005) designed a control strategy for a solid oxide fuel cell (SOFC) with frequent load changes due to variable power demand. A dynamic SOFC model, which consists of mass and energy balances and an electrochemical model that relates the fuel and air gas compositions and temperature to voltage, current density, and other relevant fuel cell variables, is used. A master controller and two typical feedback PID temperature controllers have been implemented. The master controller imposes a current density disturbance representing a change in power demand and sets the fuel and air flow rates proportional to that current (keeping the fuel utilization and air ratio constant). The PID controllers respond to the outlet fuel temperature by changing the air ratio and the molar flow around the default set. As there is no special requirement for the model structure, this kind of control strategy can be easily applied to other types of fuel cells. The controller design in an MCFC that will be proposed in Chapter 5 of the thesis is inspired by this strategy and a few other factors that will influence the performance of the MCFC are considered.

To control an MCFC System described in section 5.2 a fast and safe dynamic response during the cell current change is required. As the power load does not change very frequently an optimal steady state electric efficiency is also desired. In the ideal case the electric efficiency is dynamically optimized such that both demands can be achieved at the same time. However, the optimization of a complex nonlinear fuel cell model in real time is very difficult. To overcome this problem, the approach adopted here is to achieve the optimal state electric efficiency in offline optimization and then to make sure that the dynamic response is as fast and safe as possible. That is, when the power load changes (i.e. the cell current changes)

a master loop switches the operating variables to their new static conditions that satisfy an optimal electric efficiency at the new load. Then in the inner loop, feedback controllers satisfy the dynamic performance criteria. This approach is similar to the control concept proposed by Aguiar *et al.* (2005) for an SOFC stack. However, in contrast to their work, a spatially two-dimensional temperature field is considered in this work. Furthermore, the concept proposed here controls the maximum temperature and the maximum spatial temperature difference at the same time. This leads to a multiple-input / multiple-output (MIMO) control problem, where the choice of suitable manipulated variables is more difficult than in the single-input / single-output case.

The steady state optimization will be introduced first and temperature response tests will then be performed in order to decide which operating variable controls which controlled variable. The control scheme and results will be given thereafter.

5.2.1 Steady state optimization

Heidebrecht (2005) optimizes the input parameters of a single cross flow cell at given cell current to yield an optimal electric efficiency while fulfilling several temperature restrictions and avoiding carbonization in the anode channel. The optimization is performed at different cell currents, so that several points of a current voltage curve with optimal operating conditions are evaluated.

The electric efficiency which is used as the objective function of the optimization relates the total electric cell power diminished by the system's parasitic power consumption to the combustion enthalpy input of the fuel gas. The optimization has several constraints concerning the solid temperature and the possibility of carbonization. The temperature must not exceed a minimum and a maximum temperature, and also the maximum temperature difference within the solid phase is limited. Three operation parameters, which can be adjusted easily in the HotModule, are chosen as optimization variables. The first optimization variable is the total

amount of fuel gas (Γ_{feed}) fed to the system. In the case of the HotModule, the fuel gas consists of steam and methane. The ratio between the flux of steam and the flux of methane fed to the system, i.e. the steam to carbon ratio (S/C), is chosen as the second optimization variable. The third optimization variable is the air number (λ_{air}), defined as the ratio between the amount of air actually fed to the burner and the amount of air required under stoichiometric conditions. Those three variables must be adjusted to meet the power demands from an external load on the cell in an optimal way. For simplicity, the effect of the external load is modeled by setting the total cell current (I_{cell}) to a fixed value within each optimization. Also the temperatures of feed gas and air are assumed to be constant. The following objective function was suggested by Heidebrecht (2005):

$$\eta_{el}(\Gamma_{feed}, S/C, \lambda_{air}, R_{back}) = \frac{P_{el,system}}{H_{feed}} = \frac{P_{cell} - P_{blower}}{\Gamma_{feed} \cdot \sum_i \chi_{i,feed} \cdot (-\Delta_c h_i^0)} \rightarrow \max! \quad (5.1)$$

subject to

$$\min(\vartheta_s(\zeta)) \geq \vartheta_{s,min} \quad (5.2)$$

$$\max(\vartheta_s(\zeta)) \leq \vartheta_{s,max} \quad (5.3)$$

$$\max(\vartheta_s(\zeta)) - \min(\vartheta_s(\zeta)) \leq \Delta\vartheta_{s,min} \quad (5.4)$$

$$U_{cell} \geq U_{cell,min} \quad (5.5)$$

$$\exists j: \Delta_R g_{Cj}(\vartheta_a(\zeta_1, \zeta_2), \chi_{feed}(\zeta_1, \zeta_2)) \geq 0 \quad \text{at every } \zeta_1, \zeta_2 \in [0 \dots 1; 0 \dots 1] \quad (5.6)$$

and additionally the steady state fuel cell model equations as equality constraints. In the above equations R_{back} is cathode recycle ratio; $P_{el,system}$ is total electric cell power (P_{cell}) diminished by the system's parasitic power consumption (P_{blower}); H_{feed} is combustion enthalpy of the fuel gas; $\Delta_c h_i^0$ is standard combustion enthalpy of component i ; $\chi_{i,feed}$ is fuel gas mole fraction of component i ; ϑ_s is solid phase temperature; U_{cell} is cell voltage; and $\Delta_R g_{Cj}$ is free enthalpy of reaction j . Equations 5.2 and 5.3 demand that the solid temperature does not exceed a minimum and a

maximum temperature at any point in the cell. In Equation 5.4 the difference between the highest and the lowest temperature is limited, and Equation 5.5 demands that the cell voltage stays above a certain level. According to Equation 5.6, at least one carbonization reaction at every location of the cell must have a positive free enthalpy of reaction in order to avoid carbon deposition.

Some typical input quantities ($I_{cell}=0.5, 0.6, 0.7, 0.8, 0.9$ and 1.0) at the optimum operating points together with additional information like temperature are listed in Table 5 - 1. The results were obtained using the simplified model introduced in section 2.3.2. For the control purpose the number of steady state optimization points should be infinite to obtain optimal steady state performance at arbitrary cell currents. In order to have more possible operation points, the table by Heidebrecht (2005) was extended by specifying I_{cell} change by 0.01 from 0.5 to 1.0. When an I_{cell} change is less than 0.01, the optimized variable values between two nearest points are interpolated. For an I_{cell} change, the master controller looks up the table, locates the column of the desired I_{cell} state and sets the three variables ($\Gamma_{feed}, S/C, \lambda_{air}$) to their corresponding numbers.

I_{cell}	0.5	0.6	0.7	0.8	0.9	1.0
Γ_{feed}	0.6783	0.8296	0.9841	1.114	1.2859	1.2920
S/C	2.4304	2.4707	2.4903	2.4321	2.3106	1.7049
λ_{air}	2.0250	2.0659	2.1913	2.3447	2.6071	2.9574
ϑ_{min}	2.9604	2.9999	2.9999	2.9919	2.9942	3.0000
ϑ_{max}	3.1604	3.2000	3.1999	3.1994	3.2017	3.2000
ϑ_{diff}	0.2000	0.2001	0.2001	0.2075	0.2076	0.2000
η_{el}	0.5391	0.5240	0.5030	0.4809	0.4384	0.3838
$\tilde{\eta}_{el}$	0.5391	0.5240	0.5030	0.4769	0.4352	0.3838

Table 5 - 1: Results of the steady state optimization of input parameters;

$\tilde{\eta}_{el}$ refers to the closed-loop case discussed in section 5.3.4

5.2.2 Solid temperature response analysis

The control objective is to fulfill the temperature constraints when the current load changes, that is, to transfer the fuel cell safely from an optimal steady state to another. The steady state optimization introduced in the previous section gives a reference of what the input parameters (Γ_{feed} , S/C and λ_{air}) would be like to achieve the desired new state, but the dynamics of transition do not guarantee the temperature constraints. In order to control the solid phase temperature during dynamic transition, temperature control loops are required. The possible controlled variables are minimum temperature (ϑ_{min}), maximum temperature (ϑ_{max}) and maximum temperature difference (ϑ_{diff}). It is found that the minimum temperature rarely exceeds the limits, so there are two controlled variables (ϑ_{max} and ϑ_{diff}) and as stated already three manipulated variables (Γ_{feed} , S/C and λ_{air}). This is a typical multi-input-multi-output (MIMO) control problem. In the following, a match of input and output variables based on physical considerations is proposed. Dynamic responses of the system model to step changes of the three manipulated variables are considered. Figure 5 - 2 shows the step responses of all the possible input and output matches when each of the three input variables changes from its corresponding optimized state at $I_{cell}=0.8$ to the state at $I_{cell}=0.7$ at time 5000 and then changes back to the optimized state when $I_{cell}=0.8$ at time 10000. The actual cell current is kept constant at $I_{cell}=0.8$. All results are given in dimensionless numbers, one dimensionless time unit corresponds to 66 seconds. For the cell current and the temperature, the following scaling is used: one current density unit equals to 840 A/m², one temperature unit equal to 298.15 K.

Figure 5 - 2(a) gives the temperature difference and maximum temperature response when switching Γ_{feed} from its optimal state 1.114 to the new optimal state 0.9841 while keeping λ_{air} and S/C at their old state. A reduction of Γ_{feed} means physically that less fuel is fed to the system. As the cell current is kept constant and the cell voltage changes only slightly, the electrical power hardly varies during the

simulation experiment in Figure 5 - 2 (a). Consequently, the reduction of Γ_{feed} results in a higher electrical efficiency and — because less chemical energy is converted to heat — in a lower average temperature of the stack. However, the new steady state with the higher efficiency, which is reached at time ~ 6000 , is not feasible as the temperature difference is above the tolerable limit. This behavior is found to be typical for changes of Γ_{feed} at different operation points. A reduction of Γ_{feed} by a small amount always leads to a spatially more inhomogeneous temperature profile and hence to an increase of the maximum spatial temperature difference. The implications of a modified Γ_{feed} on the absolute maximum temperature are less clear. Depending on the actual operation point, the temperature maximum may increase or decrease. Therefore, Γ_{feed} is a suitable variable for controlling the temperature difference but is not suitable for controlling the maximum temperature.

The system response to a variation of the steam-to-carbon ratio is qualitatively similar to the response to a variation of Γ_{feed} . An example is shown in Figure 5 - 2 (b). An increase of S/C at a constant Γ_{feed} also means a reduction of the amount of fuel fed to the system. Therefore, the argumentation used to explain Figure 5 - 2 (a) holds for Figure 5 - 2 (b), too. An increase of S/C generally causes an increase of the temperature difference, while the maximum temperature may decrease or increase, depending on the operation point. Therefore, the steam-to-carbon-ratio is another possible candidate for the control of the spatial temperature difference.

The effect of a varying air number λ_{air} is shown in Figure 2 (c). A higher amount of air in the system mainly has a cooling effect, i.e. it reduces the maximum temperature. The influence on the spatial temperature difference is not that strong. Therefore, varying λ_{air} locally around a given setpoint is a good method to control the maximum temperature of the fuel cell.

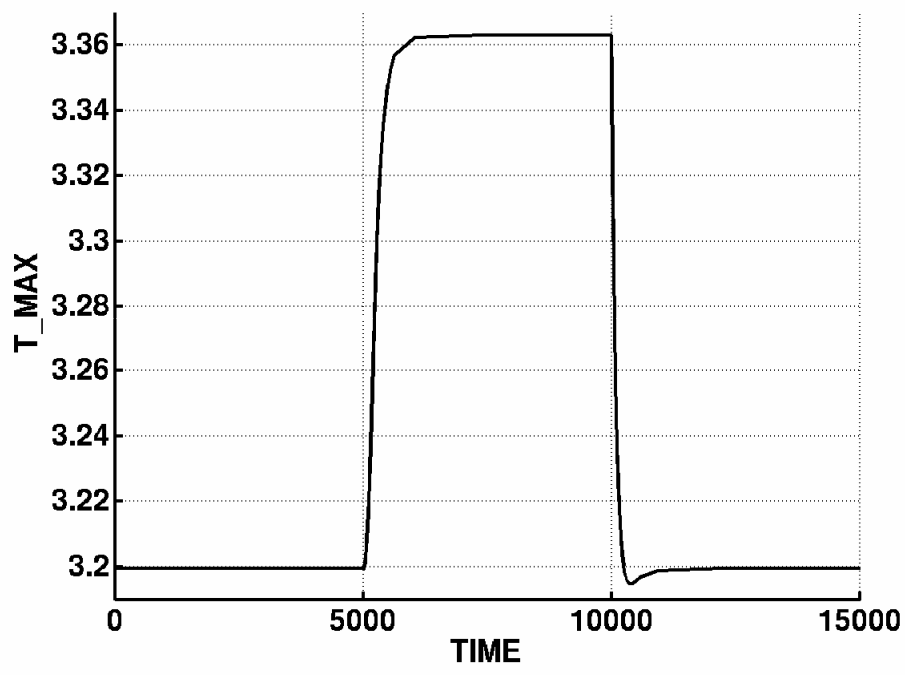
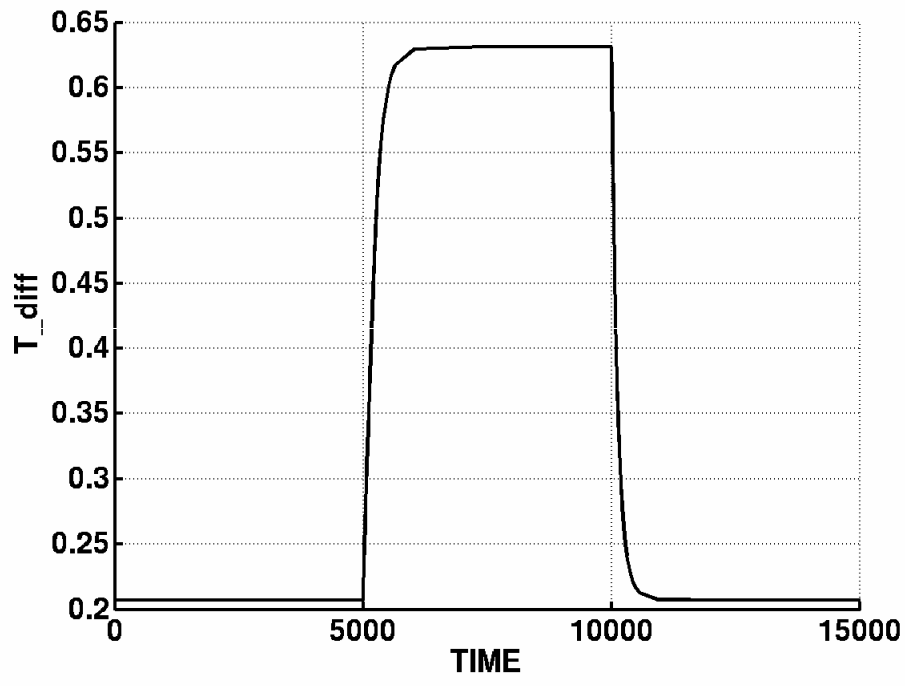


Figure 5 - 2(a): $\vartheta_{max}, \vartheta_{diff}$ response to a Γ_{feed} change; Γ_{feed} changes from the optimal value at $I_{cell}=0.8$ to the optimal value at $I_{cell}=0.7$ and back again

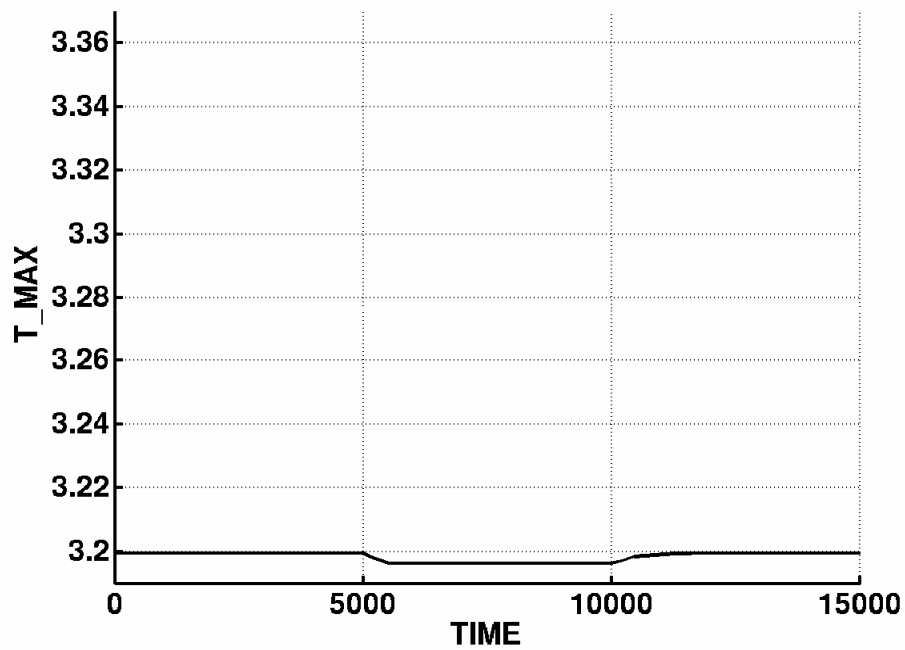
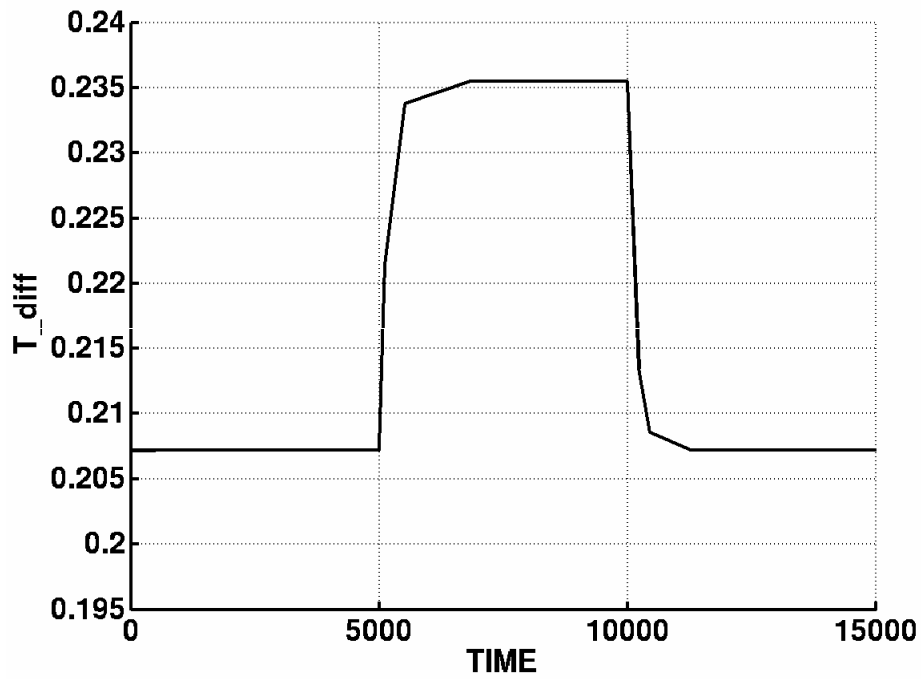


Figure 5 - 2(b): $\vartheta_{max}, \vartheta_{diff}$ response to a S/C change; S/C changes from the optimal value at $I_{cell}=0.8$ to the optimal value at $I_{cell}=0.7$ and back again

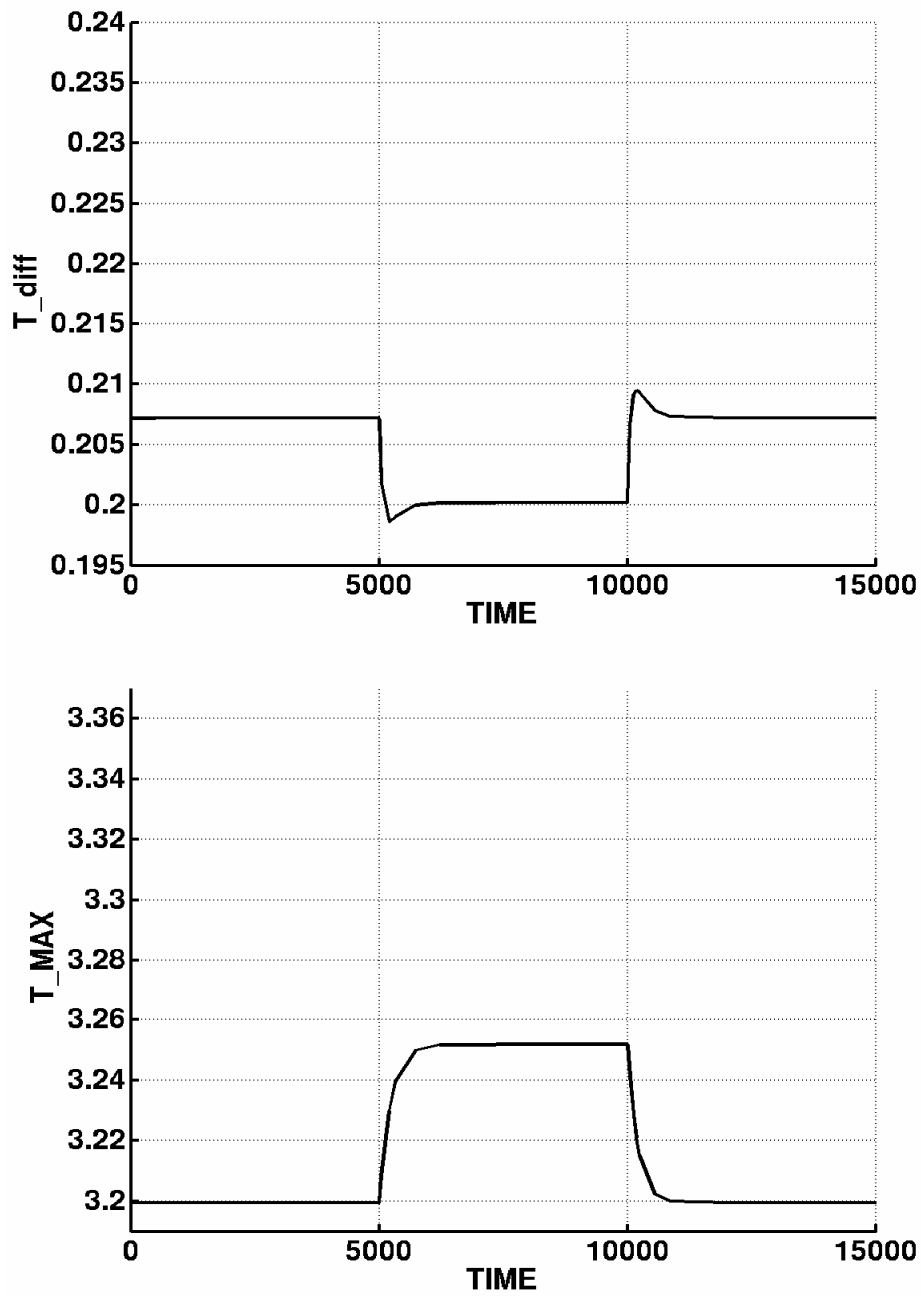


Figure 5 - 2(c): $\vartheta_{\max}, \vartheta_{diff}$ response to a λ_{air} change; λ_{air} changes from the optimal value at $I_{cell}=0.8$ to the optimal value at $I_{cell}=0.7$ and back again

To summarize the discussion of Figure 5 - 2, the air number λ_{air} has the most direct relationship to ϑ_{\max} because of its cooling effect. With respect to ϑ_{diff} , the effect of Γ_{feed} and S/C is almost the same and in this work S/C is chosen to

control ϑ_{diff} . The resulting feedforward-feedback control scheme is depicted in Figure 5 - 3. A feedforward controller sets the three manipulated variables Γ_{feed} , λ_{air} and S/C to the optimal steady state values $\tilde{\Gamma}_{feed}$, $\tilde{\lambda}_{air}$ and $\tilde{S/C}$. The air number λ_{air} is tuned by the PID controller 1 around the default set by the feed-forward controller in order to obtain a pre-defined maximum solid temperature ϑ_{max} also under transient conditions; similarly, S/C is tuned by PID controller 2 around the optimum steady state value in order to achieve a pre-defined maximum temperature difference ϑ_{diff} .

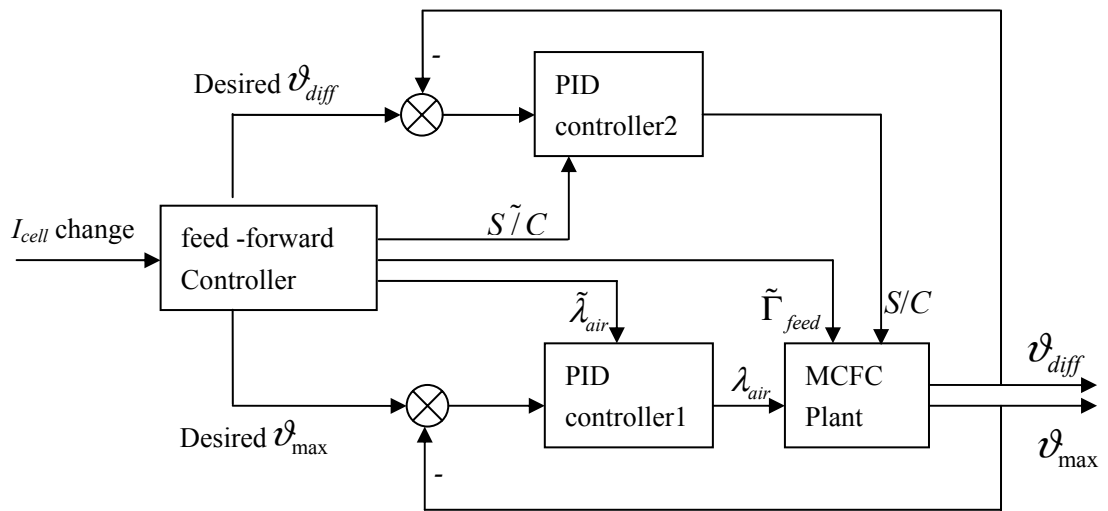


Figure 5 - 3: The feedforward-feedback control scheme

5.2.3 Control results and analysis

Figures 5 - 4(a) and 5 - 4(b) present the ϑ_{diff} and ϑ_{max} transient behavior, under open-loop and closed-loop conditions, when the cell current changes from 0.55 to 0.6 and further to 0.65, 0.75, 0.8, 0.85, 0.9, 0.95, 1.0 at every 2000 time units (0, 2000, ..., 18000) representing positive load changes and then changes back from 1.0 to 0.95, 0.9, ..., 0.5 at times (20000, 22000, ..., 38000) representing negative load changes. Note that closed-loop implies that all control loops are active, whereas

open-loop suggests that only the master controller is in operation. In the simulation shown in Figure 5 - 4, where the optimized $|\vartheta_{\max} - 3.2| \leq 0.01$, the desired ϑ_{\max} will be set to 3.2, and the desired ϑ_{diff} was always set to 0.2, resulting in a steady state electric efficiency deviating slightly from the optimal value, as can be seen from table 5 - 1.

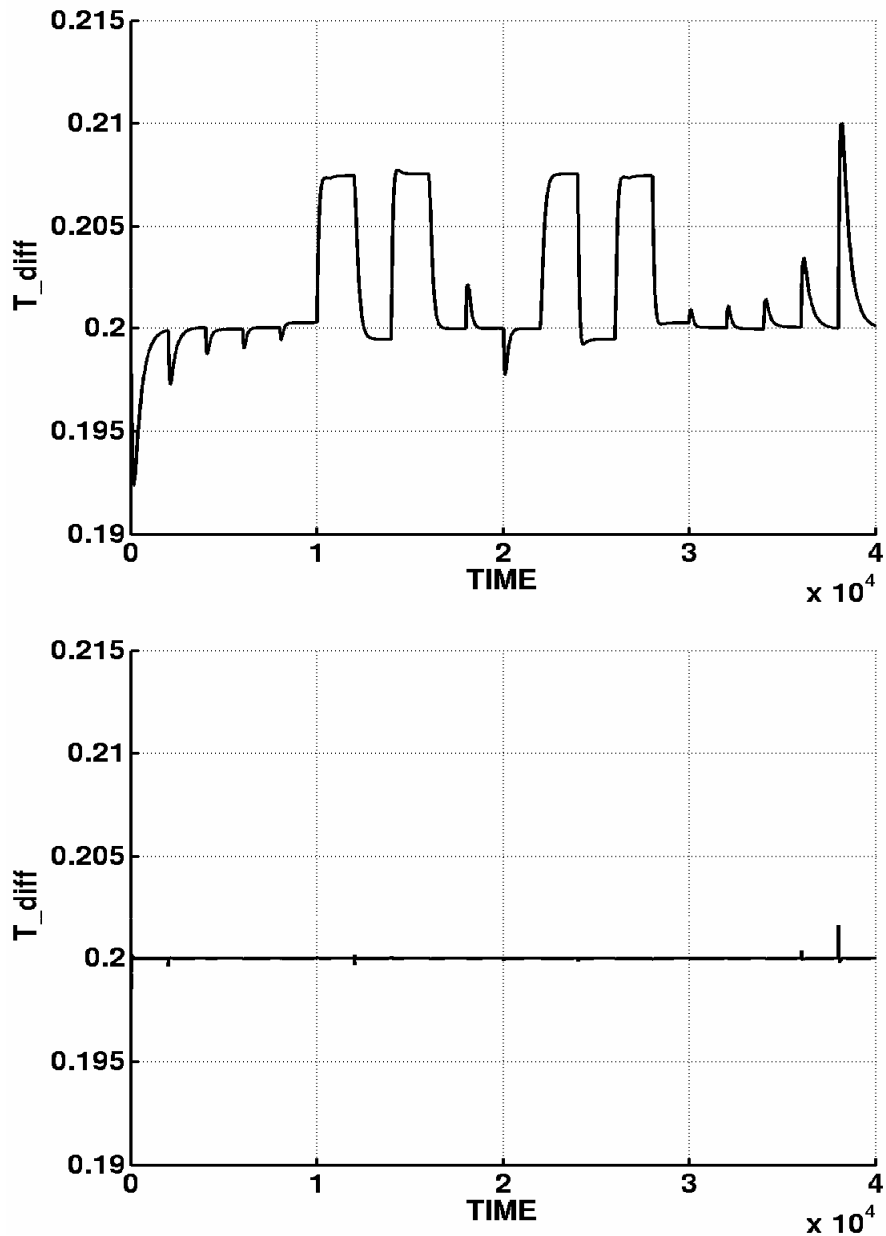


Figure 5 - 4(a): ϑ_{diff} control results (open-loop on top panel and closed-loop on bottom panel)

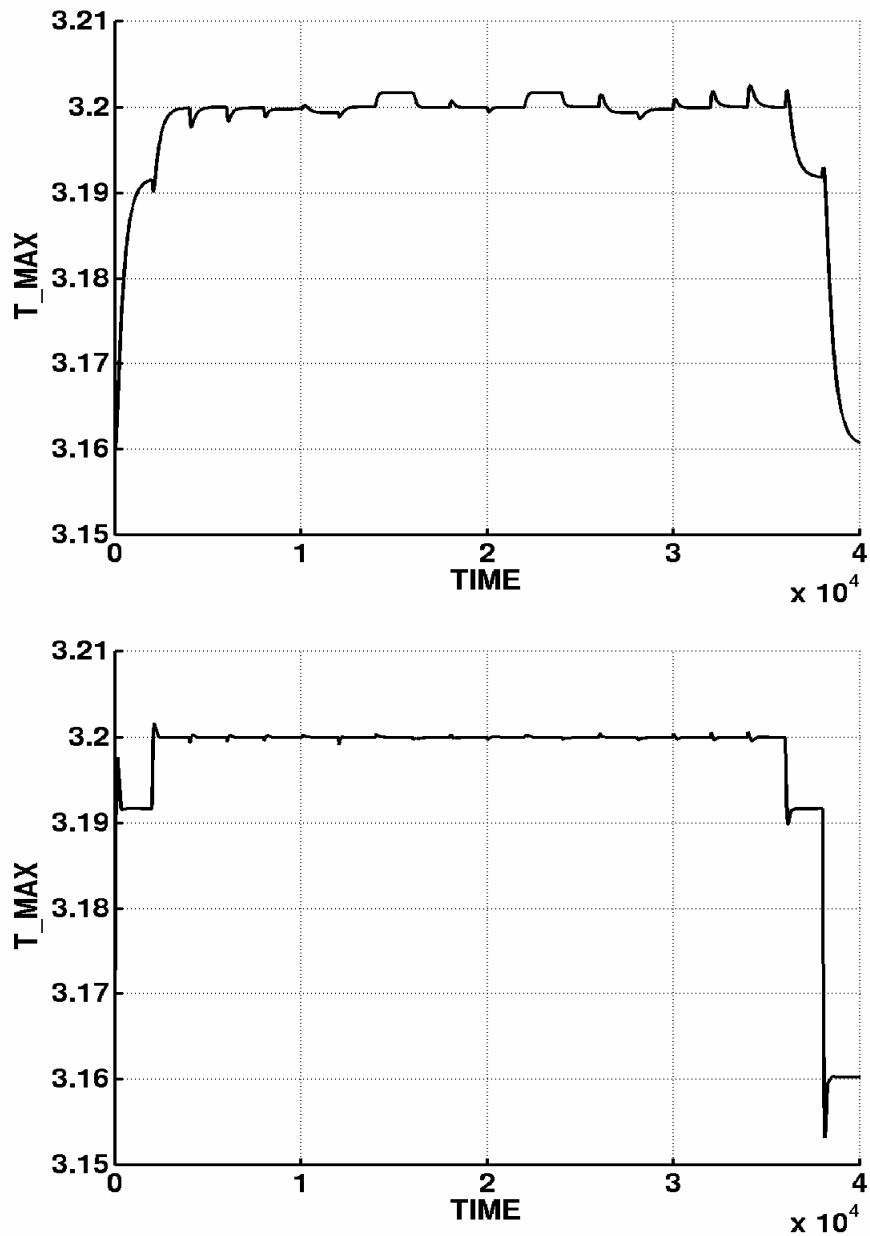


Figure 5 - 4(b): ϑ_{\max} control results (open-loop on top panel and closed-loop on bottom panel)

The parameters of the PID controllers used (ϑ_{diff} controller gain=180.0, integral time=20.0, derivative time=500.0; ϑ_{\max} controller gain=24.0, integral time=0.29, derivative time=40.0) were found to provide a fast system response. As can be seen, for the open-loop case (no temperature control), ϑ_{diff} and ϑ_{\max} usually exceed

their corresponding limits (0.2 and 3.2 respectively), while for the closed-loop case, the PID controllers successfully and quickly bring the temperatures back to their desired set-points.

5.2.4 State estimator

Usually, the required measurement information on ϑ_{diff} and ϑ_{max} is not available from an industrial fuel cell system. In most cases, temperature measurements can be taken only at a few points in the cell stack. To make the proposed control scheme applicable in practice, a state estimator or observer is required. One possible approach for state estimation is the extended Kalman filter that is based on a stochastic approach. An extended Kalman filter for the MCFC was developed and tested successfully by Grötsch *et al.* (2006). An alternative approach that is based on a deterministic approach, is the extended Luenberger observer. This approach will be studied in the following. The advantage of the Luenberger observer is that the implementation is easier and that the computational burden is smaller than in the case of the Kalman filter.

5.3 Development of a Luenberger Observer for Model Based Measurement

Usually, the measuring information available from an industrial fuel cell system is rather limited. In most cases, temperature measurements can be taken only at a few points in the cell stack, and measuring information on the composition of the gases in the cell is available only in special cases. A tool that provides information on states not accessible to direct measurements is desirable. A model-based measuring system or observer can serve as such a tool. This subsection starts with observability studies for different measurement configurations. The design of a

Luenberger observer is then described on the basis of the reduced model. The simulation results combining the developed Luenberger observer with the control strategy in the previous section are presented in the end.

5.3.1 Structure of the Observer

As a state estimator for the HotModule, a Luenberger observer is designed. The general structure of an observer is shown in Figure 5 - 5. The central part of the observer is a simulation model of the process that gives an estimate $\hat{X}(z_1, z_2, t)$ of the complete spatially distributed state vector of the cell $X(z_1, z_2, t)$, i.e. of the temperatures, gas concentrations, and electrical potentials. Due to inaccuracies of the model and due to unknown disturbances of the real process, the estimate $\hat{X}(z_1, z_2, t)$ will deviate from $X(z_1, z_2, t)$ if the observer model is not extended by a correction term. The observer correction compares the vector of measured values $y(t)$, e.g. temperature measurements at some points, with the simulated measured values $\hat{y}(t)$ computed by the observer. If the vectors differ, the correction has to change the observer states in such a way that the difference between real and simulated measurements is minimized. Consequently, the design of an observer comprises three tasks:

- the choice of an observer model that is sufficiently accurate, but can be solved in real time;
- the choice of sensor combinations that make the process observable, i.e. that permit the reconstruction of the full state vector from the available measurements;
- the design of an observer correction that reduces the observation error to a minimum.

The three tasks will be discussed in the next few sections for the MCFC system.

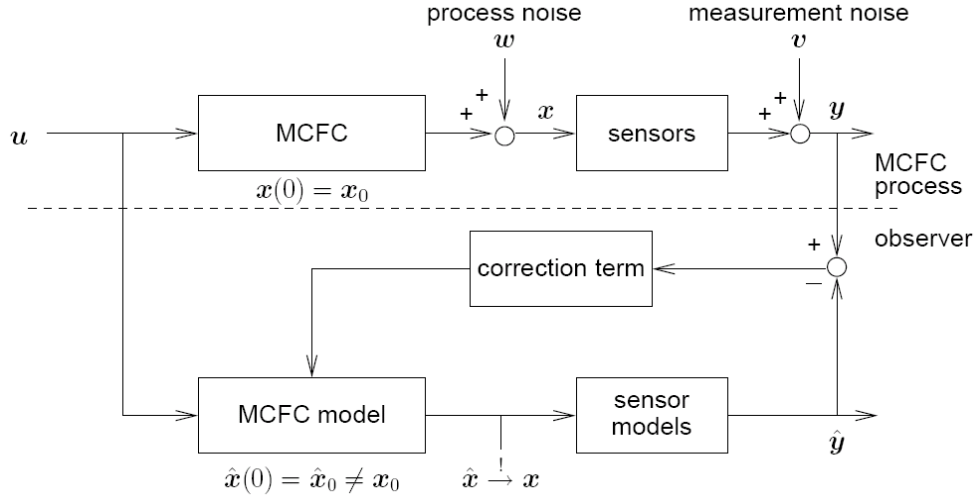


Figure 5 - 5: Block diagram of the state and parameter observer for the MCFC

5.3.2 Observer model

The reduced MCFC model of the HotModule serves as a basis of the observer model. The resulting reduced model is a differential algebraic system of differential index one that has the following structure:

$$\frac{d\vartheta_s}{d\tau} = f(\vartheta_a, \vartheta_s, \vartheta_c, \chi_i, \gamma_a, \gamma_c, \Delta\Phi_a, \Delta\Phi_c, u)$$

$$\frac{d\vartheta_c}{d\tau} = f(\vartheta_a, \vartheta_s, \vartheta_c, \chi_i, \gamma_a, \gamma_c, \Delta\Phi_a, \Delta\Phi_c, u)$$

$$0 = g(\vartheta_a, \vartheta_s, \vartheta_c, \chi_i, \gamma_a, \gamma_c, \Delta\Phi_a, \Delta\Phi_c, u) \quad (5.7)$$

In Equation (5.7), $\vartheta_i = (\vartheta_1, \vartheta_2, \dots, \vartheta_N)^T$ is the vector of the temperature amplitude functions for anode, solid and cathode. χ_i , γ_a , γ_c are the corresponding vectors for the time-dependent amplitude functions of the gas compositions and the anode and cathode flow rates, respectively, and $\Delta\Phi_a$ and $\Delta\Phi_c$ are the electrical potential differences at the anode and at the cathode; u is a vector of input variables like flow rates, inlet compositions, and inlet temperatures.

Equation (5.7) is used as a starting point for the development of a Luenberger state

observer.

5.3.3 Observability and placement of sensors

For different kinds of measuring information, local observability of the model 5.7 is checked in the following way: the system is linearized around an operation point. Algebraic variables are eliminated by solving the linearized algebraic equations. The rank of the observability matrix of the resulting linear ODE system is computed. It is found that the observability matrix possesses already full rank if a single temperature measurement or the measurement of the total cell voltage is available. Therefore, at least in theory one temperature sensor or one voltage sensor is enough to ensure observability, but, of course, additional measurements will accelerate the convergence of the observer. The investigate on of observability has been done by (Mangold *et. al* 2005). Three scenarios of different sensor configurations are considered:

Scenario 1: The average outlet temperature of the anode gases, the outlet temperature of three cathode gas channels, and the cell voltage are measured.

Scenario 2: In addition to the measurement information given in Scenario 1, the temperature at one point in the middle of the solid is measured.

Scenario 3: In addition to the measurement information given in Scenario 1, the average gas composition at the outlet of the anode gas channels and at the outlet of the cathode gas channels is measured.

(Mangold *et. al* 2005) found that the best trade-off between observability and measurement costs is achieved by scenario 1. Therefore, the further development of the state estimator is carried out on the basis of the case scenario 1.

5.3.4 Observer correction term

As a state estimator for the HotModule, in order to achieve convergence between the observer's states and the states of the real process, a correction has to be added to the model equations. The observer equations read as

$$\begin{pmatrix} \frac{d\hat{\vartheta}_s}{d\tau} \\ \frac{d\hat{\vartheta}_c}{d\tau} \end{pmatrix} = \begin{pmatrix} f(\hat{\vartheta}_a, \hat{\vartheta}_s, \hat{\vartheta}_c, \hat{\chi}_i, \hat{\gamma}_a, \hat{\gamma}_c, \Delta\hat{\Phi}_a, \Delta\hat{\Phi}_c, u) \\ f(\hat{\vartheta}_a, \hat{\vartheta}_s, \hat{\vartheta}_c, \hat{\chi}_i, \hat{\gamma}_a, \hat{\gamma}_c, \Delta\hat{\Phi}_a, \Delta\hat{\Phi}_c, u) \end{pmatrix} + \mathbf{K}_T (y - \hat{y})$$

$$\theta = g(\hat{\vartheta}_D, \hat{\vartheta}_A, \hat{\chi}_i, \hat{\gamma}_a, \hat{\gamma}_c, \Delta\hat{\Phi}_a, \Delta\hat{\Phi}_c, u) \quad (5.8)$$

In Equation (5.8), the matrices \mathbf{K}_T are constant gain matrices. They are determined in the following way.

Firstly, the reduced model equations 5.7 are linearized by the dynamic simulation tool DIVA. The linearized model can be written as

$$\mathbf{E}_D \cdot \dot{\mathbf{x}}_D = \mathbf{A}_{DD} \mathbf{x}_D + \mathbf{A}_{DA} \mathbf{x}_A + \mathbf{B}_D \mathbf{u} \quad (5.9a)$$

$$\theta = \mathbf{A}_{AD} \mathbf{x}_D + \mathbf{A}_{AA} \mathbf{x}_A + \mathbf{B}_A \mathbf{u} \quad (5.9b)$$

$$\mathbf{y} = \mathbf{C} \mathbf{x}_A$$

\mathbf{E}_D is an invertible left-hand-side matrix. Because (5.9) is a differential algebraic system with differential index 1, it is possible to solve the algebraic equations (5.9b) for the algebraic states \mathbf{x}_A .

After some rearrangement, the above Equation can be written as

$$\dot{\mathbf{x}}_D = \mathbf{E}_D^{-1} \underbrace{(\mathbf{A}_{DD} - \mathbf{A}_{DA} \mathbf{A}_{AA}^{-1} \mathbf{A}_{AD})}_{\tilde{\mathbf{A}}} \mathbf{x}_D + \mathbf{E}_D^{-1} (\mathbf{B}_D + \mathbf{A}_{DA}^{-1} \mathbf{B}_A) \mathbf{u} \quad (5.10)$$

$$\mathbf{y} = - \underbrace{\mathbf{C} \mathbf{A}_{AA}^{-1} \mathbf{A}_{AD}}_{\tilde{\mathbf{C}}} \cdot \mathbf{x}_D \quad (5.11)$$

i.e. system (5.9) can be transformed to an ODE system, and observer design methods for ODE system can be applied.

Now, \mathbf{K}_T can be chosen as a Kalman filter gain matrix as suggested by Friedland (1996). The fundamental problem in the design of an observer is the determination of the observer gain matrix K such that the closed-loop observer matrix $[\tilde{\mathbf{A}} - K\tilde{\mathbf{C}}]$ is a stable matrix.

Since the observer given by Equation 5.8 has the structure of a Kalman filter, its gain matrix can be chosen as a Kalman filter gain matrix, i.e.,

$$K = P\tilde{C}^T R^{-1} \quad (5.12)$$

where P is the covariance matrix of the estimation error and satisfies the matrix Riccati equation

$$\dot{P} = \tilde{A}P + P\tilde{A}^T - P\tilde{C}^T R^{-1} \tilde{C}P + Q \quad (5.13)$$

Where R is a positive definite matrix and Q is a positive semidefinite matrix. The matrix P is obtained by setting \dot{P} in the upper equation to zero.

But we also found our observer system is rather robust, any random matrix can be used as the gain matrix if only its elements are small enough, for instant, 0.001.

5.3.5 Test of the observer

The observer is tested with simulated measurement values generated by the simplified model. The initial condition of the observer is a steady state with $I_{cell}=0.6$, $\lambda_{air} = 2.0659$, $\Gamma_{feed}=0.8296$ and $SC=2.4707$. At time 0, the cell current is set to the correct value $I_{cell}=0.5$, $\lambda_{air} = 2.0250$, $\Gamma_{feed}=0.6783$ and $SC=2.4304$. A measurement interval of 10 time units is assumed. In the test shown in Figure 5 - 6, the simplified model is used as a reference. The observer states converge rapidly to the reference states. The convergence is much faster than the transient of the uncorrected model to the steady state.

In the next test shown in Figure 5 - 7, the dynamic behaviour is tested in a process of the following. The simplified model changes from the state in the table 5 - 1, $I_{cell}=0.5$, $I_{cell}=0.6$ to $I_{cell}=1.0$, then back to the original state at every 20000 time units. Also in this case, the observer converges quickly and only causes a small and tolerable remaining estimate error.

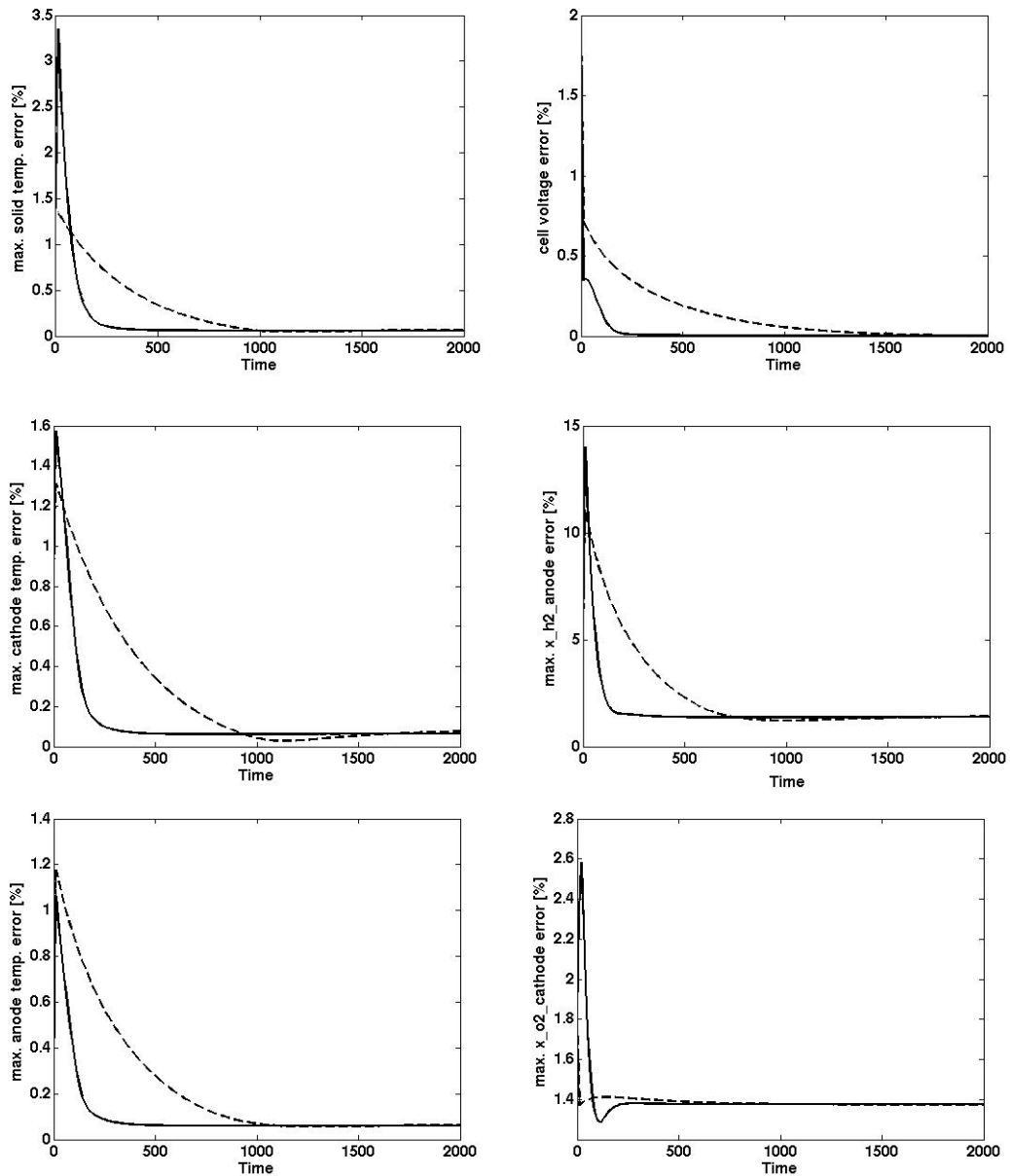


Figure 5 - 6: Convergence of the observer, when the simplified model is used as a reference; deviations of the observer states from the reference states without correction (dashed lines) and with correction (solid lines); first column from top to bottom: maximum relative error of the estimated solid temperature, the estimated cathode gas temperature, and the estimated anode gas temperature; second column from top to bottom: relative error of the estimated cell voltage, maximum relative error of the H_2 molar fraction in the anode gas, maximum relative error of the O_2 molar fraction in the cathode gas

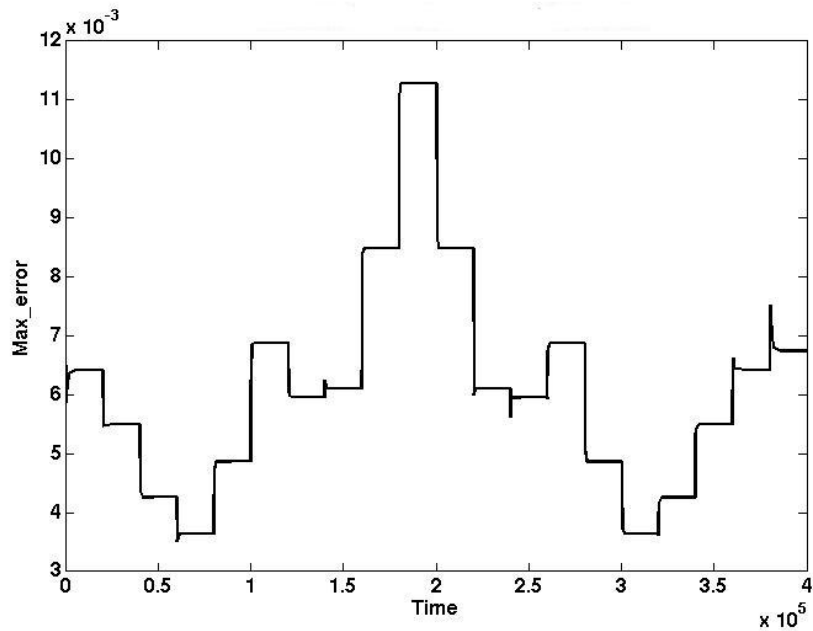


Figure 5 - 7: The maximum temperature error between observer and simplified model

5.3.6 Control results with observer

A control strategy has been designed based on the original model of the MCFC system in Section 5.3, where the controlled variables: maximum temperature and maximum temperature difference were obtained directly from the calculation of the model. To make the control strategy more applicable in practice the original model should be replaced by an observer in order to estimate the fuel cell's states that cannot be measured directly.

The control results with the observer obtained from section 5.3.5 (electrical load changes from $I_{cell}=0.5$ to $I_{cell}=0.55$ and... to $I_{cell}=1.0$, then back to the original state at every 20000 time units) are shown in Figure 5 - 8, which is comparable to Figure 5 - 4. It can be seen that the controller works very well when the observer is incorporated. The maximum temperature error between observer and full model with controller is shown in Figure 5 - 8(c), which as can be seen, is very small.

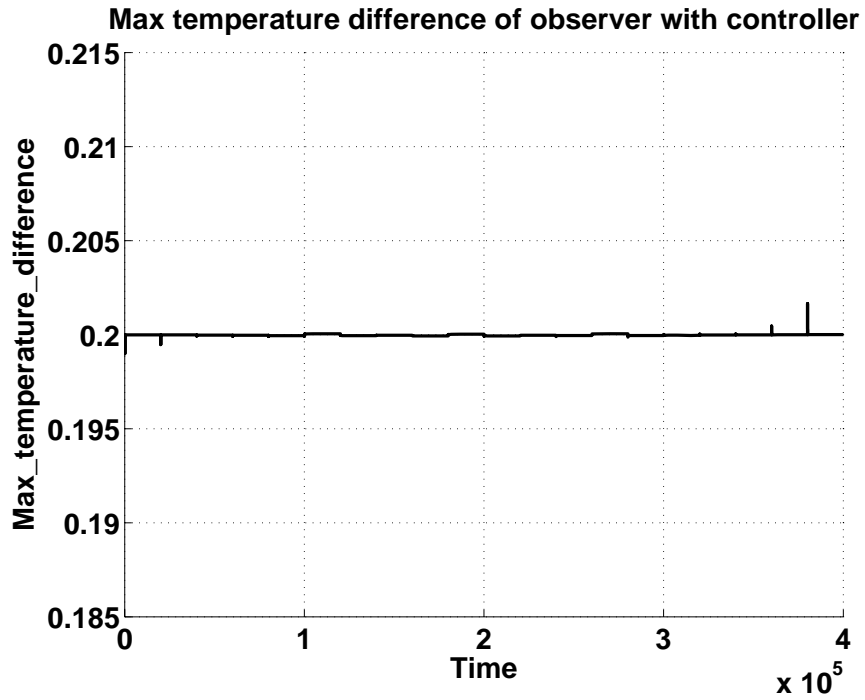


Figure 5 - 8(a): The maximum temperature difference estimated by the observer in the controlled system

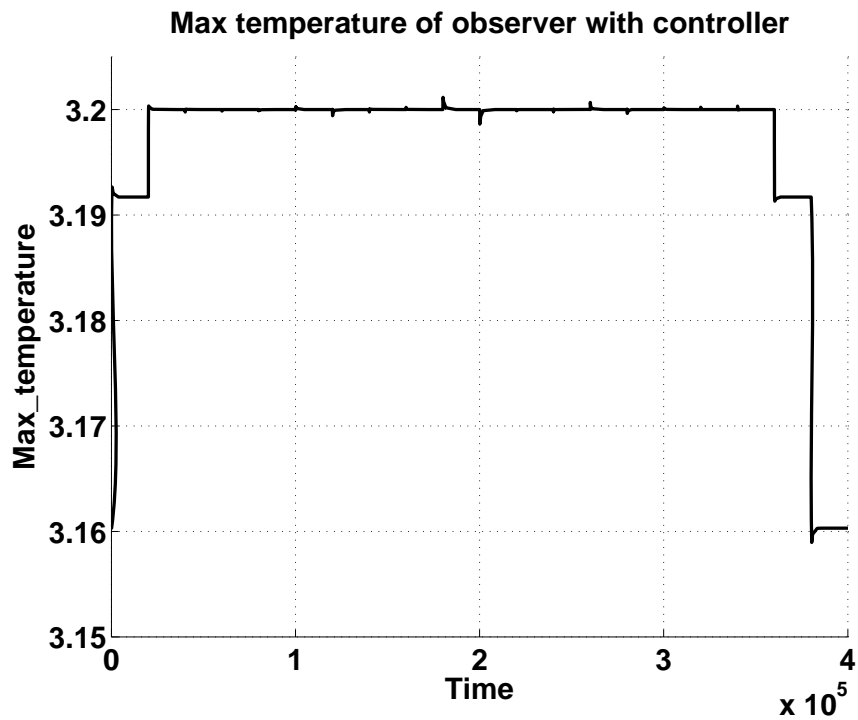


Figure 5 - 8(b): The maximum temperature estimated by the observer in the controlled system

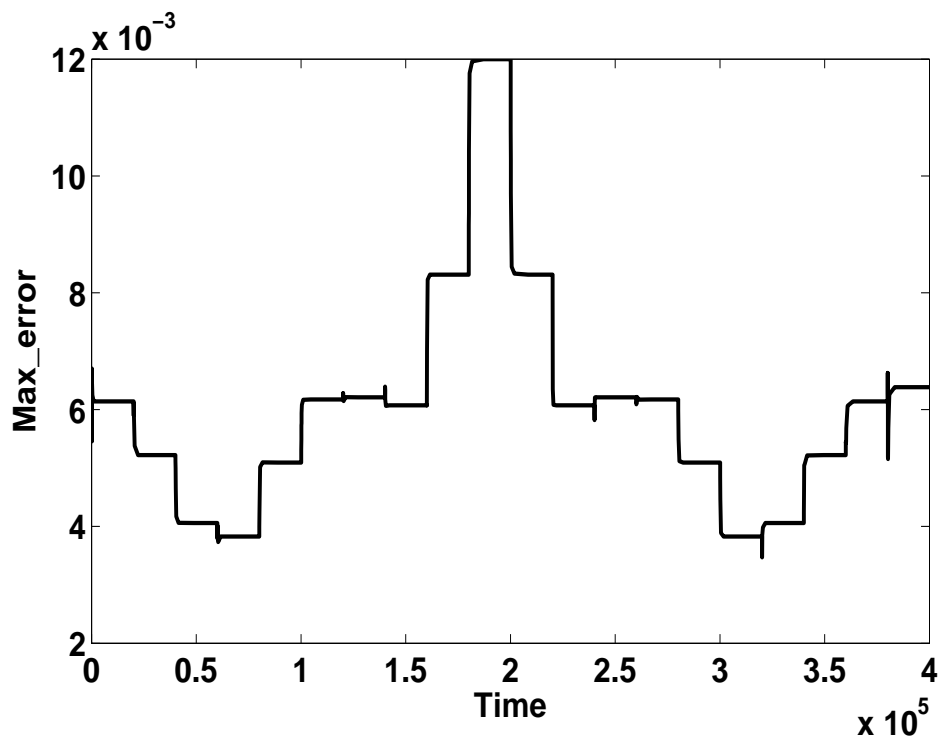


Figure 5 - 8(c): The maximum temperature error between observer and simplified model with controller

In a second test, the same scenario was applied, however, in addition five reaction kinetic parameters in the simplified model Arr_{ref1} , Arr_{ref2} , Arr_{ox1} , Arr_{ox2} , Arr_{red} are decreased by 10% and at the same time the observer and controller remain unchanged. The results are shown in Figure 5 - 9. It can be seen that the controller still works very well when these kinetic parameters are changed in the simplified model. The maximum temperature error between observer and full model with controller is shown in Figure 5 - 9(c).

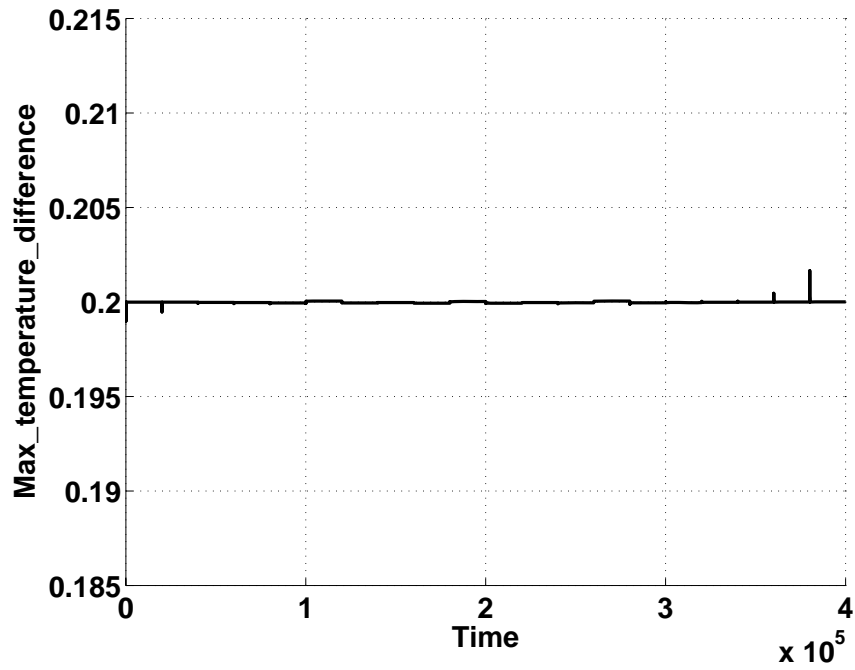


Figure 5 - 9(a): The maximum temperature difference estimated by the observer in the controlled system as Arr_{ref1} , Arr_{ref2} , Arr_{ox1} , Arr_{ox2} , Arr_{red} in the simplified model are decreased by 10%

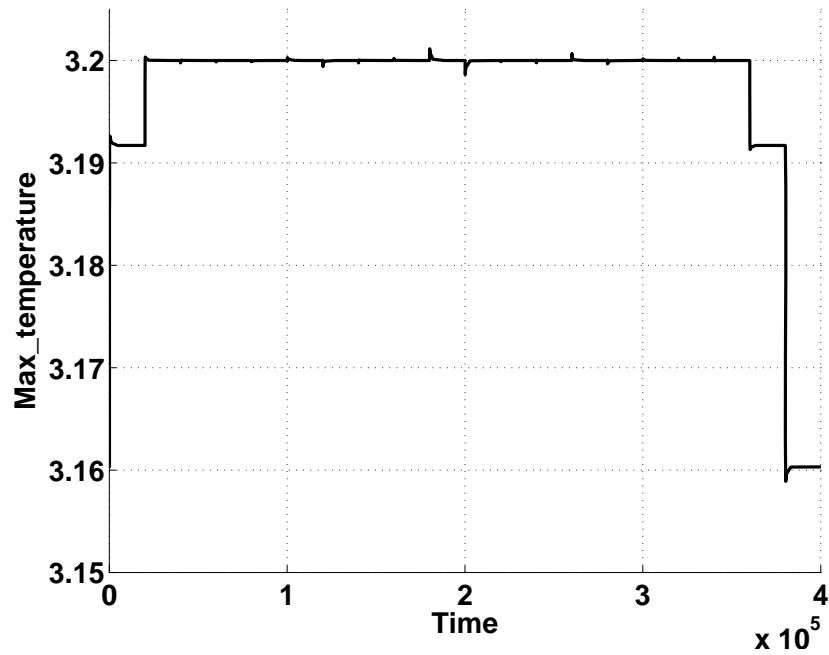


Figure 5 - 9(b): The maximum temperature estimated by the observer in the controlled system as Arr_{ref1} , Arr_{ref2} , Arr_{ox1} , Arr_{ox2} , Arr_{red} in the simplified Model are decreased by 10%

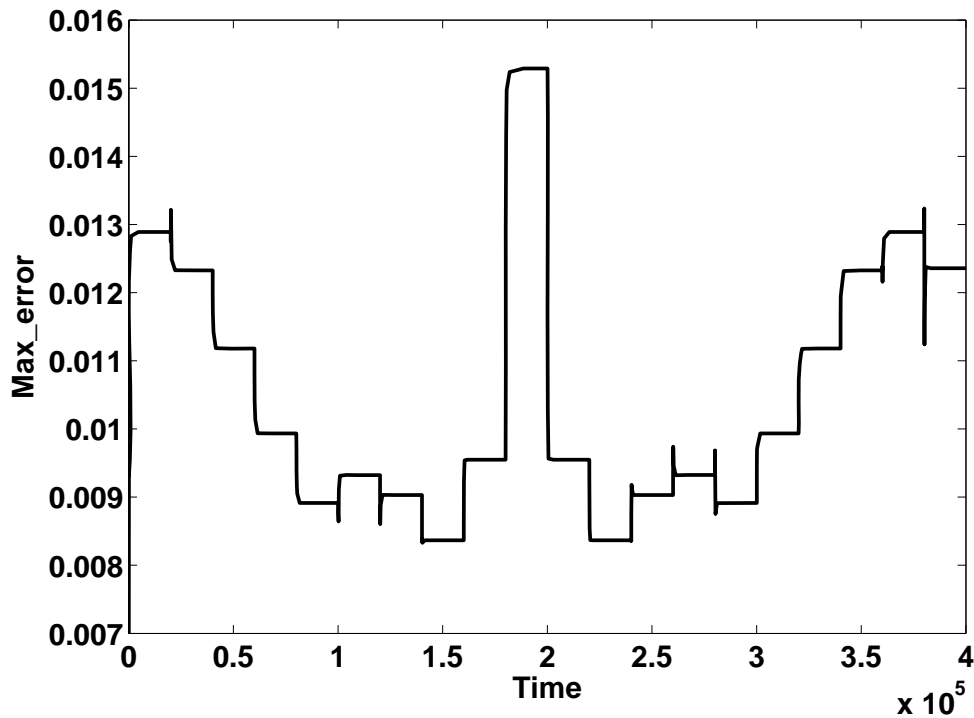


Figure 5 - 9(c): The maximum temperature error between the observer and the simplified model with the controller as Arr_{ref1} , Arr_{ref2} , Arr_{ox1} , Arr_{ox2} , Arr_{red} in the simplified model are decreased by 10%

5.4 Summary

In open literature, comparatively few publications are available on model based process control of MCFC systems. The results of this work show that a rather simple control scheme can contribute substantially to a safe and efficient operation of a high temperature fuel cell stack. Such systems are rather sensitive to local over-temperatures and spatial temperature differences. Therefore, temperature management is a key problem of the process operation of high temperature fuel cells. This work proposes a feedforward-feedback control scheme that may overcome this problem. The control scheme consists of three control loops. The first

loop is composed of a master (feed-forward) controller that imposes a load change and sets the fuel gas, the steam to carbon ratio, and the air number to their corresponding conditions for optimal steady state electric efficiency. The master-controller reads the steady state operation conditions from a look-up table. In this work, the look-up table was generated by optimizing the steady state solutions of a simplified process model; alternatively, it would also be possible to determine optimal steady state operation conditions experimentally and store them in the look-up table.

The other two loops are feedback PID controllers that are responsible for the temperature management under transient conditions. One of the PID controllers adjusts the air number in order to keep the maximum temperature below a pre-defined limit. The other PID controller corrects the steam-to-carbon ratio in order to limit the maximum spatial temperature difference. This simple control structure with linear feed-back controllers is inspired by the physical properties of the system and offers several advantages. Firstly, the actions of the controller appear to be transparent and understandable to the operating personal, a demand often made by practitioners on advanced control schemes. Secondly, the scheme has been derived from rather general properties of high temperature fuel cells and therefore may be robust to model uncertainties and applicable to many fuel cell systems.

The implementation of the developed feedforward-feedback control is especially simple, if it is possible to measure directly the maximum temperature and the maximum temperature difference, as was assumed first in this work. In practice, this measurement information is not always available. Very often, temperature measurements only can be taken at the outlets of the gas channels or at a few distinct points within the cell stack. In such cases, it possible to estimate the desired maximum temperatures and temperature differences with good accuracy from the available measurement information by using state estimation techniques. This was demonstrated in previous publications (Mangold *et al.* 2004b; Grötsch *et al.* 2006). The controller developed is then combined with a suitable state estimator in order to

make the scheme applicable under conditions, where measurement information is limited.

Chapter 6

Conclusions

Modeling a molten carbonate fuel cell system with internal reforming for control purposes and design of a control strategy are proposed in this work. Focus of this contribution is on a planar molten carbonate fuel cell and 280 kW MCFC stack 'Hot Module' by MTU CFC Solutions, Germany (Bischoff & Huppmann, 2002).

Although there has been considerable research interest in methods for modeling and controlling fuel cell systems (Chapter 2), they are either developed for a specific type of fuel cell or too complex for control purposes; and their applications on controller design are still limited. Suitable and simple-to-implement strategies of controller design also remain an open area. This background inspires the main contribution of the work. A two-dimensional detailed model of a single cross flow MCFC is first reviewed. Then a simplified form of the MCFC and a three-dimensional stack model are built based on the detailed model.

In chapter 3, firstly the simplified model is validated by comparing with the detailed model. Then the simulation of the three-dimensional stack model with indirect internal reforming was performed. The advantages and drawbacks of the 3-D model were discussed.

In chapter 4, a low order model for control purposes was derived from the two-dimensional spatially distributed cross flow model by the Karhunen-Loève Galerkin method. The basic idea of the method is to approximate the profiles of the spatially distributed variables by basis functions obtained from test simulations with a detailed reference model. The reduced model produces results that are very close to those of the original model, but it reduces the computation time by a factor

of more than 100. The reduced model itself is given in an analytical form and still contains the information on the physical correlations in the original model.

The reduced-order model obtained from the orthogonal projection method described in Chapter 4 leads to an observer model to be applied in control applications (Chapter 5). A novel control strategy, which includes three main control loops, has been implemented based on the dynamic behavior of the MCFC. The master controller assures the optimal steady state electric efficiency and the two slave controllers keep the process dynamics safe by maintaining temperature within maximum limits.

Bibliography

- Aguiar,P., C.S.Adjiman, and N.P.Brandon, (2005). Anode-supported intermediate-temperature direct internal reforming solid oxide fuel cell: II. Model-based dynamic performance and control, *Journal of Power Sources*, Vol. 147, No. 1-2, pp. 136-147.
- Atwell,J.A. and B.B.King, (2001). Proper orthogonal decomposition for reduced basis feedback controllers for parabolic equations, *Mathematical and Computer Modelling*, Vol. 33, No. 1-3, pp. 1-19.
- Baker,J. and P.D.Christofides, (2000). Finite-dimensional approximation and control of non-linear parabolic PDE systems, *International Journal of Control*, Vol. 73, No. 5, pp. 439-456.
- Bischoff,M. and G.Huppmann, (2002). Operating experience with a 250 kWel molten carbonate fuel cell (MCFC) power plant, *Journal of Power Sources*, Vol. 105, No. 2, pp. 216-221.
- Bosio,B., P.Costamagna, and F.Parodi, (1999). Modeling and experimentation of molten carbonate fuel cell reactors in a scale-up process, *Chemical Engineering Science*, Vol. 54, No. 13-14, pp. 2907-2916.
- Carrette,L., K.A.Friedrich, and U.Stimming, (2001). Fuel cells- fundamentals and applications, *Fuel Cells*, Vol. 1, No. 1, pp. 5-39.
- Cavallaro,S. and S.Freni, (1998). Syngas and electricity production by an integrated autothermal reforming/molten carbonate fuel cell system, *Journal of Power Sources*, Vol. 76, No. 2, pp. 190-196.
- Christofides,P.D. and P.Daoutidis, (1996). Nonlinear control of diffusion-convection-reaction processes, *Computers & Chemical Engineering*, Vol. 20, No. Supplement 2, pp. S1071-S1076.
- C. Prud'Homme, D.V. Rovas, K. Veroy, and A.T. Patera. Mathematical and computational framework for reliable real-time solution of parameterized

- partial differential equations. *Mathematical Modelling and Numerical Analysis*, 36(5):747-771, 2002
- Ernest, J.B., H.Ghezel-Ayagh, and A.K.Kush, (1996). Dynamic simulation of a direct carbonate fuel cell power plant, In: *Proceedings of the 1996 fuel cell seminar*, Orlando, FL, USA.
- Finlayson, B.A. (1972). *The Method of Weighted Residuals and Variational Principles*, Academic Press, New York.
- Friedland, B., Observers In: W.S. Levine, Editors, *The Control Handbook*, CRC Press, Boca Raton (1996), pp. 607–620.
- Golbert, J. and D.R.Lewin, (2004). Model-based control of fuel cells: (1) regulatory control, *Journal of Power Sources*, Vol. 135, pp. 135-151.
- Grötsch, M., M. Gundermann, M. Mangold, A. Kienle and K. Sundmacher, Development and experimental investigation of an extended Kalman filter for a molten carbonate fuel cell system . *Journal of Process Control* (2006), accepted for publication
- Gundermann, M., Heidebrecht, P., Sundmacher, K., (2006). Validation of a mathematical model using an industrial MCFC plant, *Journal of Fuel Cell Science and Technology*, accept
- Hautus, M.L.J., (1969). Controllability and observability conditions of linear autonomous systems, *Indagationes Mathematicae*, Vol. 31, pp. 443-448.
- He, W., (1994). A dynamic performance of a molten carbonate fuel cell in power generation system, *Journal of Power Sources*, Vol. 52, No. 2, pp. 179-184.
- He, W. and Q.Chen, (1995). Three-dimensional simulation of a molten carbonate fuel cell stack using computational fluid dynamics technique, *Journal of Power Sources*, Vol. 55, No. 1, pp. 25-32.
- He, W. and Q.Chen, (1998). Three-dimensional simulation of a molten carbonate fuel cell stack under transient conditions, *Journal of Power Sources*, Vol. 73, No. 2, pp. 182-192.
- Heidebrecht, P. and K.Sundmacher, (2002). Dynamic modelling and simulation of a counter current molten carbonate fuel cell (MCFC) with internal reforming, *Fuel Cells*, Vol. 2, pp. 166-180.

- Heidebrecht,P. and K.Sundmacher, (2003). Molten carbonate fuel cell (MCFC) with internal reforming: model-based analysis of cell dynamics, *Chemical Engineering Science*, Vol. 58, No. 3-6, pp. 1029-1036.
- Heidebrecht,P., (2005). Modelling, Analysis and Optimisation of a Molten Carbonate Fuel Cell with Direct Internal Reforming (DIR-MCFC), *Fortschritt-Berichte*, VDI-Verlag, Düsseldorf.
- Hoo,K. and D.Zheng, (2001). Low-order control-relevant models for a class of distributed parameter systems, *Chemical Engineering Science*, Vol. 56, No. 23, pp. 6683-6710.
- Hou,K. and R.Hughes, (2001). The kinetics of methane steam reforming over a Ni/ α -Al₂O catalyst, *Chemical Engineering Journal*, Vol. 82, No. 1-3, pp. 311-328.
- Kang,B.S., J.-H.Koh, and H.C.Lim, (2001). Experimental study on the dynamic characteristics of kW-scale molten carbonate fuel cell systems, *Journal of Power Sources*, Vol. 94, No. 1, pp. 51-62.
- Köhler,R., K.D.Mohl, H.Schramm, M.Zeitz, A.Kienle, M.Mangold, E.Stein, and E.D.Gilles, (2001). Method of lines within the simulation environment DIVA for chemical processes, in Book: *Adaptive Method of Lines* (Eds. A. Vande Wouwer, P. Saucez, W. Schiesser), Chapman & Hall/CRC, Boca Raton, pp. 371-406.
- Koh,J.-H., B.S.Kang, and H.C.Lim, (2001). Analysis of temperature and pressure fields in molten carbonate fuel cell stacks, *A.I.Ch.E.Journal*, Vol. 47, No. 9, pp. 1941-1956.
- Loève,M., (1955). *Probability Theory*, Van Nostrand, Princeton, New Jersey.
- Lückel,J. and P.C.Müller, (1975). Analysis of controllability, observability and disturbability structures in linear time invariant systems, *Regelungstechnik*, Vol. 23, pp. 163-171.
- Lukas,M.D., K.Y.Lee, and H.Ghezel-Ayagh, (2002). Modeling and cycling control of carbonate fuel cell power plants, *Control Engineering Practice*, Vol. 10, No. 2, pp. 197-206.

- Lukas,M.D. and K.Y.Lee, (2005). Model-based analysis for the control of molten carbonate fuel cell systems, *Fuel Cells*, Vol. 5, No. 1, pp. 115-125.
- Mangold,M. and M.Sheng, (2003). Nonlinear model reduction of a dynamic two-dimensional molten carbonate fuel cell model, In: *Proc.AIChE 2003 Annual Meeting*, San Francisco, USA.
- Mangold,M. and M.Sheng, (2004). Nonlinear model reduction of a two-dimensional MCFC model with internal reforming, *Fuel Cells*, Vol. 4, No. 1-2, pp. 68-77.
- Mangold,M., M.Sheng, P.Heidebrecht, A.Kienle, and K.Sundmacher, (2004a). Physical model development, model reduction, and observer design of a molten carbonate fuel cell, In: *Proc. 18th International Symposium on Chemical Reaction Engineering - ISCRE 18*, Chicago, USA.
- Mangold,M., M.Sheng, P.Heidebrecht, A.Kienle, and K.Sundmacher, (2004b). Development of physical models for the process control of a molten carbonate fuel cell system, *Chemical Engineering Science*, Vol. 59, No. 22-23, pp. 4847-4852.
- Mangold,M., M.Grötsch, M.Sheng, and A.Kienle, (2005). State estimation of a molten carbonate fuel cell by an extended Kalman filter, In: *Proceedings of SYNCOD'2005*, Springer-Verlag.
- Mangold,M. and M.Sheng, (2006). Nonlinear model reduction of a dynamic two-dimensional molten carbonate fuel cell model, in *Book: Progress in Industrial Mathematics at ECMI 2004*, pp. 262-266, Springer, Berlin.
- Park,H.M. and D.H.Cho, (1996). The use of the Karhunen-Loève decomposition for the modeling of distributed parameter systems, *Chemical Engineering Science*, Vol. 51, No. 1, pp. 81-98.
- Shen,C., G.-Y.Cao, X.-J.Zhu, and X.-J.Sun, (2002). Nonlinear modeling and adaptive fuzzy control of MCFC stack, *Journal of Process Control*, Vol. 12, No. 8, pp. 831-839.
- Shen,C., L.Yu, and G.-Y.Cao, (2004). Control-oriented nonlinear modelling of molten carbonate fuel cells, *International Journal of Energy Research*, Vol. 28, pp. 403-410.

- Sheng,M., M.Mangold, and A.Kienle, (2006). A strategy for the spatial temperature control of a molten carbonate fuel cell system , Journal of Power Sources, Vol. 162, pp. 1213-1219.
- Simoglou,A., P.Argyropoulos, E.B.Martin, K.Scott, A.J.Morris, and W.M.Taama, (2001). Dynamic modelling of the voltage response of direct methanol fuel cells and stacks Part I: Model development and validation, Chemical Engineering Science, Vol. 56, No. 23, pp. 6761-6772.
- Sun,X.-J., G.-Y.Cao, and X.-J.Zhu, (2001). A novel genetic algorithm and its application in fuzzy variable structure control of fuel cell, Journal of Intelligent and Robotic Systems, Vol. 31, No. 1-3, pp. 299-316.
- Takashima,S., K.Ohtsuka, N.Kobayashi, and H.Fujimura, (1990). Stack performance model of molten carbonate fuel cell, In: Electrochemical Society Proceedings of the Second Symposium on Molten Carbonate Fuel Cell Technology, Seattle, USA.
- Tränkle,F., M.Zeitz, M.Ginkel, and E.D.Gilles, (2000). ProMoT: A modeling tool for chemical processes, Mathematical and Computer Modelling of Dynamical Systems, Vol. 6, No. 3, pp. 283- 307.
- Yoshiba,F., N.Ono, Y.Izaki, and T.A.T.Watanabe, (1998). Numerical analysis of the internal conditions of a molten carbonate fuel cell stack: Comparison of stack performance for various gas flow types , Journal of Power Sources, Vol. 71, No. 1-2, pp. 328-336.